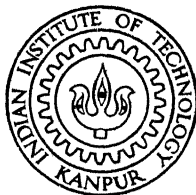# LOCAL STRUCTURES IN AMORPHOUS Ge_xSe_{1-x} SYSTEM

By

VINOD DIGAMBER CHAFEKAR

DEPARTMENT OF PHYSICS

INDIAN INSTITUTE OF TECHNOLOGY KANPUR

MARCH, 1984

LOCAL STRUCTURES IN AMORPHOUS Ge$_x$Se$_{1-x}$ SYSTEM

A Thesis Submitted
in Partial Fulfilment of the Requirements
for the Degree of

DOCTOR OF PHILOSOPHY

By

VINOD DIGAMBER CHAFEKAR

to the

DEPARTMENT OF PHYSICS

INDIAN INSTITUTE OF TECHNOLOGY KANPUR

MARCH, 1984

To

my parents

CERTIFICATE

This is to certify that this thesis entitled 'LOCAL STRUCTURES IN AMORPHOUS Ge_xSe_{1-x} SYSTEM' submitted in partial fulfilment of the requirement for the degree of Doctor of Philosophy by Mr. Vinod Digamber Chafekar, is a record of work carried out under my supervision and has not been submitted elsewhere for a degree.

(S.C. Sen)
Assistant Professor
Department of Physics
Indian Institute of Technology
KANPUR

ACKNOWLEDGEMENTS

CONTENTS

CHAPTER

CHAPTER

LIST OF FIGURES

LIST OF TABLES

SYNOPSIS

Vinod D. Chafekar
Ph. D.
Department of Physics
Indian Institute of Technology Kanpur
March 1984

'LOCAL STRUCTURES IN AMORPHOUS Ge_xSe_{1-x} SYSTEM'

In this thesis, the results of the investigation undertaken to record and analyse the X-ray absorption (K edge EXAFS), fluorescence and diffraction data of amorphous materials (Ge_xSe_{1-x} system with x = 0.1, 0.3 and 1.0) are reported. These materials belong to the amorphous semiconductor class of non-crystalline matter.

Extended X-ray absorption fine structure (EXAFS) refers to the oscillations of X-ray absorption coefficient on the high energy side of the absorption edge. Interest in EXAFS has been revived in past several years for its applications to the structure determination of amorphous materials. Although the revival of interest in EXAFS is due to the improvements in theory and experimentation, in particular the synchrotron related developments, we have in our laboratory recorded the EXAFS data with a conventional X-ray source. By operating the tube at

higher ratings the requirement of high photon flux was met. Adequate resolution ($\sim$ 4 eV) in the vicinity of absorption edge was obtained by using an exit slit of 0.05 mm width (which allows minimum increment of 0.01° in 2θ).

The analysis of EXAFS data involved number of steps with extensive use of computer. The programmes needed for the analysis have been developed. The experimental data on crystalline and amorphous germanium served to standardize the analysis procedure. The study of amorphous Ge_xSe_{1-x} system has been limited to compounds with low concentration of germanium. EXAFS is particularly useful in such a system as we can probe the environment of both kind of atoms.

Chapter I contains some introductory remarks on the local structure in non-crystalline materials and methods for its determination. The advantages and disadvantages of the relatively new technique - EXAFS over the traditional methods; X-ray diffraction (R.D.F. measurement) in particular have been briefly outlined. The possibility of ascertaining the kind of backscattering atom, particularly in system like GeSe using EXAFS has been examined.

Chapter II gives an account of the experimental details of all the three types of measurements namely

ix

the X-ray absorption (EXAFS), fluorescence and diffraction. Dispersion and resolution of the spectrometer has also been discussed.

In chapter III the theory underlying the EXAFS phenomenon and data analysis procedure has been presented briefly. Chapter IV presents the results obtained by analysing the experimental data of germanium. K edge EXAFS of both crystalline and amorphous germanium have been analysed. The effect of width of the filtering window, used to separate out the first shell EXAFS, on the phase and amplitude functions and subsequently on the determiniation of structural parameters has been discussed. The phase function was found to be least affected by the width of the window function as indicated by the same value of near neighbour distances obtained with different window widths. On the other hand the amplitude function was found to be sensitive to the changes in window width. The concepts of chemical transferability of phase and amplitudes have been used to calculate the near neighbour distance and the coordination number for amorphous germanium. The determination of near neighbour distance by comparison of experimental and theoretical phase shifts (Teo, B.K. and Lee, P.A. (1979), J. Am. Chem. Soc. 101, 2815) required that the phase functions be obtained using critical value of $E_o = E_c$ at which the phase shift is linear and the position of the peak in the magnitude of Fourier transform

is independent of the weighting factor (Stearns, M.B. (1982), Phys. Rev. B25, 2382). The analysis of X-ray diffraction data is briefly presented in the last section.

In chapter V, the analysis of experimental data of amorphous Ge_xSe_{1-x} system (x = 0.1, 0.3) is presented. K edge EXAFS of both kind of atoms (Ge and Se) has been analysed. While analysing EXAFS data, the phase functions have been extracted (at $E_0 = E_c$) following the procedure in chapter IV. It has been assumed that the first coordination shell around central atom can have both kind of atoms on account of the proximity of atomic numbers of Ge and Se. For determining the near neighbour distances two different cases are considered depending upon the kind of atom as backscattering atom, the result obtained using the experimental phase function could be interpreted in terms of the probability of that atom being the nearest neighbour to the central atom. The calculated probabilities have been used in the proposed model which is based on the probabilities of all the different possible configurations of the first coordination shell around the central atom. The experimental first shell EXAFS then could be compared with the one obtained from the proposed model to determine a set of structural parameters. DRDF analysis has been briefly presented in the last section.

Chapter VI gives the summary of the present work and also the scope for future work.

CHAPTER I

INTRODUCTION

1.1 Non Crystalline Materials

Solid materials can be broadly classified into two categories depending on their structure. The crystalline materials have a three dimensional periodic arrangement of their constituent atoms or in other words long range order (lro) exists. Structurally amorphous, non-crystalline, disordered, glassy and vitreous are synonyms, but the last two terms are generally reserved for non-crystalline solids prepared by quenching from liquid state. The amorphous materials lack the regularity of arrangement of atoms as in crystals. Diffraction experiments (X-rays, Neutron, Electron) show that the order within the amorphous phase does show some sort of similarity with that of the crystal lattice, losing however, the long range order. Amorphous solids distinctly differ from crystalline one due to lack of long range order and hence possess no readily definable translational symmetry. Figure 1.1 illustrates two different phases: crystalline and amorphous of the same chemical composition A_2O_3. There is no sharp dividing line between the crystalline and the so called amorphous materials. As the crystalline size diminishes the widths of the lines composing the powder X-ray diffraction pattern increase until the fainter lines are indiscernable and the stronger assume diffuse characters which is typical of non-crystalline substances. The
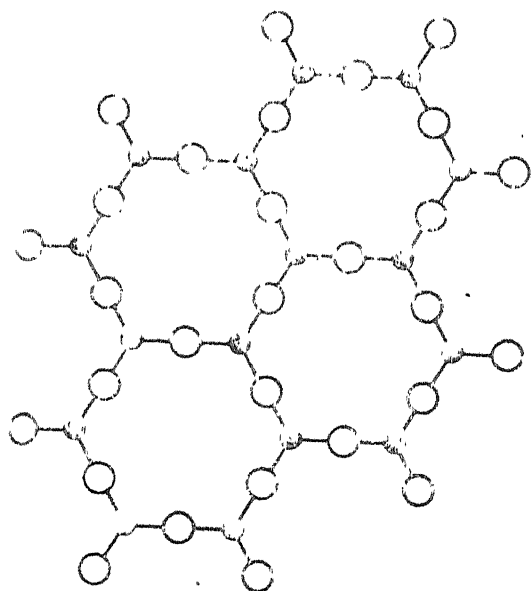
(A)
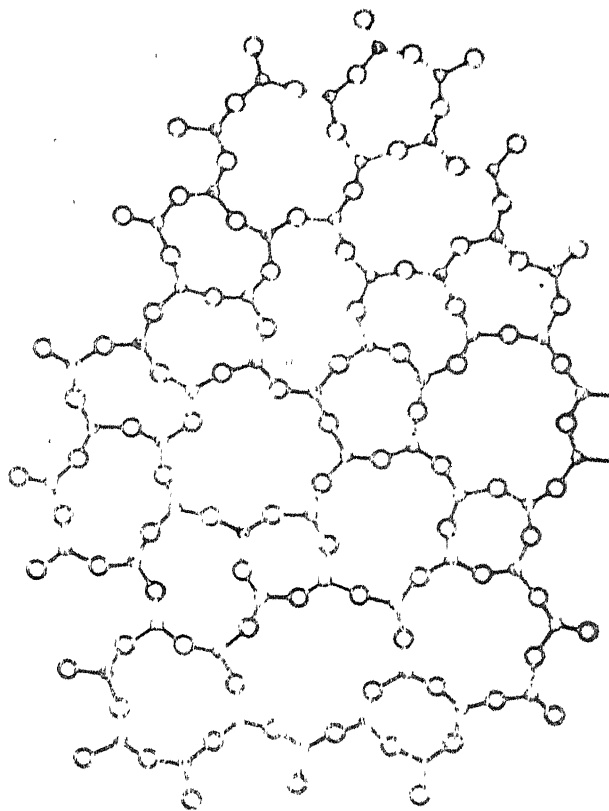
(B)

crystallite dimensions calculated from such broad bands
are often of the order of one or two unit cell dimensions,
a result very difficult to interpret on the basis of
repetitive structure pattern.

Amorphous semiconductors are well known examples
of highly disordered materials. There has been in recent
years a surge of interest in them, particularly after the
publication of Ovshinsky (1968) describing the various
types of switching phenomena which can be observed with
a large number of amorphous solids. The technological
importance soon became evident. Applications of amorphous
semiconductors either realized or anticipated include a
very wide spectrum (Feinleib et al. 1971; Hilton et al.,
1966a; Ovshinsky and Fritzsche, 1973; Neale and Aseltine,
1973; Dessaner and Clarks, 1965) such as optical recording
devices, optical lenses, windows and filters, continuous
dynode electron multipliers (channeltron), optical mass
memory, phase contrast holograms, high energy particle
detectors, ultrasonic delay lines and microfiche trans-
parencies, in addition to the exciting switching and
memory devices and the well established applications in
xerography. This is indeed a very impressive list,
specially in view of the fact that the understanding of
the amorphous semiconductors today is still far from
satisfactory. Further the advantage of producing amorphous

semiconducting materials in the form of thin films makes
them adaptable to integration with other solid state
technologies.

The field of amorphous semiconductors as a whole
is of fundamental interest. Ordered materials (crystal-
line) are known to have universal features in their
electronic structures. It can be expected that amorphous
semiconductors may also possess such universal features.
Considerable efforts are being made to obtain the rigorous
theoretical interpretations of the experimental observa-
tions. An understanding of the properties of amorphous
semiconductors requires not only familiarity with solid
state physics but rather a detailed knowledge of the
results obtained from the combined fields of physics,
chemistry, metallurgy and electrical engineering. Consi-
derable exploratory work on amorphous semiconductors was
carried out during the early fifties. In recent years,
intensive research work in several countries has been
directed to improve the understanding of structural,
electrical, optical, mechanical, magnetic and other pro-
perties of these materials in order to attain the same level
of understanding as in case of crystalline semiconductors.
In the present work we are concerned with the structural
aspects.

1.2 Determination of Local Structure

A complete description of the properties of any
compound requires a full knowledge of its structure.
There are basically two main approaches for determination
of local structure in non crystalline materials, which
have have been used in the past, namely the diffraction
methods and the spectroscopic methods. In the first
group, the interaction of radiation with matter leads to
information which can be analysed as such in the Fourier
space or transformed to real space, either mathematically
as in case of X-ray or neutron diffraction or physically
as in case of electron microscopy.

The electron or X-ray diffraction pattern of amor-
phous materials consist of a few broad halos rather than
sharp Bragg reflections. A small crystalline size, strains
and imperfections broaden the sharp crystallite reflections
and as the crystal size gets smaller a point is reached
where the crystallite reflections overlap and diffraction
pattern appears like that of amorphous materials (Germer
and White, 1941; Piggott, 1966). The probability of find-
ing an atom on a sphere of radius r or the Radial Distribu-
tion Function (RDF) $4 \pi r^2 \, \rho(r)$, $\rho(r)$ being the atomic
density, is used to give a one dimensional description
of the atomic distribution. When RDF is normalised,

it contains a number of peaks at some values of r and area
under each peak corresponds to the number of atoms contained
in the coordination shell. To illustrate, figure 1.2 shows
the RDF of $Ge_{.42}Se_{.58}$ as obtained from X-ray diffraction
data by Bienenstock et al. (1976). It can be noted that
the first and second neighbour peaks are well defined in
this case, but that little information is obtainable about
more distant coordinations.

As we know, the diffraction methods give us only a
one dimensional information - the result of RDF and intri-
cate separation methods using different radiations, it is
only by means of modelling that one can obtain a three
dimensional information.

Zacharaisen in 1932 (Zacharaisen, 1932) in a paper
which led to the foundations of our understanding of glassy
structure insisted that "It must be frankly admitted that
we know practically nothing about the atomic arrangement
in glasses". Knowledge about the non-crystalline materials
remained almost static in the following thirty years.
Zacharaisen's random network - the father of subsequent
models of amorphous solids - remained a mathematically
unhandable concept. Diffraction experiments of Warren
(Warren et al., 1936, Biscoe and Warren 1938) on vitreous
silica and boron oxide were consistent with random network
model and similar concepts were used by Bernal in probing
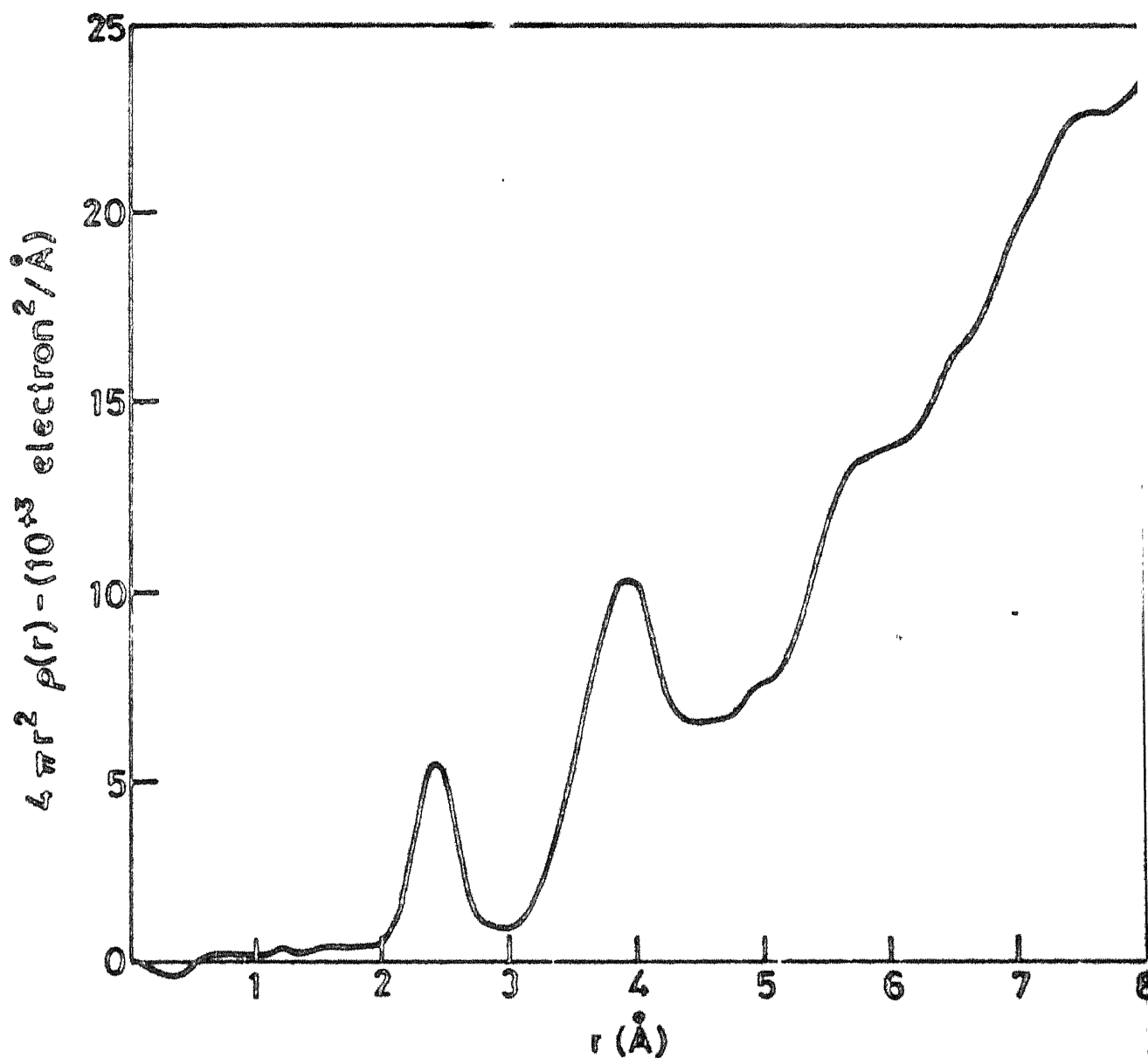
Fig.1.2   Radial distribution function for $Ge_{.42}Se_{.58}$, as obtained from X-ray diffraction data by Bienenstock et al. (1976).

the structures of water and simple liquids (Bernal and Fowler, 1933, Bernal, 1937, 1959), but the concept remained underdeveloped and largely unappreciated.

There has been a rapid growth of interest in amorphous solids in the past decade ranging from covalent glasses such as vitreous silica through the related amorphous tetrahedral systems of Si, Ge and H_2O. Depending upon the method of preparation and the nature of molecules concerned, one might expect variety of amorphous structures. Despite this variety, all amorphous substances can, following Zacharaisen, be treated within the same conceptual framework: an irregular topology of linked subunit molecule. Although distinctivley microcrystalline materials can be prepared (Wagner et al., 1968), diffraction experiments on the amorphous solids cannot convincingly be explained in lattice terms (Cargill, 1970; Mozzi and Warren, 1969; Moss and Graczyk, 1969). As a first approximation one tries to develop an idealised model which describes the essential structure of group of systems. Modelling two extreme types of amorphous structures based upon an idealised tetrahedral geometry and upon spherically symmetrical atoms cover many of the systems of most practical interest. In each case, real physical models were built in laboratory. Later, digital computers were used to build and refine the models. In the present investigation models based on tetrahedral geometry are of interest.

The idealised tetrahedral network is topologically similar to other non-crystalline aggregates. The ground work for realising Zacharaisen's random network concept was led in 1960's, when a series of tetrahedral models were built in an attempt to understand the structures of vitreous silica and water (Ordway, 1964; Evans and King, 1966). The vitreous structural models may be classified as microcrystallite, amorphous clusters, continuous random network (CRN), the chain model (Hilton et al., 1966b) suggested for GeTe and chain crossing model (Fawcett et al., 1972) suggested for $Ge_x Se_{1-x}$ system ($x \leqslant 0.3$) and so on. In its simplest form, the microcrystallite structure of the tetrahedrally coordinated as well as of other types of solids is considered to be an assembly of crystallites with their orientations and shapes distributed as they might be in recrystallised solids. The amorphous cluster models were developed specially for application to tetra-hedrally coordinated systems. In an "ideal" random network structure, every atom is bonded to the number of nearest neighbours required to satisfy the chemical valence so that there are no internal "dangling" bonds. The structure can be enlarged indefinitely without breaking bonds or increasing deviation of the bond angles from their ideal values. For example this model seems to describe adequately the RDF of amorphous germanium (Grigorovici and Manila, 1969; Polk, 1971; Turnbull and Polk, 1972).

The model describing the RDF gives us the nearest neighbour separations, the coordination numbers and the bond angles, all of which are vital parameters for any basic theory that hopes to explain in detail the electronic properties of non-crystalline materials. The problem often encountered with this approach is that quite different reasonable structural models yield almost exactly the same first neighbour peak area so that they can not be distinguished. This sort of ambiguity pervades much of the chalcogenide glass RDF work. It is quite extreme in Ge-chalcogenide because the structures of crystalline and amorphous Ge-monochalcogenides are strikingly different (Bienenstock, 1973a) so that the knowledge of former gives little guidance concerning the nature of the later. Ge-Se system poses the worst problem because the two atomic numbers are almost identical. From figure 1.2 it is apparent that the first peak may have contributions from Ge-Se, Ge-Ge and Se-Se first neighbour pairs. Herein lies the essence of the ambiguity in its interpretation.

All the diffraction techniques directly detect the lro and in particular the unit of periodicity. For the case of non-crystalline materials, the diffraction techniques, as has been pointed out earlier, have only

limited applicability. On the other hand the other group of methods namely the spectroscopic methods could be used as filters to select from the vast number of models those which have a higher probability of being real and reject those which are not compatible with experimental results. The spectroscopic methods include Raman spectroscopy, NMR, IR and the relatively new methods such as positron annihilation and specially EXAFS which provides new ways of probing the environment of atoms in the structure. It is this technique which has been used in the present work.

1.3 Some Special Advantages of X-ray Absorption Spectroscopy

Although there exist several theoretical and experimental difficulties in satisfactorily interpreting X-ray absorption spectra, this technique has certain special advantages (Cauchois, 1948) which are stated below:

a) It is very specific regarding the element or the ion under investigation.

b) All types of substances, solids (crystalline, amorphous, metallic and non-metallic, elemental and compounds), liquids and gases in different physico-chemical states can be studied by this method.

c) Wide energy range is covered in the same spectra. With a high resolution curved crystal spectrograph, the

different features of a discontinuity such as position, shape, width and fine structure give information about different single particle states as well as collective states simultaneously (Mande and Nigavekar, 1967).

d) Information regarding the empty states in the conduction band is obtained in the absorption spectra making use of relatively narrow inner states as a scanning probe.

e) It is a non-destructive technique and comparitively a small amount of the material is required for the investigation.

f) X-ray absorption spectra are sensitive to chemical combination and can therefore be used in the study of chemical bonding.

g) Amongst the different techniques used in the study of the solid state, it is relatively simple and inexpensive.

h) Oscillations in the absorption coefficient on the high energy side of the absorption discontinuity (EXAFS) provides information about local structure around the absorbing atom.

1.4 Extended X-ray Absorption Fine Structure (EXAFS)

The term extended X-ray absorption fine structure refers to the oscillations of the X-ray absorption coefficient on the high energy side of the absorption edge

extending to about 1000 eV above the edge. There has
been, in recent years, a revival of interest in EXAFS.
Several sophisticated theories (Stern, 1974; Lee and
Pendry, 1975; Lee and Beni, 1977) have been putforth to
explain the occurrence of EXAFS. Experimental methods
for recording the X-ray absorption spectra have also
improved in the last decade.

In late 1930s, X-ray absorption spectra were taken
in transmission with low power conventional tubes, a dis-
persive Bragg spectrometer and photographic film as
detector (Kossel, 1920; Kronig, 1931, 1932). Lytle (1966)
improved the measurements using modern counting and auto-
mation techniques. The replacement of conventional X-ray
tubes with synchrotron radiation signalled the beginning
of new era in measurement techniques (Kincaid and Eisenberger,
1975). A transmission technique using a channel cut mono-
chromator and an ion chamber was developed, followed by
development of fluorescence detection technique based on
solid state detector (Jaklevic et al., 1977). A new
graphite array system was developed (Hastings et al., 1979)
which extended the limits of EXAFS experiments. The
synchrotron related developments have been responsible
for the renewed interest in conventional rotating anode
X-ray tubes coupled with curved crystal monochromator
to perform laboratory based transmission experiments

(Knapp, 1978). Even the conventional sources coupled with flat crystal monochromator yield data of fairly good quality (Lytle et al., 1975) and in the present work we have used a similar set up for recording the EXAFS data. The requirement of high photon flux is met by operating the tube at higher ratings.

It is believed that study of EXAFS can give valuable and very precise information about the interatomic distances in all kinds of materials. The RDF studies measure distances between all possible pairs in a multicomponent system whereas EXAFS can provide information about the immediate environment of an individual species in the system. EXAFS being basically an sro phenomenon, it is most useful for studying the disordered materials. Recently EXAFS is being used in disordered systems (Crozier and Seary, 1981; Crozier et al., 1977), Catalysts (Lytle et al., 1980), Biological systems (Shulman et al., 1975, Sayers et al., 1976) and so on. The distances could be determined to an accuracy of $\pm 0.01 \overset{\circ}{A}$ and the coordination numbers within 20% accuracy. The accuracy is mainly determined by the quality of experimental data and the data analysis procedure used to extract the relevant parameters. The main problem in the analysis is to obtain the smooth free atom absorption, $\mu_o(K)$, required for normalising the EXAFS modulations to per atom scale (Criteria for

automatic background removal and normalisation has been
recently suggested by Cook and Sayers (1981)). Any error
in normalisation directly affects the amplitude of the
normalised EXAFS and subsequently the determination of
coordination number. Other factors which could affect
the EXAFS amplitudes are thickness of the absorber (Stern
and Kim, 1981), many body effects (Stern et al., 1980) and
the temperature. The temperature dependent Debye-Waller
type factor is a measure of both the thermal as well as
static disorder in the material. This factor must be known
for determination of coordination number. In many cases the
effective Debye-Waller approximation is inadequate in dis-
ordered systems (Eisenberger and Brown, 1979; Crozier and
Seary, 1980) and one has to resort to modelling for obtain-
ing meaningful results.

1.5 Scope of the Present Work

Considerable attention has been provoked to the
study of amorphous chalcogenides, specially amorphous
Ge_xSe_{1-x} system (R. Tronc et al., 1977 and Yoshimura et al.,
1978) because of their possibilities for numerous applica-
tions in areas such as optical storage, imaging, replica-
tion of patterns and phase holography (Goldschmidt et al.,
1977; Zembutsu et al., 1975; Terao et al., 1972). An
understanding of the properties of amorphous chalcogenides
requires a full knowledge of their structure. However, the

local structures of these chalcogenides have not been well
established. Attempts have been made for determining their
local structure (Bal and Chamberlain, 1978; Bletskan and
Gerasimenko, 1978; Kawamura et al., 1982). The Ge chalco-
genides, in particular the Ge_xSe_{1-x} system poses difficulty
as the bond lengths Ge-Ge, Ge-Se and Se-Se are not very
different and hence could not be resolved (Fawcett et al.,
1972). One could imagine, quite readily, that such a glass
is phase separated into $GeSe_2$ and GeSe. The $GeSe_2$ would
have four fold coordination of Ge by Se atoms and two fold
coordination of the Se atoms by Ge atoms, as in amorphous
SiO_2. The GeSe might have each atom coordinated by three
of the other species, as discussed by Bienenstock (1973b).
Alternatively, it might phase separate into $GeSe_2$ plus Ge,
so that all Ge atoms are four fold coordinated, instead of
some being three, and all the Se are twofold coordinated
by Ge. Another model considers the system as homogeneous
molecular Ge_2Se_3. Here, each Ge is coordinated by one Ge
and three Se's while each Se is coordinated by one Ge and
one Se. For Se rich alloys ($x \leqslant 0.3$) we can expect amorphous
Se structure to be maintained. The structural element of
Se lattice is an isosceles triangle (Richter, 1972). It
is determined by shortest atomic distances $r_1 = 2.32$ $\overset{\circ}{A}$
and $r_2 = 3.69$ $\overset{\circ}{A}$ within the screw chain of lattice. The
shortest chain distance is $r = 3.46$ $\overset{\circ}{A}$. In one of the

models suggested for Se rich alloys, this Se chain structure is maintained and Ge atoms act as chain crossing points (CCM model). In the other model (RCM) Ge atoms are allowed to bond to other Ge atoms as readily as the two fold coordinated Se atoms. Both of these models adequately describe the RDF (Fawcett et al., 1972). The diffraction methods thus met with several limitations. Now that EXAFS has emerged out as a powerful tool for the determination of local structures in amorphous systems (Gurman, 1982), it is therefore worthwhile to study the $Ge_x Se_{1-x}$ system using EXAFS.

In this thesis, we report our investigations on

a)   EXAFS associated with K X-ray absorption discontinuity in crystalline and amorphous germanium.

b)   EXAFS associated with the K X-ray absorption discontinuity of germanium in $Ge_x Se_{1-x}$ system (x = 0.1, 0.3).

c)   EXAFS associated with K X-ray absorption discontinuity of selenium in amorphous $Ge_x Se_{1-x}$ system (x = 0.1, 0.3).

d)   X-ray diffraction studies of amorphous Ge and $Ge_x Se_{1-x}$ (x = 0.1, 0.3).

e)   X-ray fluorescence studies of these materials.

Many theoretical difficulties are involved in analysing EXAFS data. Inspite of these difficulties the author has made a successful attempt to develop computer programs for the analysis of EXAFS data.

CHAPTER II

EXPERIMENTAL

2.1 Specimen Preparation

The amorphous chemical compounds $Ge_{0.1}Se_{0.9}$ and $Ge_{0.3}Se_{0.7}$ were prepared as per the following procedure. Appropriate amounts of constituent elements were mixed and sealed in a quartz tube under high vacuum. The elements used were of five nine purity. The bulk samples were obtained by melting, annealing and then quenching in air. Amorphous germanium was prepared, in the form of thin film, by evaporating five nine pure germanium in 10^{-6} Torr vacuum on aluminium substrate. The substrate temperature was $300^{O}K$.

The X-ray diffraction patterns of all the samples were recorded. The patterns showing a broad peak vanishing rapidly at high diffraction angle are typical of amorphous compounds. Figure 2.1 shows such a pattern obtained for $Ge_{0.1}Se_{0.9}$ which peaks about 15.5^{O} (2θ). Application of Debye formula (Klug and Alexander, 1954) for this pattern reveals that the average crystalline size in this sample is around $11 \overset{O}{A}$. The compositions of the constituent elements were confirmed by X-ray fluorescence analysis (sec. 2.5).

2.2 Experimental Procedure - EXAFS

The basic experiment involves the measurement of absorption coefficient, μ, as the X-ray photon energy is varied across, and beyond the K-absorption edge. The absorption coefficient is related to the logarithmic
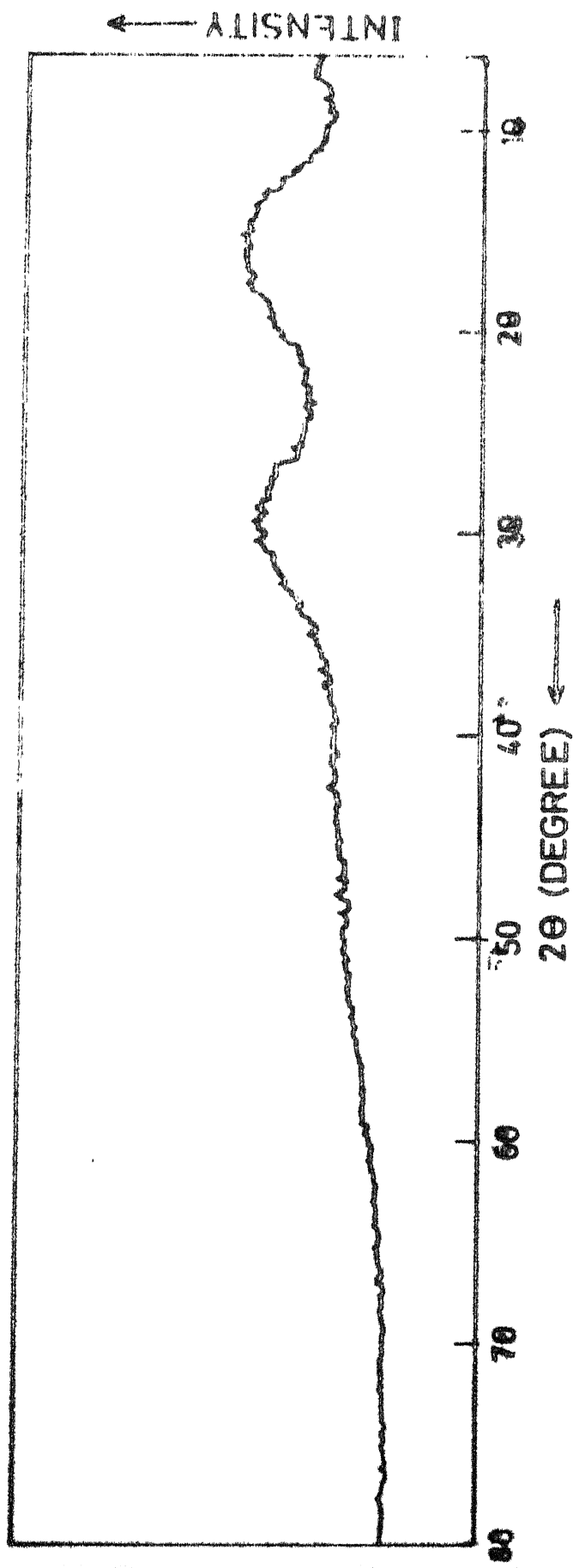
Fig.2.1 X-ray diffraction pattern of Ga.1Ge.9

ratio of the incident and transmitted intensities at a particular energy (or wavelength). Thus the experiment consists of basically the measurement of X-ray intensities as a function of photon energy. The following sections briefly describe the experimental procedure for EXAFS measurements.

2.2.1 Dispersion

Since X-ray absorption experiment involves detection of X-rays having different wavelengths, single crystals are invariably employed for separating out a particular wavelength. Crystal dispersion arrangements may be broadly classified as flat-crystal and curved crystal. Actually, curved crystals do not focus X-rays in the true optical sense, but diffract them in such a way that they converge to a line or a point. In our experimental set-up a flat-crystal arrangement has been used. A single crystal of LiF cut at its (200) plane (2d = 4.028 $\overset{\text{o}}{\text{A}}$) served as an analyser. X-rays incident at a glancing angle θ, only a particular wavelength given by Bragg's formula

$$2d \sin\theta = n\lambda \qquad (2.1)$$

are detected by the detector. The harmonic contribution would also be there, but being negligibly small compared to the first order, may be neglected.

2.2.2. Geometry of the experiment

Figure 2.2 shows the geometry of X-ray diffraction from the analysing crystal. Crystal is set in position A. For every wavelength a cone of divergent rays from the absorber intersects the crystal surface at range of angles. One of the rays is likely to intersect the crystal at the Bragg angle, as shown for the lower ray in the figure. The other ray is diffracted at the same point if the crystal is rocked. Each wavelength present undergoes the same phenomena at its own Bragg angle, as is diffracted to a different point on the spectrometer circle, resulting in the dispersion of the spectrum on the basis of wavelength. This flat crystal arrangement is called Bragg-Brentano parafocussing (Brentano and Landasy, 1954).

2.2.3 Spectral range

In principle, the largest wavelength which a crystal can diffract is equal to twice the interplaner spacing (2d) of the crystal planes parallel to its surface. For LiF (200) this limit is ~ 4.02 Å. The K-absorption wavelength corresponding to germanium (1.11652 Å) and selenium (0.97977 Å) lie well within this range. Knowing the absorption edges, the position 2θ on the goniometer circle is immediately ascertained by Bragg relation (2.1). The corresponding energy (E_o) of the photon is given by

$$E(eV) = 12398.52/\lambda \ (\overset{\circ}{A}) \tag{3.2}$$

FOCUSING CIRCLE

DETECTOR

CRYSTAL

θ

R

SPECTROMETER
CIRCLE
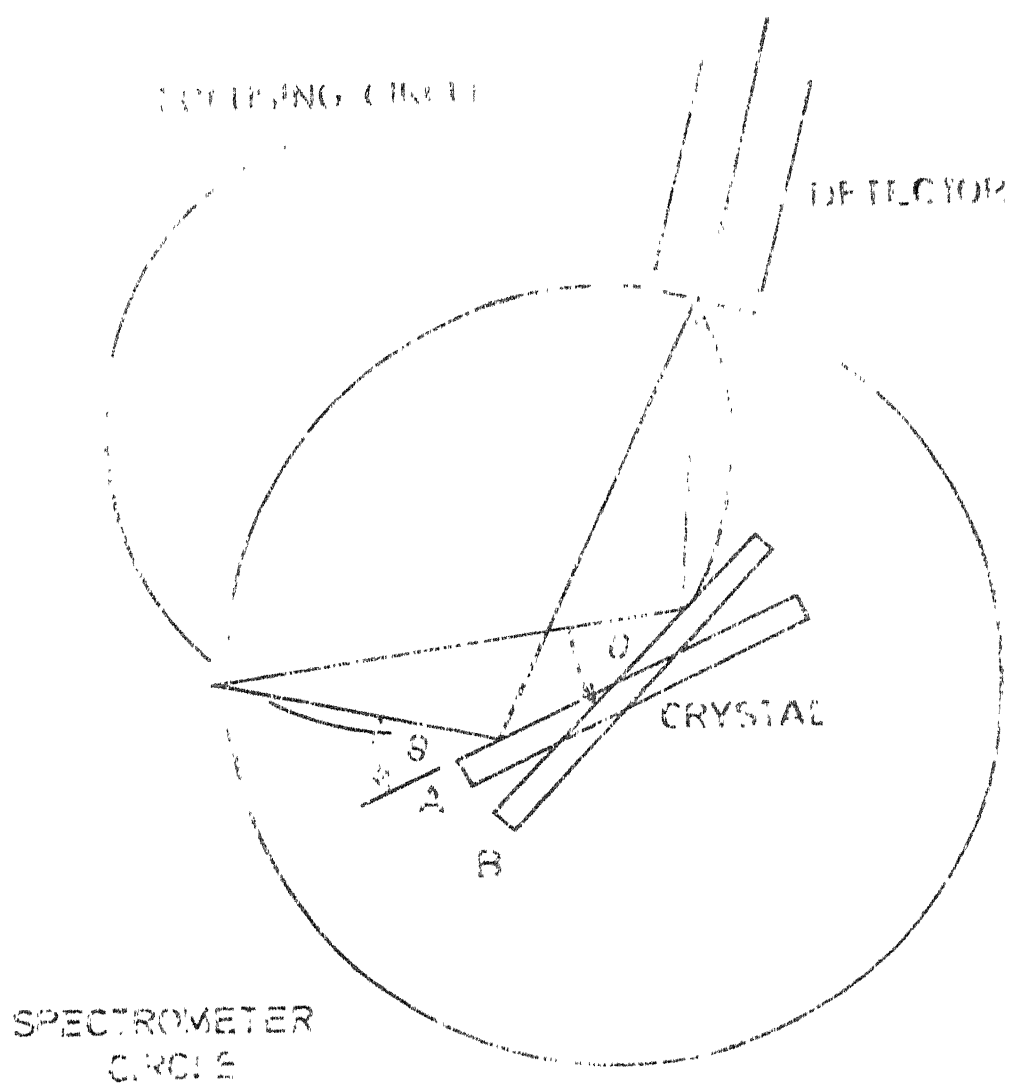
Figure 3 Bragg-Brentano parafocusing

The spectral range of interest for the K-absorption edge is about 1000 eV on high energy side and about 200 eV below on the low energy side of the edge. The corresponding wavelengths and Bragg angles can be calculated using relations (2.1) and (2.2). The range on 2θ scale for the K-absorption edge of germanium comes out to be 29.4° to 33.8°. The corresponding range for selenium K-absorption edge is 28.1° to 29.3°.

2.2.4 Preliminary adjustments

In the present investigation, a Seifert's X-ray spectrometer with auto-step scanning mechanism has been employed. At the centre of the goniometer of radius 17.5 cms is a stage which could be rotated, the axis of rotation being also the goniometer axis. The LiF crystal, after polishing, is mounted on this stage. X-rays from the sealed X-ray tube pass through entrance slit and are incident on the analysing crystal at Bragg angle θ. The width of the entrance slit can be adjusted to a desired size. A lead absorber was kept before the detector to avoid damage of detector when goniometer is in 0° position. The crystal holder at the centre was rotated slightly in such a way that maximum intensity is received at the detector. In this position half the beam is obstructed by the crystal and remaining passed parallel to its surface to the detector.

After this 0° adjustment, the spectrometer is said to be aligned.

The target of the sealed X-ray tube usually contain some impurities which produce emission lines at their respective Bragg angles. These impurity lines were used to redetermine the interplaner spacing (2d value) of the crystal. With the present adjustments the 2d value for LiF crystal using FeKα line turns out to be equal to 4.0262 $\overset{\circ}{A}$.

The X-ray beam, diffracted from the crystal, passes through another slit called the exit slit before it reaches the detector. The size of this exit slit determines smallest increment in 2θ and consequently the resolution. Resolution is different from the angular dispersion. The resolution or resolving power is defined as $\lambda/d\lambda$ or $E/\triangle E$. From (2.1)

$$2d\cos\theta \, \triangle\theta \; = \; n\triangle\lambda \qquad\qquad (2.3)$$

Using (2.2) and (2.3) it can easily be shown that

$$\triangle E \; = \; E\cot\theta \; \triangle\theta \qquad\qquad (2.4)$$

Thus for higher resolution, intensities should be measured at smallest possible increment $\triangle\theta$ and according to Rayleigh's criterion of resolution, the width of the exit-slit should have maximum $2\triangle\theta$ divergence. The

requirement of high photon flux in EXAFS experiment
constraints one from using an exit slit of very small
divergence. An exit slit of .05 mm width, which corres-
ponds approximately to 0.02^{O} divergence, was put before
the detector. This allows a minimum increment in 2θ
equal to 0.01^{O}. In case of K-edge of germanium, for
instance, $2\theta = 32.1^{O}$ and $E_{O} = 11104$ eV. Equation (2.4)
gives $\triangle E \sim 3.35$ eV.

2.2.5 Preparation of absorber

Because of the high absorption by all materials
to X-rays having energies close to their absorption edges,
the chief problem in experimental X-ray absorption spec-
troscopy is the preparation of homogeneous samples having
requisite uniform thickness, typically of the order of
few microns. Ideally nothing but the substance itself
should be placed in the path of X-ray beam. A convenient
method is to prepare the absorber in the form of uniform
thin film. In case of amorphous compounds $Ge_{0.1}Se_{0.9}$
and $Ge_{0.3}Se_{0.7}$ absorbers were prepared by spreading a
fine powder of the sample on an adhesive cellotape. The
homogenity of the absorber was tested by recording the
transmitted intensity through different parts of the
absorber (rotating the absorber). The fact that the
thickness of the absorber affects the fine structure has

been appreciated for quite some time. Since counter has been employed for measuring intensities, additional criterion is enforced by counting statistics. Assuming that the statistical precision of all the experimental points is the same, it was suggested (Parratt et al. 1957) that the thickness should be such that $I/I_O \sim 0.1$ where I and I_O are transmitted and incident intensities respectively. Thickness effect on EXAFS amplitudes has been recently discussed by Stern and Kim (1981). Significant distortion in EXAFS amplitudes occurs when $\Delta \mu_O x \gg 1.5$, where $\Delta \mu_O$ is the K-edge step in the absorption coefficient. In practice, however, the thickness of the absorber can not be controlled and several thicknesses of samples were tried before the final measurement was made.

2.2.6 Recording absorption spectra

After the preliminary adjustments discussed in section 2.3.4, the absorber was placed in the path of X-ray beam. It is generally believed that the absorber can be placed anywhere in the path of the X-ray beam. Actually it is better to place the absorber ahead of the crystal or near the detector so that any fluorescent radiation emitted by the absorber does not reach the detector. Both the positions were tried. Since the transmitted intensity from the absorber depends on the intensity of the beam incident on it, the placement of

absorber ahead of the crystal reduces the transmitted
intensity. Because of the requirement of high photon
flux, the absorber was finally placed near the source.

The spectral region to be scanned for a particular
K-absorption edge was calculated (section 2.3.3). The
detector was moved to the initial 2θ position. The
detector is either a proportional or a scintillation
counter. Since the fluorescence is generally completed
in 10^{-8} seconds, the recovery time of scintillation counter
is excellent. Counter signals are proportional to the
energy of X-ray photons in both counters. Scintillation
counter was preferred because the maximum useful count
rate, without substantial coincidence loss, for scintil-
lation counter (10^6 counts /sec.) is higher than that for
a proportional counter (10^5 counts/sec.).

The sealed X-ray tube with Cu-target was operated
at 50 KV, 30 mA to get the maximum possible intensity.
The intensity could be measured in either preset count
mode or preset time mode. To have equal statistical
precision for all experimental points, the intensities
were measured in preset count mode (10^5 counts). The
goniometer was operated in auto-step scanning mode. The
auto-reset and auto-print switches were in 'ON' position
and step-scanning was activated. The selector switch was

kept on 'external-pulse' position. The step in 2θ could
be adjusted within a range of $0.01°$ to $0.99°$. Since the
exit-slit of .05 mm was used at the detector, the lowest
step of $.01°$ in 2θ was adjusted. The print-pulse activates
the scanning motor, and the detector is advanced to next
2θ position with a specified step. The detector is locked
in this position till the next print command is executed,
giving the time for preset number of counts. The time T
with absorber in the path of the beam was printed on a
machine role. The scan was repeated without the absorber
to give T_o at each 2θ position. The intensity I_o may
change with time, however the change was found to be
within the statistical precision.

Knowledge of the start position and step size in
2θ allows calculation of X-ray wavelength for each data
pair (T, T_o) and the absorption μx can be calculated. The
total experimental data consisted of 350-450 data pairs.

An elementary computer program was developed which
incorporated i) calculation of the absorption μx according
to equation 3.1, wavelength and energy at each point,
ii) fitting a Victoreen curve of the form $A \lambda^3 + B \lambda^4$
to absorption data below the edge and iii) extrapolation
and subtraction of Victoreen curve from data above the
edge. The resulting data gives the contribution to
absorption exclusively due to K-shell.

2.3   Experimental Details - X-ray Diffraction

For the calculation of Radial Distribution Function (RDF), the experimental data consists of X-ray diffraction intensity from the sample normalized to electron units. Normally the powdered sample is prepared in a slid cavity of perspex which contributes to the measured X-ray diffraction intensity. For this reason experiment is performed in two steps involving measurement of intensity from substrate and sample mounted on substrate (slid cavity) separately. Following sections describe the experimental procedure briefly.

2.3.1   Geometry of the experiment

Geometry for recording the X-ray diffraction pattern is very similar to the one used in EXAFS experiment. Monochromatic X-ray beam, from X-ray tube with cu-target is obtained using a Ni filter. After passing through an entrance slit, beam is incident on the powder sample at glancing angle θ and the diffracted beam is received at the detector at an angle 2θ. Figure 2.3 illustrates schematically the geometry of the counter diffractometer.

The sample O is the flat-faced briquet of powder. Monochromatic radiation diverges from the entrance slit E, which is just a line focus on the target. The diffracted radiation is selected by a narrow receiving slit R. Distances
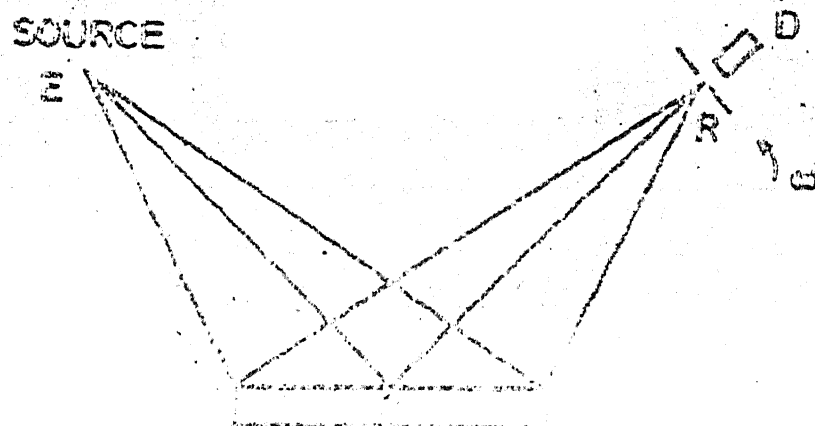
Figure 3. Schematic representation of the source and receiver as used for recording perfect pressure.

EO and OR are equal and since the sample face is maintained symmetrical with respect to the primary and diffracted beams, there is an approximate focussing condition. The radiation passed by the receiving slit (or the exit slit) is detected by the scintillation counter D. For recording the diffraction pattern the counter turns at an angular velocity ω and the sample turns at rate $\omega/2$ to maintain the focussing conditions.

2.3.2 Correction factors

The X-ray diffraction intensities measured in arbitrary units have to be corrected by various correction factors before being used in calculation of RDF. The major corrections arise due to the unpolarized beam used and the absorption in the sample. The other corrections are noise in the data, multiple scattering in the sample etc.

The characteristic radiation from X-ray tube is considered unpolarized (Bearden, 1928). But such a radiation after being scattered or diffracted is polarized, the amount of polarization depending on the angle through which it is scattered or diffracted. The true intensities are obtained after dividing by the polarization factor

$$P(\theta) = (1 + \cos^2 2\theta)/2$$

The other measure correction is due to the substrate scattering. Experimentally recorded intensity $I_{SC}(2\theta)$

constitute scattering from both the sample and the substrate. To separate out the contribution from substrate, experiment is repeated with sample removed from the substrate (intensity $I_C(2\theta)$). However $I_C(2\theta)$ does not represent the actual contribution from the substrate to $I_{SC}(2\theta)$ because of the absorption in sample.

Thus the actual experimental intensity from the sample is given by

$$I_{expt}(2\theta) = I_{SC}(2\theta) - I_C(2\theta) \cdot e^{-2\mu t cosec\theta} \qquad (2.5)$$

where μ is the absorption coefficient of the sample and t is the thickness of the sample.

2.3.3 Intensity measurement

The sample holder used in the experiment was made up of perspex. It was cleaned with acetone and was mounted on the stage at the centre of the goniometer. After the preliminary adjustments for aligning the diffractometer, the step was adjusted at 0.5^O in 2θ. The intensity was measured in preset time mode with time preset at 15 seconds. Step scanning is activated and intensity in arbitrary units (counts per 15 seconds) at each 2θ position equally spaced in 2θ is printed on machine role. The range was from 6° to about 130° in 2θ. The experiment was repeated with powder in the sample holder. The tube was operated at 30 KV, 20 mA.

2.4 Experimental Details - X-ray Fluorescence

When X-rays are absorbed within the sample, a bound electron is ejected from the atoms of the constituent elements. Electrons from higher levels jump into the newly created hole and emit X-ray photon of corresponding energy. This process is called X-ray fluorescence. The fluorescence spectra contains the emission lines of the constituent elements, the intensity of the peaks being proportional to the concentration.

The essential features of X-ray fluorescence crystal spectrometer are shown in figure 2.4. The experimental fluorescence spectra were taken on XRD-6 spectrometer of General Electric Co. with a fluorescence attachment. The primary X-ray beam from X-ray tube with tungsten target irradiates the specimen A held in some type of drawer B in the specimen compartment C. A lead shutter mechanism (not shown in figure) is provided to block the primary beam at X-ray tube window when specimen is inserted and removed from its compartment. The secondary radiation thus excited contains many wavelengths and is emitted in all directions. But only those rays directed substantially parallel to the foils of the solar collimator D emerge from specimen compartment and reach the angular crystal (LiF)E. Different wavelengths are detected at
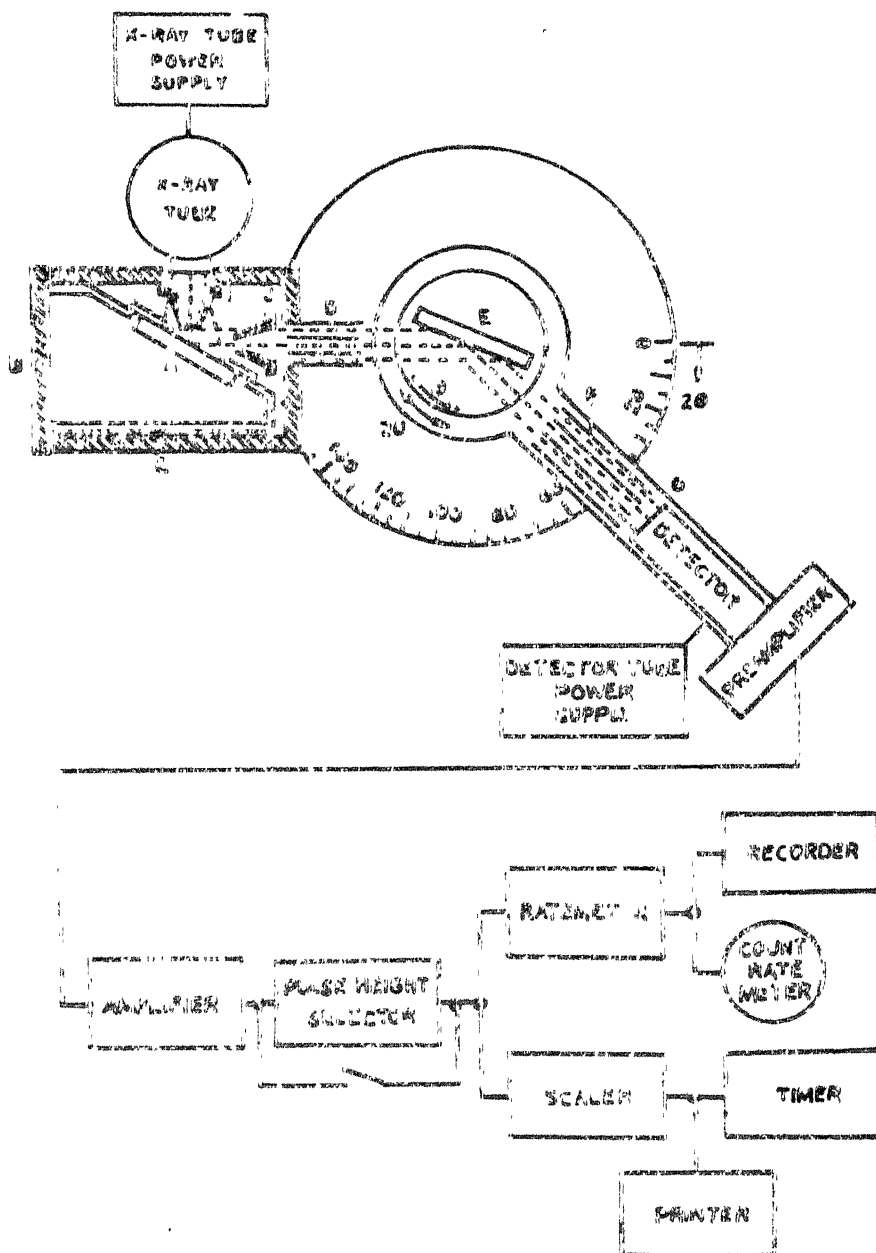
Fig.2.4 X-ray secondary emission (fluorescence) spectrometer.

different 2θ angles. The chart recorded with continuous scan (1.5^O per minute) gives peaks corresponding to the emission lines of the elements. The measurements on Ge_xSe_{1-x} system were used to confirm the concentration of constituent elements.

CHAPTER III

THEORY AND ANALYSIS OF EXAFS

3.1 Mechanism of X-ray Absorption

The experiment of Bragg and Bragg (1913), which demonstrated that X-rays could be reflected from crystal planes, laid the foundation of X-ray spectroscopy. The interaction of X-rays with matter results in a number of interesting phenomena, such as scattering, photoelectric absorption, radiation damage, pair production (in case of X-ray of energy greater than 1.02 MeV), secondary emission, Auger emission, etc. The analysis of the attenuation of X-ray intensity when X-rays penetrate through matter requires the segregation of various physical processes involved of which photoelectric absorption is usually the most important and is referred to as the true absorption.

When an X-ray beam passes through a medium the intensity of transmitted beam I is attenuated logarithmically (Azaroff, 1974). According to the classical equation, if the incident beam with intensity I_o has travelled a distance x, then the absorption coefficient μ_ℓ will be given by

$$\mu_\ell = -\frac{1}{x} \ln(\frac{I}{I_o}) \qquad (3.1)$$

It follows from the above equation that dimensions of μ_ℓ are reciprocal centimeters so that it represents the attenuation of the beam per unit length travelled and is called the linear absorption coefficient. It turns out to depend on the energy (or wavelength) of the X-rays.

Calculation of the linear absorption coefficient is complicated by this last fact so that it is convenient to define a mass absorption coefficient

$$\mu_m = \mu/\rho \qquad (3.2)$$

where ρ is the density of the absorbing medium, μ_m is the cross-section of the mass unit.

The variation of the mass absorption coefficient with the wavelength λ in $\mathring{A}$ (10^{-8} cm) is shown in Fig. 3.1. It is evident from the figure that as the wavelength of the transmitted X-rays increases, the photoelectric absorption increases as λ^3 until a critical wavelength is reached. For wavelengths larger than the critical wavelength at the absorption edge, incident X-rays have insufficient energy to knock out a particular kind of bound electron in the atom, and photoelectric ejection of such electrons no longer contributes to the absorption process. The absorption edges in Fig. 3.1 are called K, L_I, L_{II} and L_{III} edges respectively according to the inner electron whose binding energy equals the energy at the absorption edge. Following the photoelectric ejection of an inner electron, the excited atom typically emits an X-ray photon, as an outer electron falls into the newly created hole, and this phenomenon is termed X-ray fluorescence.
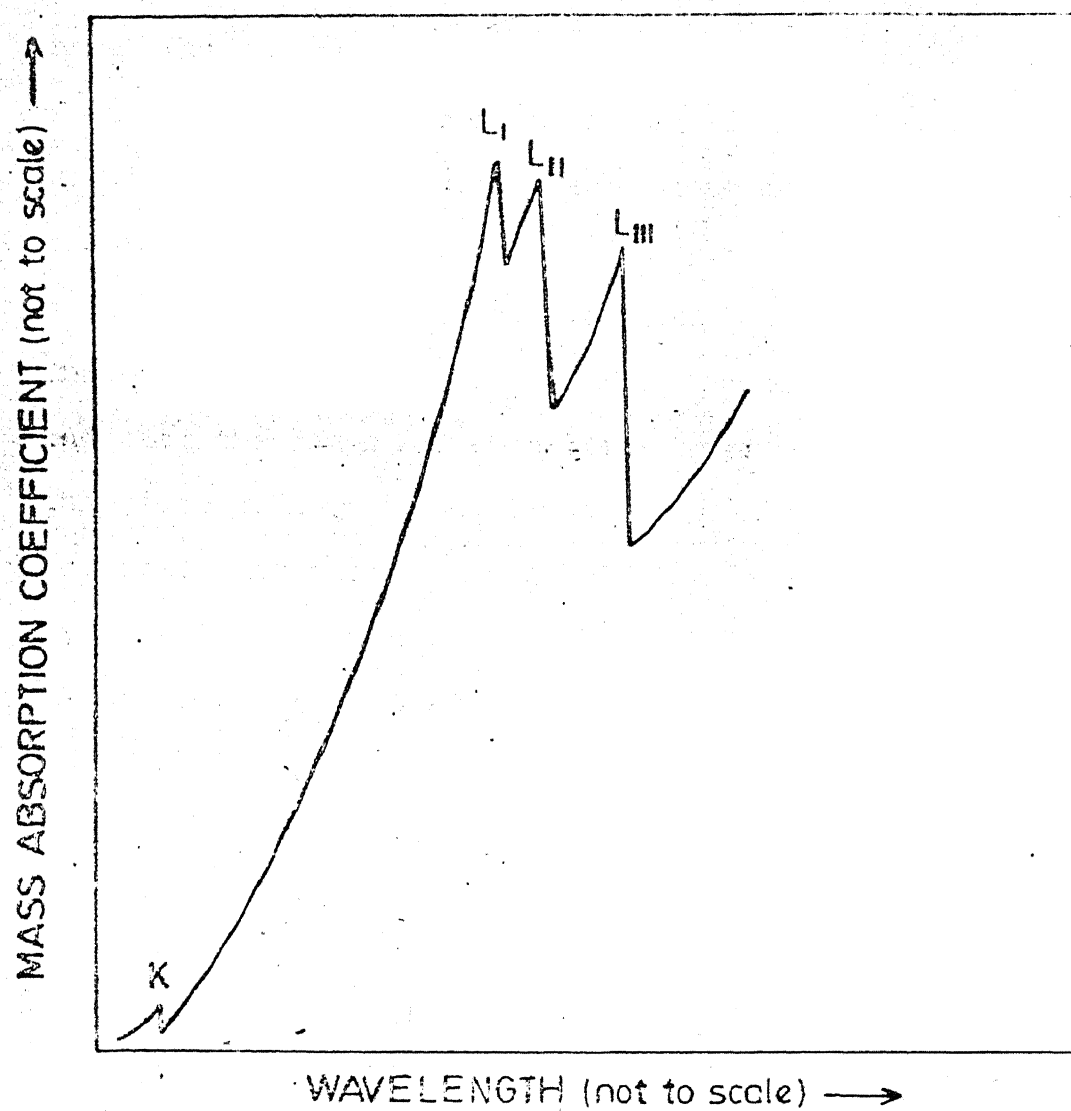
Fig. 3.1 Schematic illustration of the variation of the mass absorption coefficient with wavelength.

3.2   Extended X-ray Absorption Fine Structure (EXAFS)

When the horizontal range in Fig. 3.1 is expanded,
the saw-toothed character of an absorption edge is replaced
by a fine structure that extends to about hundreds of
electron volts on the high energy side (or low wavelength)
of the main edge. This is termed as the Extended X-ray
Absorption Fine Structure (EXAFS). Absorption process
refers to the transition of a bound electron to some
unoccupied final state. The fine structure appearing at
and near the observed absorption edge (within a few eV)
therefore reflects the distribution of unoccupied states
for absorbing atom. As is well known, proximity of other
atoms modifies such quantum states and their relative
densities, so that EXAFS can be utilised in their study.
This fine structure was previously observed (Kronig, 1931)
only for crystalline substances but later it was observed
for nearly all types of materials. This was first explained
by Kronig (1931) for crystalline absorbers.

3.3   Theories of EXAFS

The first theory explaining the fine structure
was proposed by Kronig (1931). According to his theory,
the origin of fine structure is ascribed to the zone
structure of energy levels of the electrons in the crystal
which is the periodic field in the crystal. The X-rays

are absorbed by electrons which make transitions from X-ray
levels to empty levels lying above the Fermi surface. These
empty levels are grouped into zones and there exist forbidden
and allowed bands. Because the absorption coefficient is
proportional to the product of transition probability and
the density of states, a fine structure occurs. In his
theory variation of transition probability was neglected
and the fine structure was explained mainly by the electronic
state density. For the structure of gas molecules he computed
(Kronig, 1932) the fluctuation of absorption coefficient
caused by the variation of the state function of the final
state of the transition. He assumed that final state is
sum of the plane waves of photoelectron and the scattered
waves.

Peterson (1933) applied this theory to explain
absorption curve of chlorine but subsequent experimental
measurements by Lindh and Nilson (1943) deviated appreciably
from his theoretical calculations. Also measurements on
$GeCl_4$ (Shaw, 1946; Stephenson, 1947; Glaser, 1951) did not
agree with the predictions of Hartree et al. (1934).

After failure of Kronig's theory to explain "general
features" of the absorption curves of all materials,
Kostarev (1941, 1949, 1951) presented a more general theory
based on consideration of nearest neighbour atoms which
could explain absorption edge structure of $GeCl_4$ (Hartree et al.

1934). The gist of Kostarev's argument is that the ratio $\chi(k)$ is determined by transition probabilities from initial K state to the final F state according to

$$\chi(k) \;=\; \frac{|\bar{P}_{KF}|^2}{|\bar{P}_{KF}|^2_{\text{free atom}}}$$

and is independent of variations in the density of states underlying Kronig's theory for solids.

A different interpretation was offered by Hayasi (1949) who suggested that the maxima are superimposed on free atom curve and they are additive. Shiraiwa et al. (1958) considered the life time of the state of the electron ejected by absorption of photon in analysing the original Kronig's theory. Assuming that the density of states varies as $E^{1/2}$, where E is the energy of photon, they concluded that the absorption coefficient

$$\chi(k) \propto E^{1/2} P(E)$$

where P(E) is the transition probability.

It is possible to distinguish these theories from early Kronig's theory by realising that Kronig's theory (also Hayasi's) is based on the existence of long range order (lro) in a crystal whereas other theories consider only the nearest neighbour atoms, i.e., the short range order (sro). This makes sro theories more general in that

they are applicable to amorphous solids and gases as well whereas lro exists only in crystals.

Lytle (1963) began measurements with the initial goal of extending Hanawalts temperature effect to cryogenic temperatures (Hanawalt, 1931) to sharpen the fine structure as well as improving and automating the instrumentation (Lytle, 1966) so that high quality of the data could be obtained. Although his theory bears certain similarity to the Hayasi theory, it was successful in extracting accurate first neighbour distances from fine structure data.

Sayers et al. (1970) have reported improved measurements and theory of EXAFS. Over past few years considerable improvement in the theoretical understanding of EXAFS has occurred. Theories of EXAFS (Stern, 1974; Ashley and Doniach, 1975; Lee and Pendry, 1975) based on the single scattering of an ejected photoelectron by atoms in coordination shells surrounding the absorbing atom give an expression for normalised EXAFS $\chi(k)$ as

$$\chi(k) = \sum_j A_j(k) \sin(2kr_j + \phi_j(k)) \qquad (3.3)$$

where the summation extends over j coordination shells, r_j is the radial distance from the central absorbing atom to atoms in the jth coordination sphere and $\phi_j(k)$ is a total phase shift due to interaction of the photoelectron with central atom potential and scattering from atoms in the jth

3-20, Ramnagar Society
Behind Mehsananagar Society
Chhani Road, Vadodara - 390002
GUJRAT

DR. Chandan Singh
Maths, Stat & Computer Group
R. & D Centre
Jyoti Ltd.
Vadodara - 390003
GUJRAT.

$$A_j(k) = (N_j/k.r_j^2)F_j(k) \exp(-2\sigma_j^2 k^2) \qquad (3.5)$$

where N_j is the number of atoms in the jth shell and σ_j is the root mean square deviation of the interatomic distance about r_j which may contain both static and temperature effects. The amplitude factor, $F_j(k)$ accounting for elastic electron backscattering amplitude $f(\pi,k)$ and inelastic effect is

$$F_j(k) = f(\pi,k) \exp(-2r_j/\lambda) \qquad (3.6)$$

λ being the inelastic mean free path. $f(\pi,k)$ is the EXAFS electron backscattering form factor and is a function of the type of scattering atom.

The exponential term $e^{-2\sigma^2 k^2}$ accounts for the effect of lattice vibration and disorder which was first discussed by Schmit (1961) and treated more completely by Beni and Platzman (1976). This EXAFS Debye-Waller factor differs

from the Debye-Waller factor for X-ray diffraction in an interesting way. It is the mean square average of the difference of displacements and may, in general, be different from the mean square displacement. The Debye-Waller factor has been extracted by studying the temperature and the k^2 dependence of the logarithm of the ratio of EXAFS amplitudes (Stern et al., 1975).

The exponential term containing mean free path accounts for the inelastic losses in the medium. This effect is further dealt with in the following sections.

Knowledge of backscattering amplitude and the phase shift due to scattering from atoms in the coordination shell is essential in comparing the experimental EXAFS with expression 3.3. There have been several earlier attempts and ab initio calculations of amplitude and phase shift by Hartree-Fock (HF) method (Lee and Pendry, 1975; Kincaid and Eisenberger, 1975; Pettifer and McMilan, 1977) and by Hartree-Fock-Slater (HFS) (Ashley and Doniach, 1975; Lagarde, 1976). Neither scheme provided very satisfactory results. What is needed is a relatively simple scheme which interpolates between the low energy region where HFS method has been tested, and the high energy region where HF approach is expected to be more reasonable. Such a scheme based on the local density functional formalism was introduced by Lee and Beni (1977). Teo and Lee (1979)

have calculated amplitude and phase functions for nearly
half of the elements in the periodic table using an
electron-atom scattering theory of Lee and Beni (1977).
These values have been used in the analysis and found
to give satisfactory results (Shulman, et al. 1978;
Teo et al., 1977; Lee et al., 1977, Teo et al., 1978a,
1978b).

3.4 EXAFS Analysis

One of the earliest attempts of successful extrac-
tion of structural parameters from the EXAFS data was based
on the Fourier transform of the data expressed in momentum
space (Sayers et al., 1971). The absolute value of the
transform was found to peak at distances shifted from known
values by several tenths of $\overset{o}{A}$. When corrected for these
shifts using systems with known distances, bond lengths
could be extracted. However, this method is not very
accurate because the peak value of the Fourier transform
depends in general on such factors as the weighting of the
data and the choice of the threshold energy E_o and because
the phase shift $\phi_j(k)$, which is largely responsible for the
shifted Fourier peak, is not a linear function of k.
Citrin et al., (1976) extracted the phase function $\psi_j(k)$
by direct curve fitting to eqn. 3.3 to show that these
functions could be transferred to other simple systems to

extract bond lengths with an accuracy 0.01 $\overset{o}{A}$ to 0.02 $\overset{o}{A}$.
This approach, however, is not generally applicable to
systems of more than one principle distance. The two
methods of Fourier transform and curve fitting have been
combined to analyze more complicated systems. Following
sections provide a relatively detailed account of the
Fourier transform filtering method which has been used
in the present investigation.

3.4.1 Extraction and normalization of EXAFS

The removal of oscillatory part (EXAFS) of the X-ray
absorption coefficient from the smooth monotonically decrea-
sing background is the most difficult problem as the smooth
absorption of an isolated atom $\mu_o(k)$ is not generally
available experimentally, and the present theoretical
calculations of $\mu_o(k)$ are not sufficiently accurate for
most EXAFS work, (nearly .01%). There are several background
removal methods that could be tried such as simple polynomial
fit over the whole range of data, iterative low order poly-
nomial fitting combined with fitting EXAFS, orthogonal poly-
nomial fitting, Fourier transform, extrapolation of an assumed
functional form of the background from below the absorption
edge and the most flexible cubic spline fitting. In our
analysis the EXAFS signal was separated from low frequency
background and high frequency noise by Fourier filtering

technique (Lytle et al. 1975). A sixth order polynomial fitted to the data (EXAFS + background) over the whole range approximated $\mu_0(k)$ and used to obtain the normalized EXAFS.

3.4.2 Fourier transform filtering

The next step in the analysis is a Fourier transform. To perform the Fourier transform, the data must be transformed from the energy to wave number k-space. The transformation is given by

$$\hbar^2 k^2 / 2m = E - E_0 \qquad (3.7)$$

where E is the energy of the X-ray photon and E_0 is the "inner potential" caused by the atomic potentials and represents the "zero" above which kinetic energy must be added to determine the total energy E. In metals at low energy, E_0 can be approximated by Fermi energy, but at higher energies (> 30 eV or so) this is no longer true, since the exchange and correlation energies go to zero in a complicated way with increasing energy, and the pseudopotential of the ion core is energy dependent.

Several workers have fixed E_0 arbitrarily at a special feature in the spectra such as a point of inflexion (Hayes et al.,1976 ; Cramer et al., 1978). The effect of the choice of E_0 and its determination are discussed in the later part of the chapter.

To make the Fourier transform less sensitive to the choice of E_O , the normalized EXAFS is multiplied by k^3 and then Fourier transformed. The k^3 multiplication has the effect of weighting the EXAFS oscillations more uniformly over the range of data ($k > 4\overset{O}{A}{}^{-1}$) and also assures that the chemical effects on EXAFS information, which are most significant at small k are effectively cut off. The magnitude of Fourier transform peaks at several distances shifted towards origin by an average slope of phase shift $\phi(k)$.

The first shell contribution to EXAFS can be isolated by applying a smooth filter window function. Both the real and imaginary parts of Fourier spectrum are filtered identically so that the phase error is minimised. The essential feature of a good filter window function is that it does not produce gross distortions in the data and almost any smoothly varying function satisfies this requirement. The first shell EXAFS can be decomposed into amplitude and phase functions using the Fourier transform method (Shulman et al., 1978).

3.4.3 Empirical phase shifts and chemical transferability

The argument of sine function in eqn. 3.3 is $\psi_j(k) = 2\ kr_j + \phi_j(k)$ which can be obtained experimentally for a model system. At sufficiently high photoelectron kinetic energies, typically above 50 eV where EXAFS

scattering processes are dominated by core electrons, phase shifts are insensitive to chemical environment. This is the principle underlying the concept of chemical transferability in which it is assumed that the phase shift ϕ_j in the case of model system is the same as that in the case of the unknown system. Determination of $\psi_j(k)$ for an atom pair in a given model system of known distance r_j^m enables the determination of distance r_j^u in an "unknown" (different) system containing the same atom pair as is evident from the following.

For the model system, the phase function is

$$\psi^m(k) = 2kr^m + \phi(k)$$

where $\phi(k)$ is the scattering phase shift defined earlier.

For the unknown system containing the same atom pair

$$\psi^u(k') = 2k'r^u + \phi(k)$$

using the concept of transferability of phase shift. The wave vector k' for unknown system is not, in general, same as k of the model due to the chemical shifts, i.e., because of the change in the threshold E_o.

The plot of $\psi^m(k) - \psi^u(k')$ as a function of k should be a straight line with zero intercept and slope

equal to $2(r^m - r^u)$. E_o is varied in such a fashion so as to reduce the intercept of the line to minimum. A closely related analysis method of varying E_o until the "slope" remains constant over a large range of k has been used successfully by Martens et al. (1978).

Another flexible method which has been used in our analysis, of determining E_o and r simultaneously, is the least square fitting the experimental phase shift $\phi(k)$ with the theoretical phase shift (Teo and Lee, 1979). Since $\phi(k) = \psi(k) - 2kr$,

$$\Delta_r \phi = 2k \Delta r$$

Thus changes in r affect $\phi(k)$ mainly at higher k values. Also $\Delta_k \phi = 0.263 \, \Delta E_o / k$ indicates that changes in E_o affects only at lower k values. Thus it is not possible to produce an artificially good fit by adjusting E_o with a wrong distance r. This method has been widely used and the nearest neighbour distances could be determined to within 0.03 $\overset{o}{A}$ (Reed et al., 1977, 1978; Teo et al., 1978a, 1978b).

3.4.4 Amplitude transferability

The amplitude function obtained after decomposition of first shell EXAFS contains information about the coordination number, the kind of atoms involved, the amount of

disorder and the effective photoelectron mean free path.
In principle, it is possible to obtain all these para-
meters by the direct method of curve fitting. But in
practice, the experimental amplitude is usually off by
$\sim 50\%$. This discrepancy is expected to be somewhat
sensitive to the chemical environment and will depend
on distance r_j (due to an exponential factor $e^{-2r_j/\lambda}$).
Moreover, reduction in amplitude is due to the many body
effects (Stern et al., 1980) which are not considered in
the theory. The EXAFS amplitude is also affected by thick-
ness and non-uniformity of the absorber (Stern and Kim, 1981).
Because of these reasons and the strong correlation between
the various parameters determining the amplitude function,
the curve fitting technique is not suitable.

Analogous to the chemical transferability of phase
shifts, in principle, it is possible to extract these
quantities assuming chemical transferability of amplitudes,
i.e., using model compounds as standard for unknown systems.
For a single shell containing N identical atoms, the
amplitude function is given by

$$A(k) \;=\; \frac{N}{kr^2} \, F(k) \, e^{-2\sigma^2 k^2} \, e^{-2r/\lambda(k)} \qquad (3.8)$$

Denoting the model and unknown systems by m and u
respectively, the logarithm of their ratio gives

$$\ln\left[\frac{A_m(k)}{A_u(k)}\right] = \ln\left[\frac{N_m}{N_u} \cdot \frac{R_u^2}{R_m^2}\right] + 2k^2\left[\sigma_u^2 - \sigma_m^2\right] + 2\left[\frac{R_u}{\lambda_u(k)} - \frac{R_m}{\lambda_m(k)}\right]$$

$$\dots\dots (3.9)$$

If it is assumed that $\lambda_u(k) \approx \lambda_m(k)$ and $(r_u - r_m) \ll \lambda(k)$, then the third term becomes negligible and the parameters of the straight line obtained by plotting the logarithmic ratios of the amplitude versus k^2 enable the evaluation of N_u and σ_u. A similar analysis could be used for determining N_j for different shells.

There are several difficulties that can be encountered with this approach. The first involves empirical determination of $A(k)$. The finite value of k_{max} (the maximum value of k) affects the magnitude of the Fourier transform and in turn affects the amplitude function than its phase. Another factor is the relative mean free path of the two systems. Differences as little as 1-2 A^o at a given k are actually non-negligible because of the logarithmic form of the above equation (Citrin et al., 1979). This problem has also been discussed by Eisenberger and Lengeler (1980) and Stern et al. (1980).

CHAPTER IV

CRYSTALLINE AND AMORPHOUS GERMANIUM

4.1 Introduction

In this chapter are presented the results on crystalline and amorphous germanium. Both crystalline and amorphous germanium have been studied before with X-ray diffraction (Shevchik and Paul, 1972; Temkin et al., 197?) and EXAFS (Sayers et al., 1971, 1972; Crozier and Seary, 1981). Earlier work of Sayers et al. (1972) demonstrated that EXAFS could provide quantitative information regarding the local structure around the absorbing atom. In view of the progress made in theoretical aspects and data analysis procedures in the last decade, it is worthwhile to study crystalline and amorphous germanium with EXAFS. Experimental data on crystalline germanium (c-Ge), which serves as model system in the analysis of amorphous germanium (a-Ge), has been used to standardize the analysis procedure. Although information about second and higher coordination shells is important in distinguishing different structural models for disordered systems, first shell parameters provide a useful aid. The different data analysis procedure for near neighbour distance determination, in particular, have been examined.

4.2 Elementary Analysis

The absorption μx as a function of incident X-ray phton energy for K-absorption discontinuity in c-Ge is

depicted in figure 4.1. The abrupt change in the absorption
near the absorption edge around 11 KeV amounts to nearly 1.5.
A sharp peak in the vicinity of edge on the high energy side
is the white line (WL). It may be compared with the earlier
work of Lytle et al. (1975). The broadening of the white
line observed may be attributed to the scattering effects
and relatively higher thickness of the absorber (Agrawal,
1979). The broad peaks after the WL vanishing far above
the edge are due to EXAFS which are clearly visible in the
figure. The slowly decreasing absorption on the low energy
side of the absorption edge is due to the substrate and any
other contribution resulting from the other bound electrons
in the atom. This was approximated by a Victoreen curve of
the form $A\lambda^3 + B\lambda^4$ with A = 0.349; B = 0.0124 (shown by
dashed curve in figure 4.2(a)). The contribution to absorp-
tion exclusively due to K shell was obtained by extrapolating
and subtracting this curve from the data on the high energy
side.

The wave vector at every point above the edge $(> 60$ eV)
was calculated using the equation 3.4. The value of energy
at which the kinetic energy of the photoelectron is zero
was obtained by comparing the slopes of the absorption edge
at every point on it. The average of the energy of the point
at which the slope starts decreasing and that of the prece-
eding point was chosen as the zero point energy ($E_o = o$).
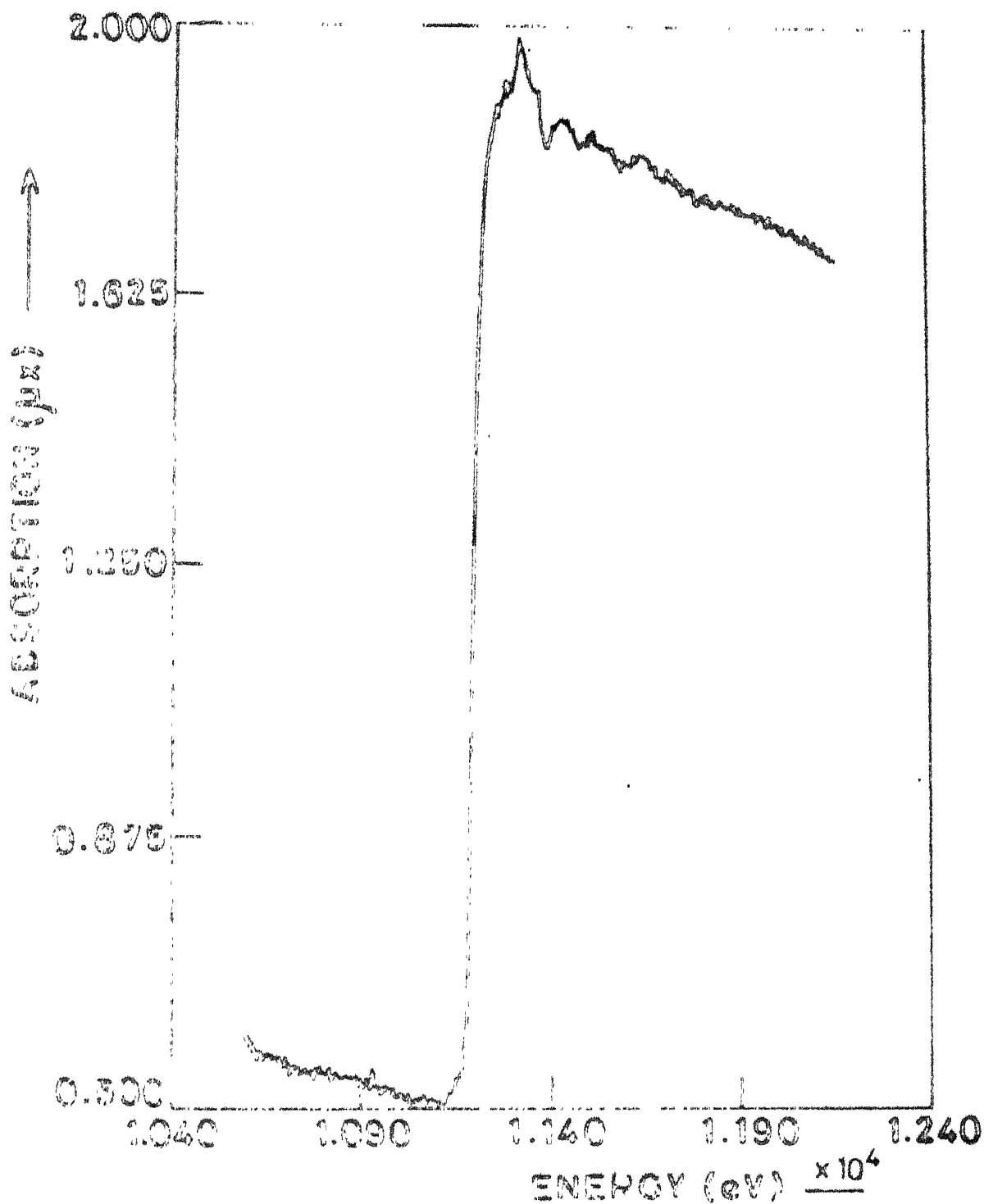
Fig.4.1 X-ray absorption spectrum of crystalline germanium, sharp rise in absorption μx near 11 KeV is the K edge and oscillations above the edge is EXAFS

This approximately corresponds to the inflection point of the edge (11129 eV). Since the wave vector is non linearly connected with the Bragg angle θ, the k values are not, equally spaced. A quadratic interpolation programme (see Appendix I) has been used to interpolate the data onto a grid of equally spaced k values ($\triangle k \sim 0.02 \text{ Å}^{-1}$). The resulting data now serves as input to the Fourier transform routine in the next step of analysis.

4.3 Removal of Free Atom Absorption $\mu_o(k)$ and Normalization

One of the most difficult problems in the EXAFS analysis is the removal of background and the normalization of EXAFS oscillations to per atom scale. Direct Fourier transform of the raw data after adding zeroes from 0 to k_{min} and from k_{min} to about 12π indicated that the background frequencies. (low frequencies) extend to the intermediate EXAFS frequencies. The EXAFS frequencies could be easily estimated because the first shell radius for crystalline germanium is known to be equal to 2.45 Å. Therefore all the Fourier coefficient (a_n's and b_n's) corresponding to r values greater than ~ 1.8 Å. to about 7 Å represent the EXAFS signal. A sixth order polynomial in wave vector k, which also approximates $\mu_o(k)$ was fitted to the data (EXAFS + background). Fourier transform after separating $\mu_o(k)$ gives EXAFS frequencies well separated from the low frequency background. EXAFS in k-space was obtained by performing an inverse Fourier

transform (IFT) after removing low frequencies corresponding
to any residual background and the high frequencies corres-
ponding to r greater than 7 $\overset{o}{A}$ representing noise. This was
then normalized to per atom scale using the polynomial fit
($\mu_o(k)$).

Figure 4.2(b) shows the resulting normalized EXAFS
$\chi(k)$. As is evident from the figure, EXAFS peaks around
3 $\overset{o}{A}{}^{-1}$ and decays at high k-values almost exponentially.
Relatively high value at low k is due to the distortions
produced in the process of extraction and normalization
of EXAFS and such distortions are not desirable for further
analysis. The difficulty is resolved by multiplying $\chi(k)$
with a Hanning window function (Bergland, 1969) defined as

$$\frac{1}{2}\left\{ 1 - \cos 2\pi (k - k_{min})/(k_{max} - k_{min}) \right\}$$

This function has been used in the region of k-values
corresponding to the first and last 10% of the range investi-
gated. As a result $\chi(k)$ is forced to assume a half cosine
bell shape terminating at k_{min} and k_{max} (Lytle et al. 1980).

4.4 Fourier Transform Filtering

The normalized EXAFS thus extracted is, in principle,
capable of giving the local structure parameters such as
radii of different coordination shells, corresponding coor-
dination numbers and the disorder parameters σ_j^2 etc. by the
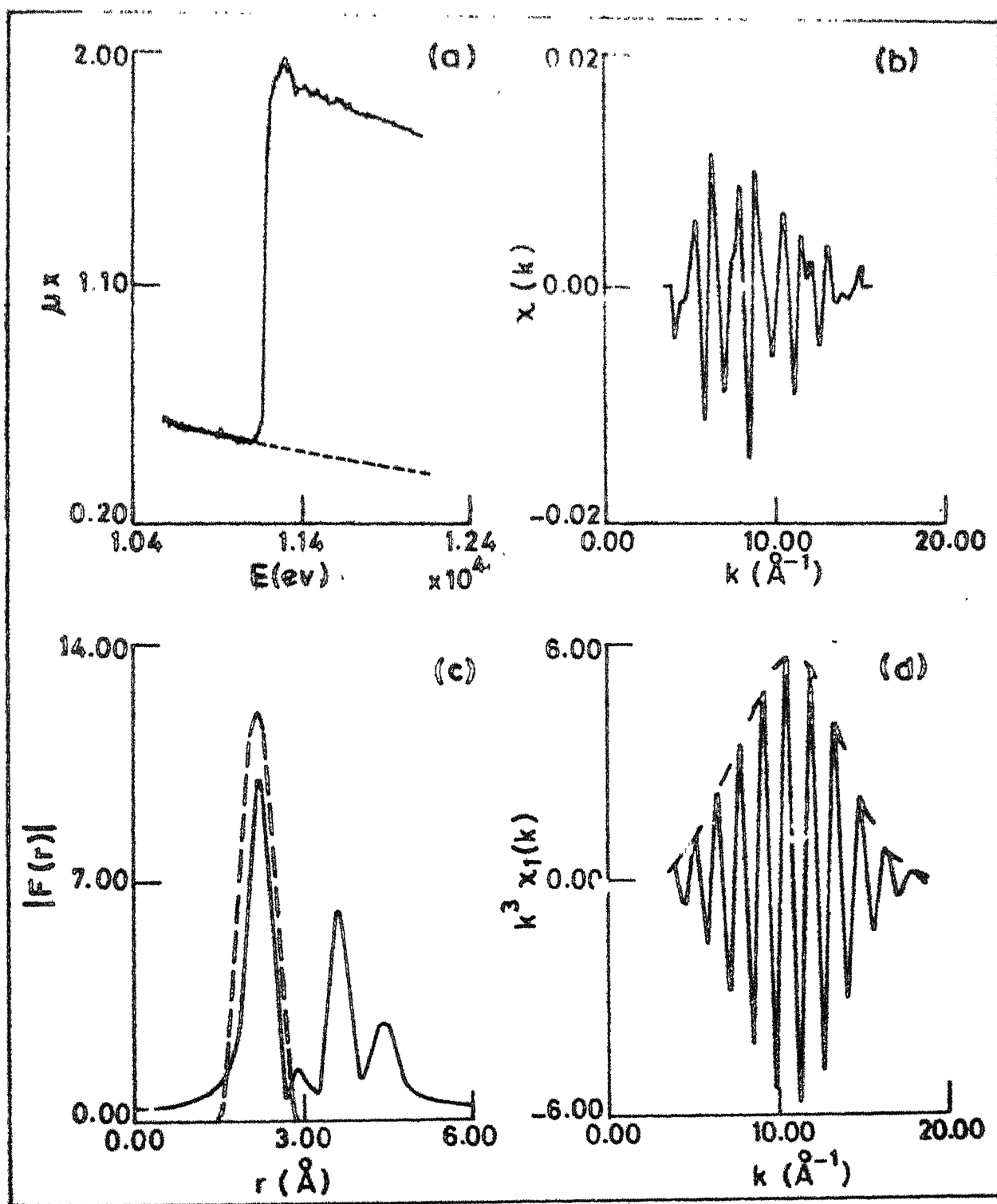
Fig.4.2 a) Absorption spectrum of c-Ge as in Fig.4.1. The dashed curve is Victoreen curve 0.349 λ^3+0.012 λ^4. b) Normalised EXAFS $\chi(k)$ extracted from (a). c) Magnitude of Fourier transform $k^3 \chi(k)$. The dashed curve is the filtering window and d) First shell EXAFS $k^3 \chi_1(k)$. The dashed curve is the amplitude function $k^3 A_1(k)$.

method of least squares fit using equation 3.3. However
the list of parameters is so large that such a least squares
minimization is practically not possible. Another flexible
method briefly described in the previous chapter, namely
the Fourier transform filtering, has been employed here.

Figure 4.2(c) shows the magnitude of Fourier transform
(FT) of $k^3 \chi(k)$. The k^3 weighting of the EXAFS data approxi-
mately equalizes the amplitude over the whole range and
weighs the data at large k values properly. This further
makes the position of the peaks in the FT less sensitive
to the choice of E_o. Recently it has been shown (Stearns,
1982) that at a particular choice of E_o the phase shift
$\phi(k)$ is linear and the position of peak in the FT is
independent of the weighting factor (k, k^3, k^5). This will
be discussed later.

The first large peak is observed at 2.27 $\overset{o}{A}$ and
corresponds to the contribution of the first coordination
shell to EXAFS. The other prominent peaks correspond to
the higher coordination shells. Structure beyond 6 $\overset{o}{A}$ is
not visible as it was filtered out during the extraction
of EXAFS. The dashed curve encompassing the first peak
is the smooth filtering window which was used to separate
out the first shell EXAFS. The resulting first shell
EXAFS, $k^3 \chi_1(k)$ obtained after performing IFT is shown
in figure 4.2(d). If before performing IFT, the coefficients

corresponding to the negative r-values were removed, the resulting inverse transform would be a complex quantity (see Appendix II) from which the amplitude and phase functions could be readily evaluated. The amplitude function $k^3 A_1(k)$ obtained in such a way is shown by the dashed envelope in figure 4.2(d). The phase function $\psi_1(k) = 2kr_1 + \phi_1(k)$ is shown in figure 4.3. As $\Phi_1(k)$ is very small compared to the factor $2kr_1$, the curve $\psi_1(k)$ is almost a straight line with slope equal to $2(r_1 - \alpha)$ where α is called the bonding parameter ($\phi(k) = -2\alpha k + \beta$). The peak in the FT is shifted by an amount α towards the origin. The least squares straight line fit gives value of $\alpha = 0.19 \overset{O}{A}$ using the known value of $r_1 = 2.45 \overset{O}{A}$. This may be compared with the earlier work of Lytle et al.(1975) where the value of α is equal to $0.24 \overset{O}{A}$. The discrepancy is due to the value assigned to E_o. Change in value of E_o changes the position of the peak in FT and subsequently the value of α obtained. Thus any physical significance to α could be assigned only when certain criterion for the choice of E_o is fixed.

4.5 Linear Phase Shifts and Bond Length Determination

As noted earlier the weighing of the EXAFS data reduces the sensitivity of position of the peak in the magnitude of FT on the choice of E_o. The fact that the
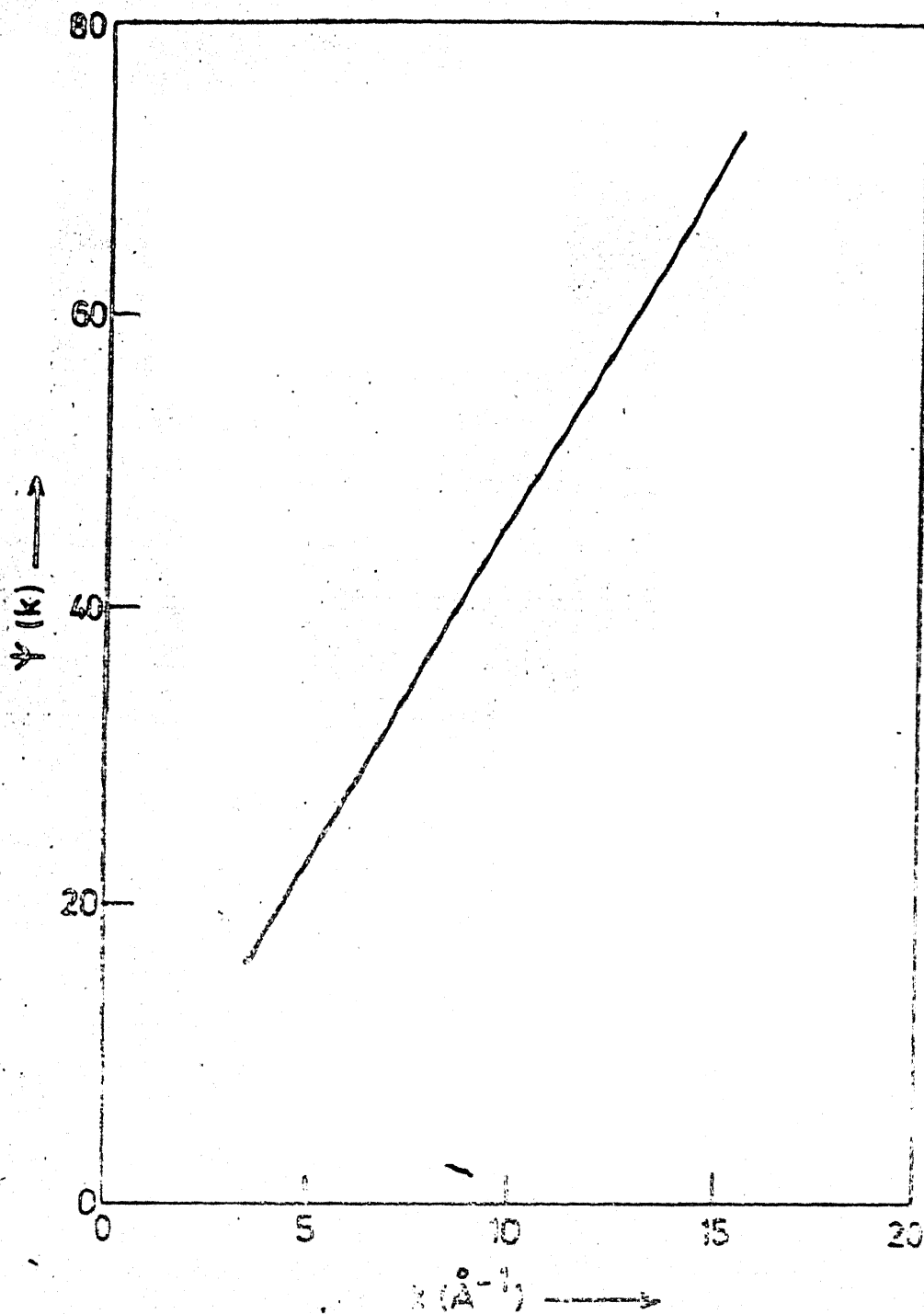
Fig. 4.3 The phase function $\psi_1(k) = 2kr_1 + \phi_1(k)$ derived from Fig. 6.3(d) as explained in the text.

peak position depends on the weighting factor as well as on the choice of E_O has been posing a problem in determining the accuracy with which bond lengths could be determined with EXAFS. Recently (Stearns, 1982) it has been pointed out that there exists for any material a particular value of $E_O = E_C$ at which the peak position in the magnitude of FT is independent of the weighting factor (k, k^3, k^5) and that the phase shift derived at this value of E_O is linear. For a particular weighting factor, the variation of peak position as a function of E_O is nearly a straight line, the slope of which diminishes with increase in degree n of the weighting factor. The lines for different values of n intersect at a particular point which gives the value of E_C. Further the existence of such a crossover point can be used to assess the quality of the experimental data.

Using the method outlined above, the value of E_C has been determined for c-Ge as well as for a-Ge (see section 4.7). Figure 4.4(b) shows the variation of the position of first peak as a function of E_O and weighting factors k, k^3 and k^5 for c-Ge. The crossover point obtained gives value of $E_C = -25$ eV and is comparable with $E_C = -26$ eV as obtained by Stearns (1982). The near neighbour distance can now be determined from the phase function obtained at $E_O = E_C$ by comparison of experimental and theoretical phase shifts. Figure 4.5 shows the two phase shifts obtained
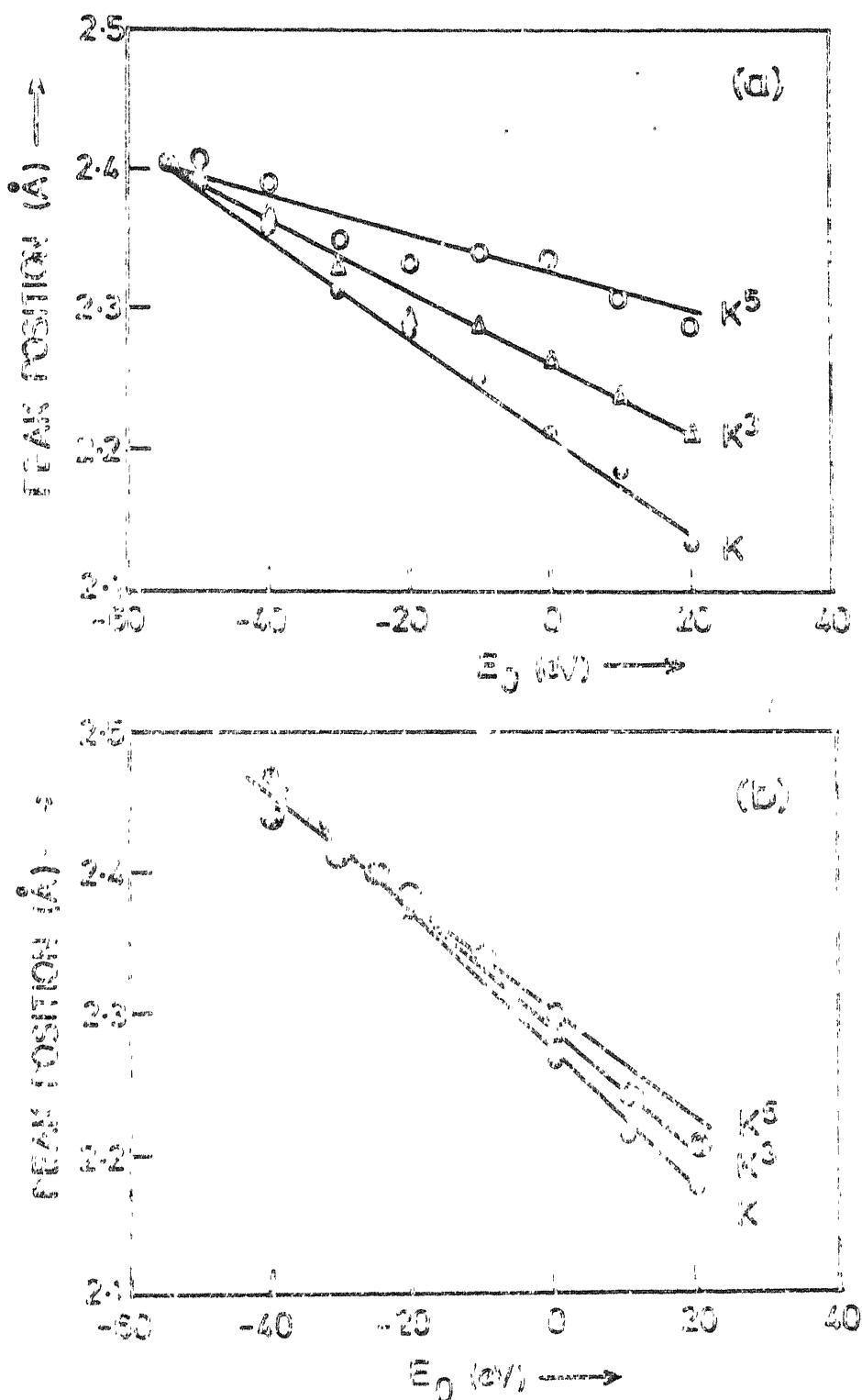
Fig.4.4 Variation of peak position as a
function of change in the threshold E_0
and weighting factor (k, k^3, k^5) for (a)
a-Ge and (b) a-Si.
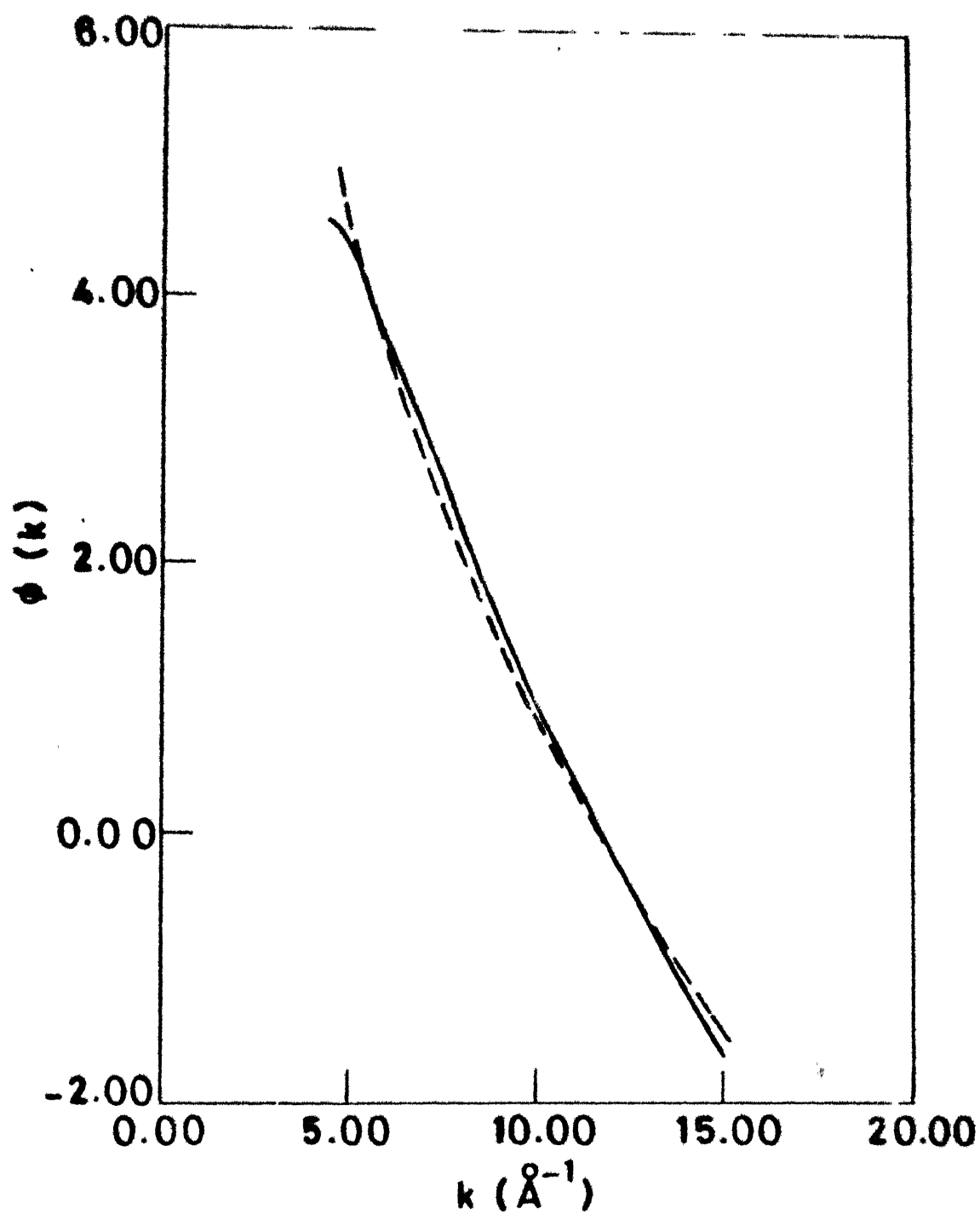
Fig.4.5 Comparison of experimental (dashed)
and theoretical phase shifts for c-Ge.

after the minimization procedure. The dashed curve is
the theoretical phase shift (Teo and Lee, 1979). The
parameters determined are ΔE_O = 30 eV, r_1 = 2.46 $\pm$ 0.01 $\overset{O}{A}$
(with width of the filtering window equal to 1.25 $\overset{O}{A}$).

4.6 Effect of the Width of the Filtering Window

The effect of the width of the filtering window on
the phase and amplitude function and subsequently on the
determination of local structure parameters has been
investigated by analysing the normalized EXAFS data with
different widths of the filtering window. The phase func-
tions were used to determine the near neighbour distance
by comparison of the experimental and theoretical phase
shifts. The changes in the phase functions could be
immediately ascertained from the values of α and the near
neighbour distance obtained for different widths of the
filtering window. The results are summarised in Table 4.1.
The value of r_1 determined by comparison of phase shifts
with different widths is same and equals 2.46 $\overset{O}{A}$ with the
accuracy of $\pm$ 0.01 $\overset{O}{A}$. The value of α or slope of the phase
function does change with the width of the window. However
this does not affect the value of r_1.

Unlike the case of phase function, the width of the
filtering window not only affected the magnitude but also
the shape of the amplitude function. This is illustrated

Table 4.1

Effect of width of the filtering window on phase function
$(E_O = -25 \text{ eV})$

Width ($\overset{O}{A}$)	α ($\overset{O}{A}$)	ΔE_O (eV)	r_1 ($\overset{O}{A}$)
0.535	−0.058	34.05	2.46
0.714	−0.059	34.04	
0.892	−0.060	33.80	2.46
1.071	−0.058	33.11	2.46
1.250	−0.042	30.20	2.46
1.428	−0.013	25.00	2.47
1.607	−0.015	19.70	2.47

by plotting the amplitude function $A_1(k)$ for five diffe-
rent widths of the filtering window in figure 4.6. As
is evident from the figure a too narrow window has comple-
tely washed away the details in the amplitude function.
With increasing width all the amplitude functions start
with a lower value and peak around 7 $\overset{o}{A}{}^{-1}$ (except for
'narrow' window). Thus for sufficiently large window
width it is only the low k information which is mostly
affected. The theoretical calculations of backscattering
amplitudes (Teo and Lee, 1979) suggest that the amplitude
function for Ge has a peak around 7-8 $\overset{o}{A}{}^{-1}$ and then decays
at large k values. For extracting the structural informa-
tion from the experimental amplitude by comparing it with
the theoretical one (equation 3.8), the two functions must
be consistent. Non-uniqueness of the amplitude function
naturally causes concern and great caution should be
exercised while determining the structural parameters from
this function. In our analysis we have used an optimum
width (1.25 $\overset{o}{A}$) for which the details in the amplitude
function are retained.

4.7 Results for Amorphous Germanium

Similar analysis has been carried out for the K
absorption discontinuity of Ge in amorphous germanium
(a-Ge). The results are presented in graphical form in
figure 4.7. Figure 4.7(a) shows the experimental absorption
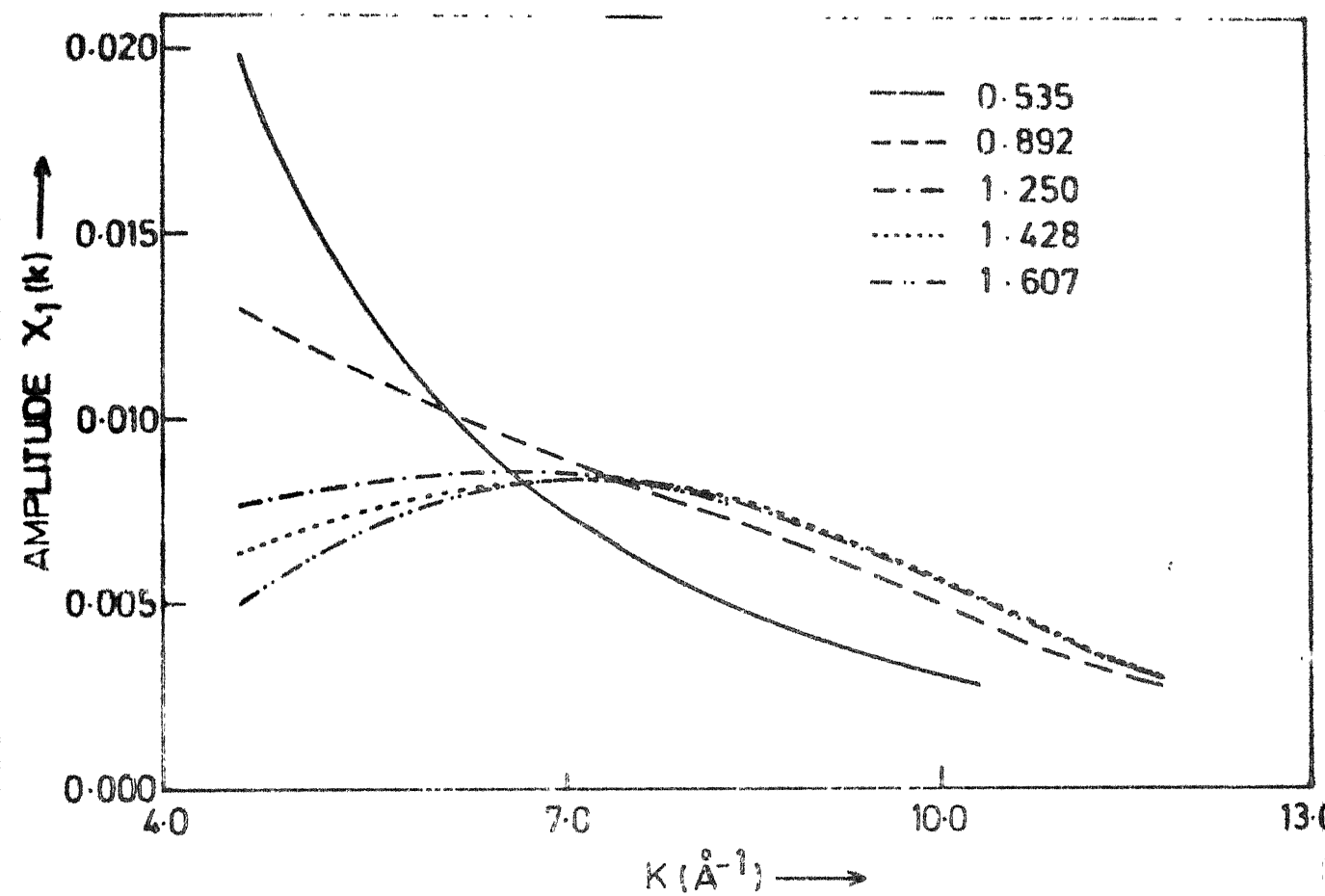
Fig.4.6 Amplitude functions $A_1(k)$ of c-Ge for five different window widths (in Å).
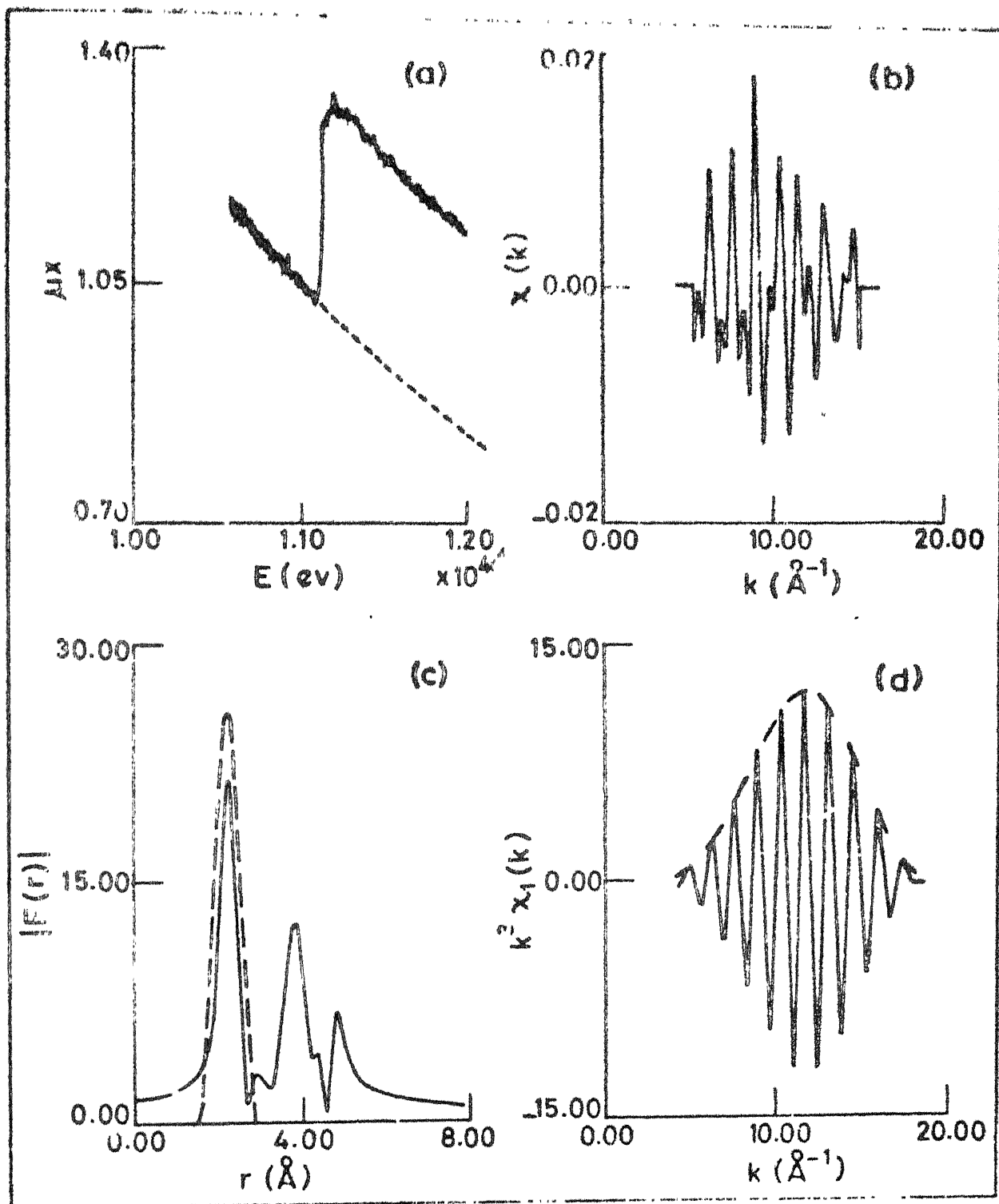
Fig.4.7 a) Absorption spectrum for a-Ge. The dashed curve is the
Victoreen curve $0.931 \lambda^3 - 0.175 \lambda^4$. b) Normalized EXAFS $\chi(k)$ extracted
from (a). c) Magnitude of Fourier transform of $k^3 \chi(k)$, dashed curve
being the filtering window. d) First shell EXAFS $k^3 \chi_1(k)$. The dashed

spectrum with dashed curve representing the Victoreen fit
(A = 0.9319; B = -0.1749). The steep decrease in absorp-
tion as compared with corresponding spectrum for c-Ge is
due to the substantial contribution to absorption by the
substrate (absorber was prepared by sandwitching several
thin films together). The normalized EXAFS obtained from
raw data after background removal and subsequent normaliza-
tion to per atom scale appears in part (b) of the figure.
The nature of EXAFS oscillations is similar to that obtained
in the case of c-Ge except the rapid changes in the negative
half. The reason for this could be explained by considering
the absorption spectra of c-Ge and a-Ge. The absorption
spectra of a-Ge contains a lot of noise as compared with
that of c-Ge spectrum. Since the noise frequencies are
uniformly distributed throughout the entire frequency range,
it is not possible to separate the noise completely.

Figure 4.7(c) shows the magnitude of FT of $k^3 \chi(k)$
with dashed curve being the filtering window. The first
large peak is observed at 2.31 $\overset{o}{A}$. The overall spectrum
is similar to the one obtained for c-Ge. In figure 4.7(d)
is depicted the first shell EXAFS $k^3 \chi_1(k)$. It rises
sharply and peaks around 12.5 $\overset{o}{A}{}^{-1}$. The dashed envelope
is the amplitude function $k^3 A_1(k)$. The phase function
$\psi_1(k)$ gives the value of α (calculated using $r_1 = 2.45 \overset{o}{A}$)
equal to 0.16 $\overset{o}{A}$, lower than that obtained for c-Ge (0.19 $\overset{o}{A}$).

This deviation of nearly 0.03 $\overset{o}{A}$ in the value of α indicates a larger value of r_1 in a-Ge. The position of the first peak in the magnitude of FT which is shifted by an amount α towards origin gives $r_1 = 2.50.\overset{o}{A}$ for a-Ge (using α of c-Ge).

The value of E_c for a-Ge was determined by the procedure described in section 4.5 and turns out to be -55 eV (fig. 4.4(a)). The first shell radius now can be determined from the phase function extracted at E_c = -55 eV. Figure 4.8 shows the comparison of experimental and theoretical phase shifts obtained after minimization. The parameters obtained are $r_1 = 2.49 \overset{o}{A}$, ΔE_0 = 59 eV. The value of r_1 obtained by this method agrees well with the straightforward method of using α for c-Ge (at E_0 = 0).

4.8 Empirical Phase Shifts and Chemical Transferability

The concept of chemical transferability has already been outlined in section 3.4.3. Accordingly a difference in phase functions of c-Ge (model) and a-Ge was calculated. A least squares straight line fitted to this had intercept -2.31. Non-zero value of intercept indicates that the threshold in a-Ge and c-Ge differ. ΔE_0 was varied using the method of bisection till the intercept reduced to nearly zero. Using the predetermined value of r_1 for c-Ge (2.46 $\pm$ 0.01 $\overset{o}{A}$), value of slope of the straight line yields r_1 = 2.49 $\pm$ 0.01 $\overset{o}{A}$ for a-Ge. Figure 4.9 shows the
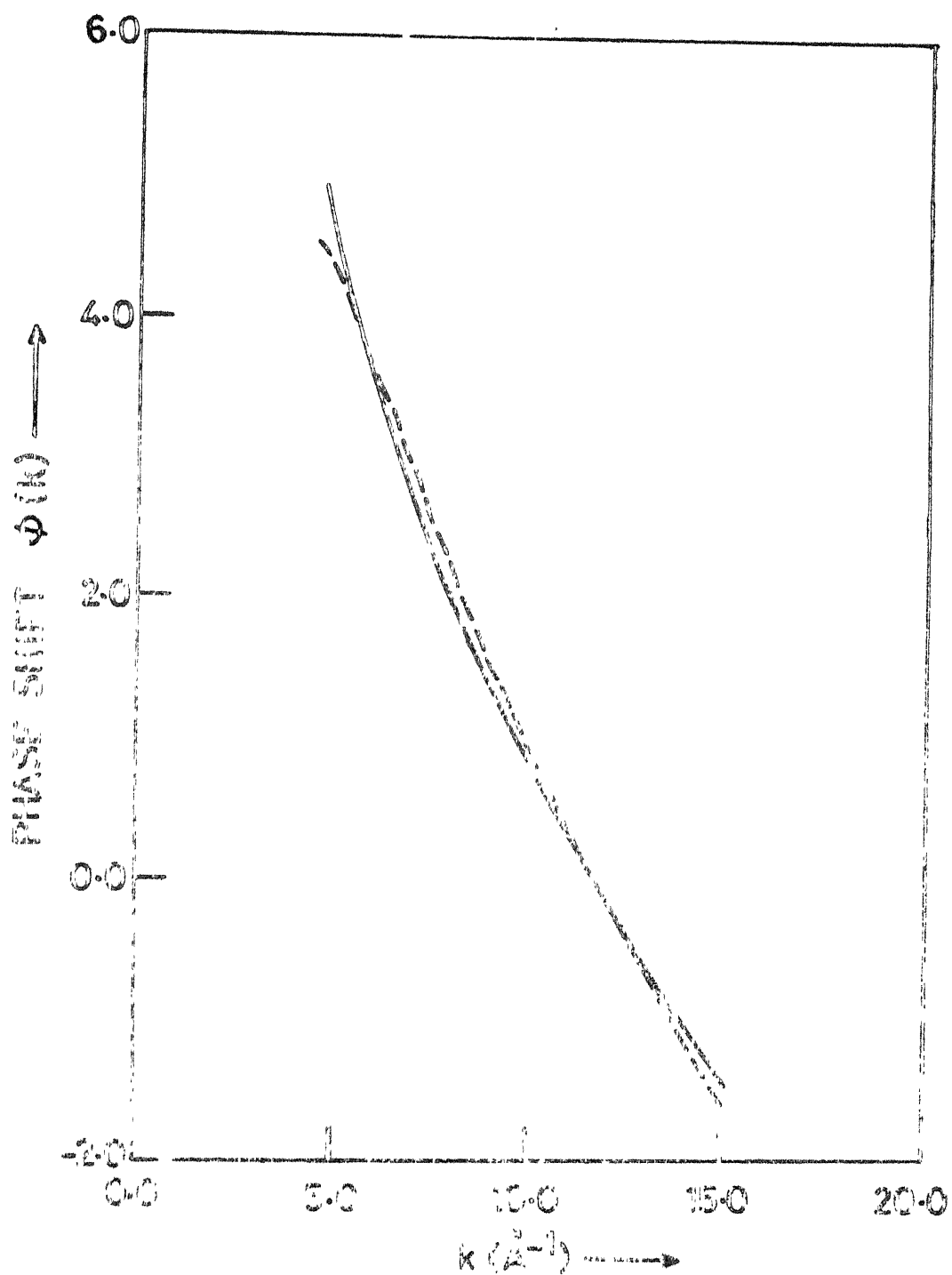
Fig.3.8 Fit of the experimental phase shift
with the theoretical phase shift (dashed).
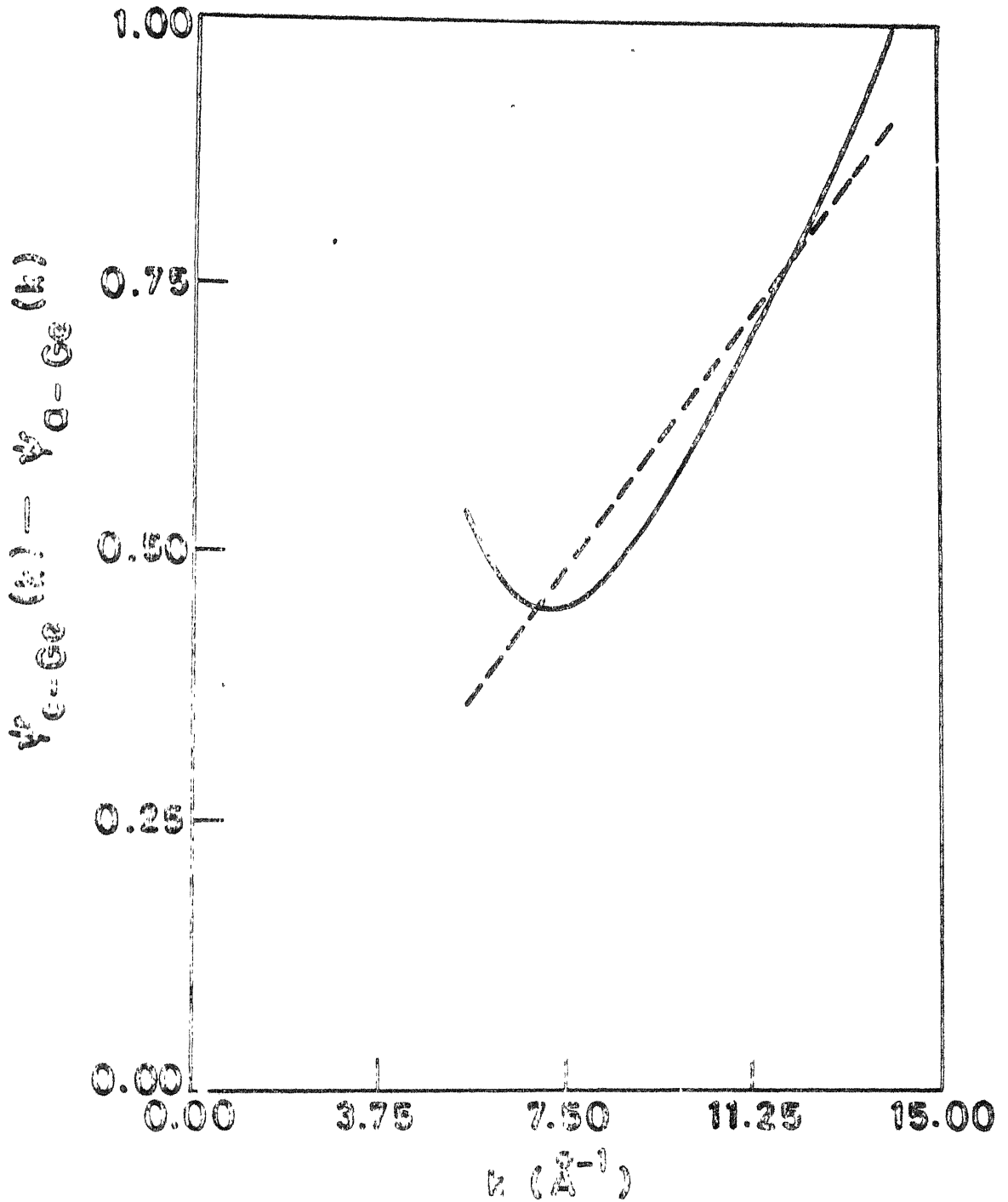
Fig.4.9 Difference of phase functions Ψ_{c-Ge}
and Ψ_{a-Ge} as a function of wave vector
$k(Å^{-1})$. The dashed line is the least squares
fitted straight line.

plot of the difference of phase functions and the least squares fit. The straight line clearly passes through origin.

4.9 Determination of Coordination Number

Information about the coordination number is contained in the amplitude function obtained by FT filtering. Comparison made between measured EXAFS amplitudes for nearest and more distant neighbour coordination shells in wide variety of known compounds at room temperature and liquid nitrogen temperature reveal the significant sensitivity of amplitudes to chemical environment (Eisenberger and Lengler, 1980). Absence of exact quantitative theoretical calculation of amplitude function and systematic errors in the experimental data makes the determination of coordination number by direct comparison of amplitude function unreliable. However an overall scaling factor determined for model system may be used, to a first approximation, in the other chemically similar system to determine the coordination number. The other widely used method is chemical transferability of amplitudes with known chemically similar model system (see section 3.4.4).

4.9.1 Comparison of amplitude functions

The amplitude function for the first coordination shell is given by expression 3.8. Mean free path λ can

be assumed to be independent of the photoelectron wave vector k. Using the coordination number for c-Ge system (4.0) and the quantitative theoretical values of back-scattering amplitudes (Teo and Lee, 1979), an overall scaling factor and Debye waller type factor σ_1^2 could be determined from the experimental amplitude function for c-Ge. Figure 4.10 shows the final result of the minimization run. Dashed curve is the theoretically calculated $kA_1(k)$ curve. The parameters namely the overall scaling factor and σ_1^2 are 0.2336 and 0.0034 $\overset{O}{A}{}^{+2}$ respectively. Using these parameters in fitting the amplitude function for a-Ge with theory, the coordination number for a-Ge was determined and is equal to 4.4 ± 0.8. In figure 4.11 the two functions $kA_1(k)$ for the case of a-Ge have been compared.

4.9.2 Amplitude functions and chemical transferability

Assuming that the two amplitude functions for c-Ge and a-Ge are transferable (i.e. backscattering amplitudes $F(k)$ remain same in both), logarithmic ratio of the two functions was plotted against the square of the wave vector k. However the plot is no more a straight line as could be expected from the expression 3.9 (after neglecting the third term). Therefore a least squares fit with a straight line was obtained. It was found that the slope and the intercept of this line vary depending on the range of
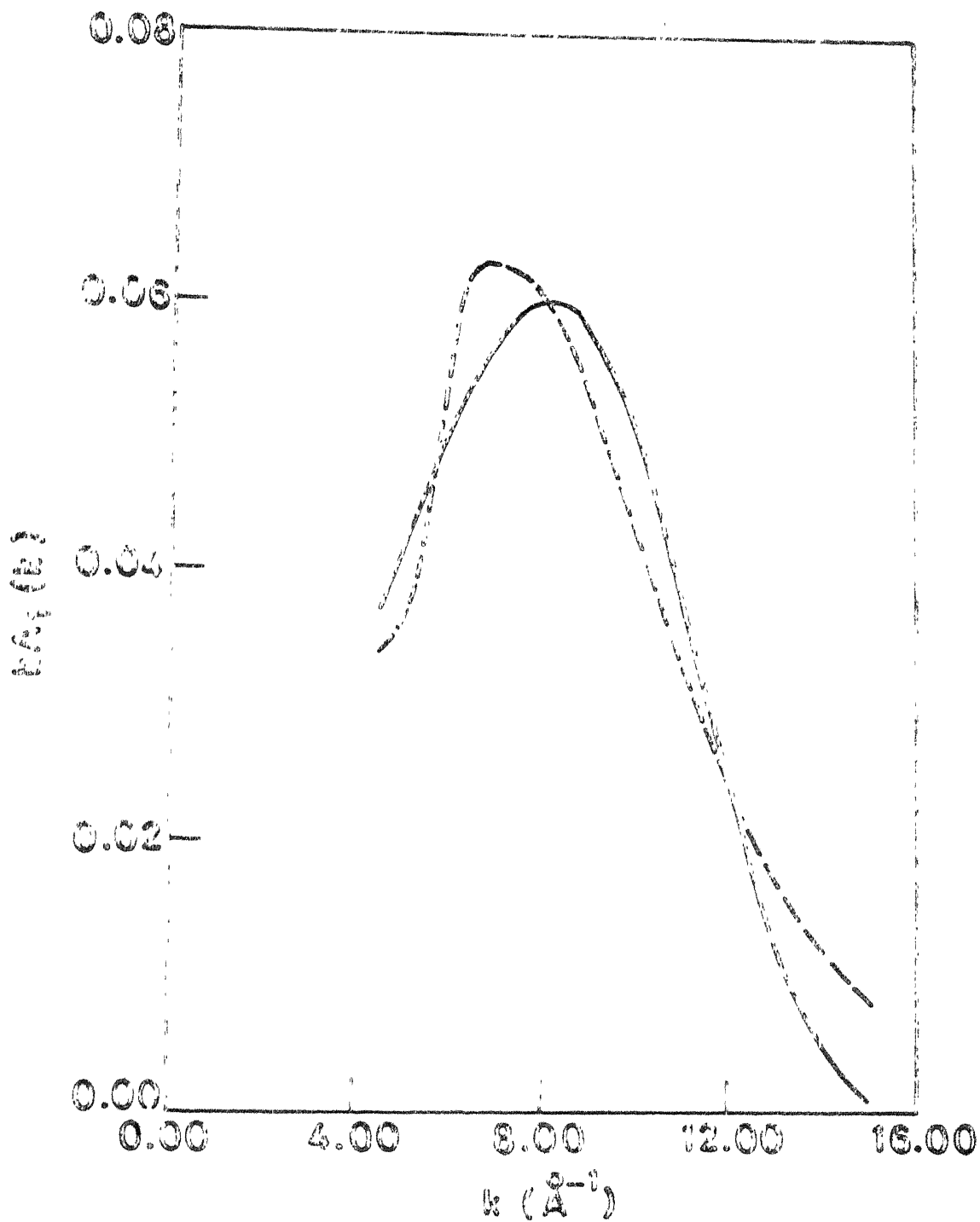
Fig.4.10 Comparison of experimental (solid curve) and theoretical amplitudes $kA_1(k)$ for c-Ge.
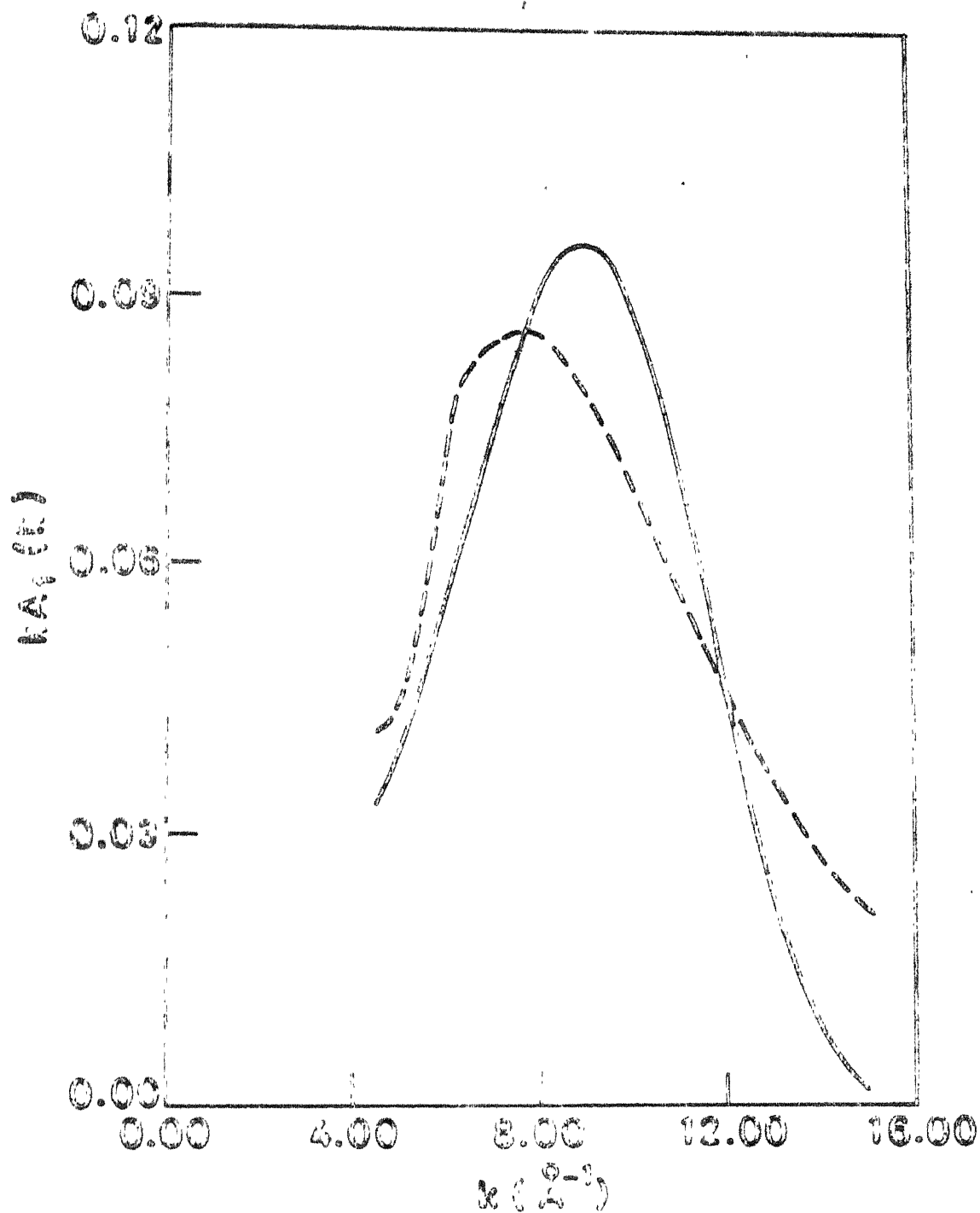
Fig.4.11 Comparison of experimental and
theoretical (dashed) amplitudes $xA_1(x)$ for
$a=0_0$.

k-values over which the fit is obtained. Therefore the parameters namely the coordination number for a-Ge and the difference in σ_1^2 values for c-Ge and a-Ge could be determined only approximately. Figure 4.12 shows the logarithmic ratio and the fitted straight line plotted against k^2 over a range 5 - 15 $\overset{o}{A}^{-1}$. The slope and intercept thus determined are -0.00048 and -0.072 respectively. Neglecting the third term in equation 3.9, the coordination number for a-Ge turns out to be 4.49 $\pm$ 0.5.

4.10   Results: X-ray Diffraction

X-ray diffraction pattern of a-Ge films show broad halos and absence of any sharp peaks which indicate the amorphous nature of the films. The experimental data consisted of measured intensity from the Al-substrate and the film (I_o and I respectively). The contribution to intensity I from the Al-substrate was subtracted using equation 2.5. The intensity in arbitrary units was further corrected for polarization, compton scattering and dispersion of form factors. The normalized intensity is obtained by requiring that intensity curve at high s($4\pi\sin\theta/\lambda \overset{o}{A}^{-1}$) oscillates about the total independent scattering curve (Halder et al., 1966). Figure 4.13 shows the normalized intensity curve. The normalized intensity I_{eu} is related to the radial distribution function as follows :
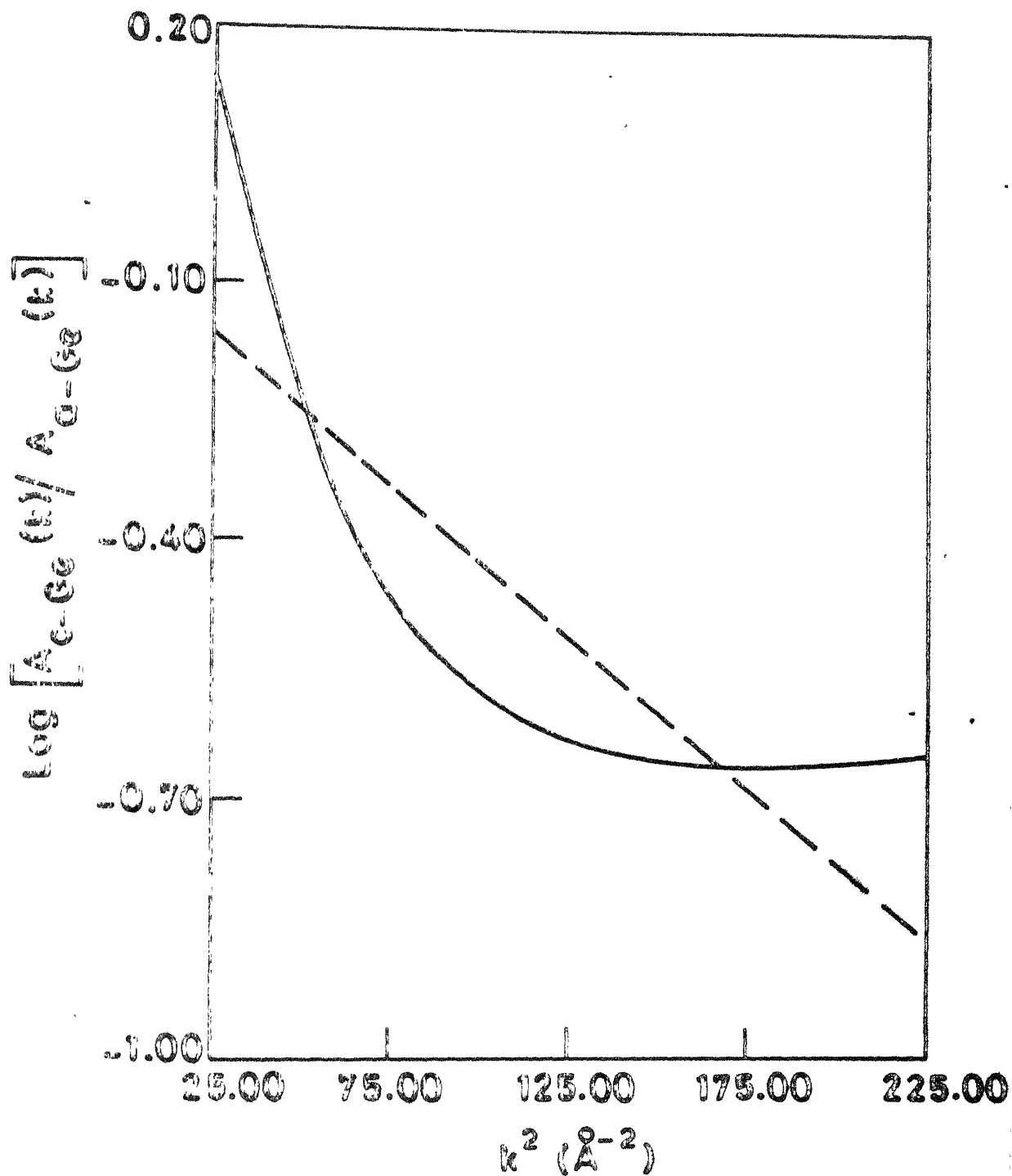
Fig.4.12 Logarithmic ratio of amplitudes plotted against k^2 ($Å^{-2}$). Dashed line is a least squares fitted straight line.
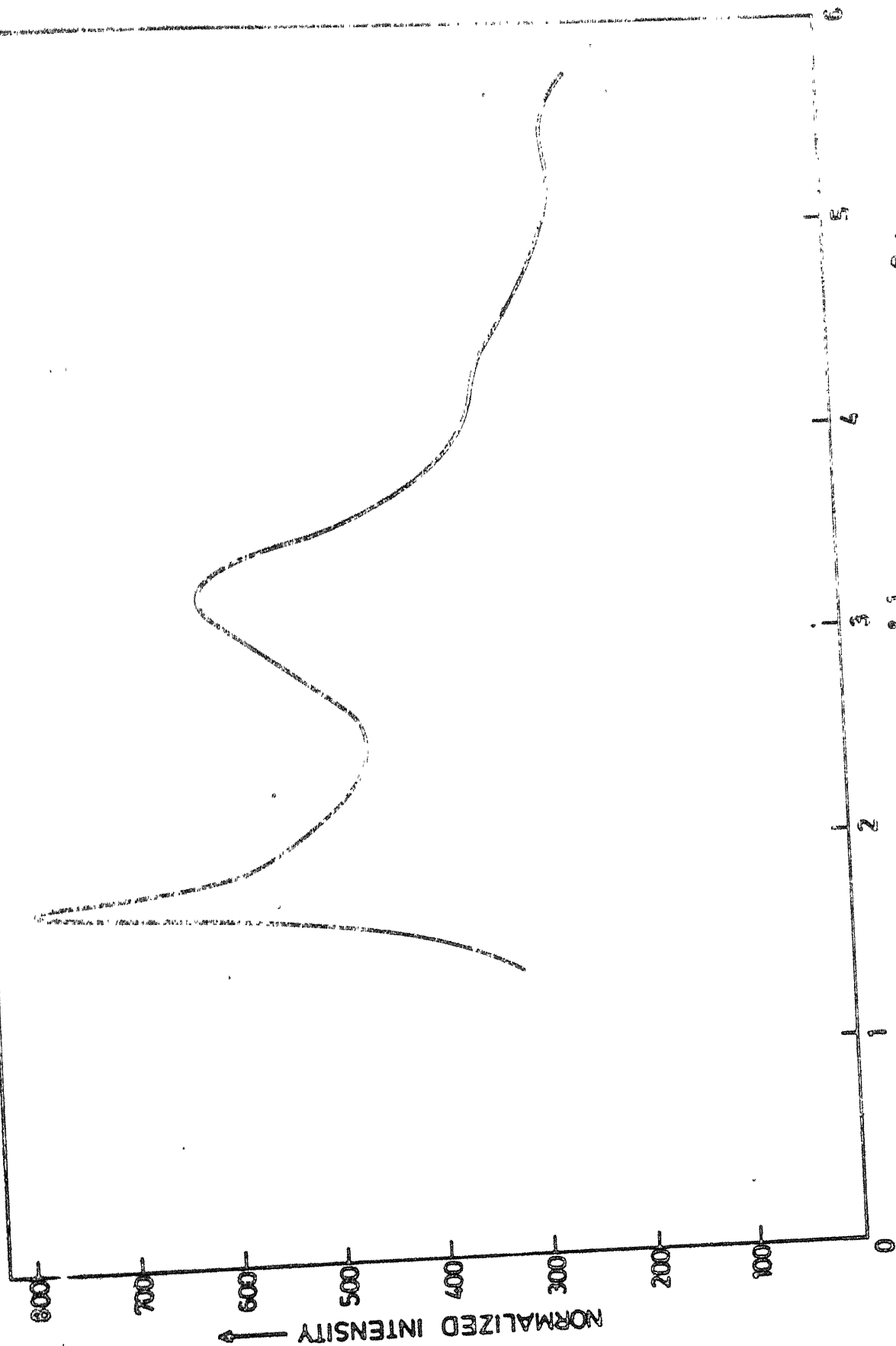
Fig. 6.15 Normalized intensity as a function of s (Å^{-1})

NORMALIZED INTENSITY
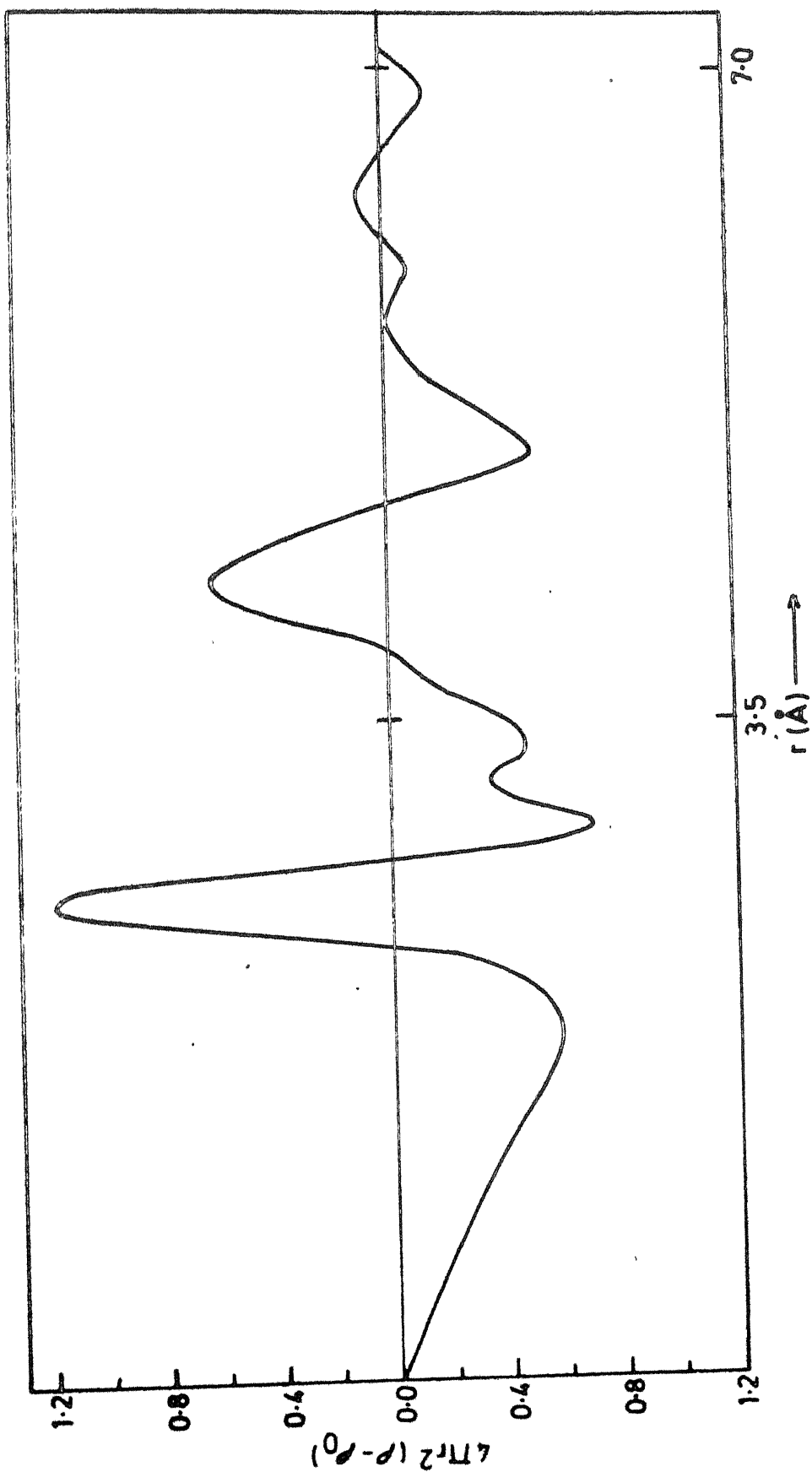
Fig.4.14 G(r) function obtained using data of Fig. 4.13.

$$F(s) = s \left\{ \frac{I_{eu}}{f^2} - 1 \right\} = \int_{0}^{\infty} G(r) \sin sr \, dr$$

where f is the atomic scattering factor, r is the radial distance from an atom at an arbitrary origin; $G(r)$ equals $4 \pi r (\rho - \rho_0)$ and is the Differential Radial Distribution Function (DRDF); s equals $4 \pi \sin\theta/\lambda$; ρ is the atomic density, atoms per unit volume, at a radial distance r, and ρ_0 is the average atomic density.

Fourier inversion of the above equation yields

$$G(r) = \frac{2}{\pi} \int_{0}^{\infty} F(s) \sin rs \, ds$$

Following the termination correction procedure (Kaplow et al., 1965), the final $G(r)$ function was obtained and is shown in figure 4.14. The near neighbour distance, from the first large peak, is $2.46 \pm 0.03 \, \overset{O}{A}$. This is in agreement with the value obtained from EXAFS analysis.

CHAPTER V

$Ge_x Se_{1-x}$ SYSTEM

5.1   Introduction

Ge_xSe_{1-x} compounds can be obtained in crystalline and amorphous structure depending on the concentration of germanium (x = 0.33 and 0.5, the compounds have crystalline structures). The system Ge_xSe_{1-x} system has been studied earlier by X-ray diffraction methods (Fawcett et al., 1972; Bienenstock,1970b) and also by EXAFS (Sayers et al., 1972, 1974) and Raman spectroscopy (Nermanich et al., 1978; Kawamura et al.,1982). The X-ray diffraction studies, in particular, met with several limitations. For low concentration of germanium (x≤ 0.33) both the chain crossing model (CCM) and Random covalent model (RCM) were equally probable. Earlier studies with EXAFS on amorphous GeSe and $GeSe_2$ too could not point at a particular model which would describe the experimental results completely. The present work on this system is limited to compounds with low germanium content.

In this chapter are presented the results obtained for two compositions x = 0.1 and x = 0.3 (hereafter referred to as I and II respectively). The experimental data of both X-ray diffraction and X-ray absorption (EXAFS) experiments have been analysed with more emphasis on later.

The K X-ray absorption discontinuities of germanium as well as selenium have been recorded in both I and II.

Analysis of EXAFS associated with particular kind of absorbing atom provides information about local structure around that atom. However the proximity of atomic numbers of Ge and Se poses some problem in determination of near neighbour distance using experimental phase function. An entirely different approach has been used, for the above mentioned reason, which leads to a model based on probabilities of all the possible configurations. The experimental first shell EXAFS could then be described in terms of this model.

5.2   Results: EXAFS

In all the cases the elementary analysis and extraction and normalization of EXAFS has been carried out by procedures described in the previous chapter. The results for Ge K absorption discontinuity in I and II are presented graphically in figures 5.1 and 5.2 respectively. The fine structure is clearly visible in both the absorption spectra (part (a) of the figures). Incident photon energy at the inflection point ($E_O = 0$) in both cases is ~ 11126 eV. The background absorption below the edge is more in case of I. This is because the sample of same thickness could not be prepared with the particular method used for preparing the absorption screens (see section 2.2.5). The normalised EXAFS shown in (b) part of the figures is
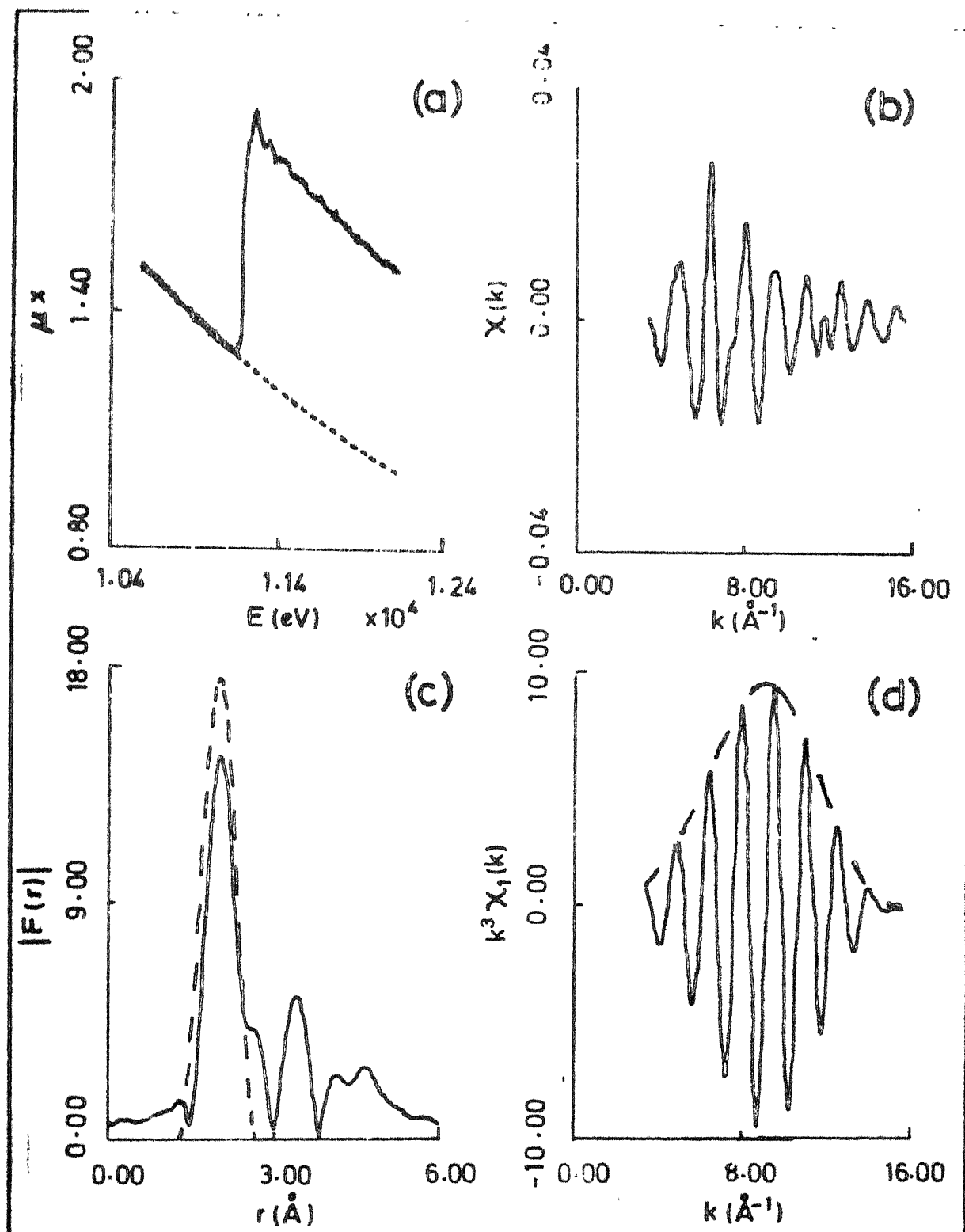
Fig.5.1 a) Absorption spectrum of Ge K edge in I. The dashed curve is
Victoreen curve 0.807 λ^3+0.122 λ^4. b) Normalized EXAFS χ(k) extracted
from (a). (c) Magnitude of Fourier transform of $k^3 \chi$(k) with a filter-
ing window (dashed curve) and (d) First shell EXAFS $k^3 \chi_1$(k). The das'-'
curve is amplitude $k^3 A_1$(k).
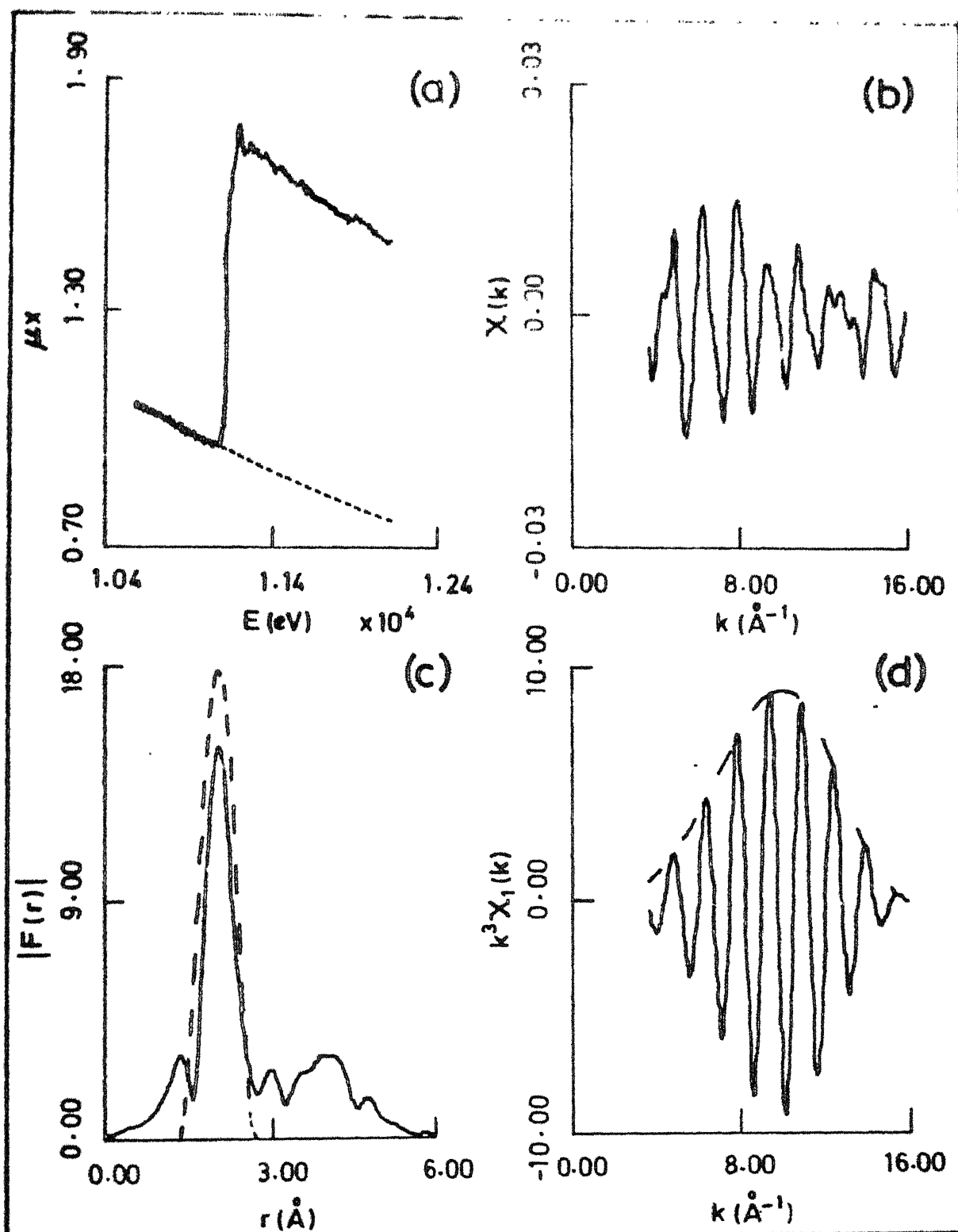
Fig.5.2 a) Absorption spectrum of Ge K edge in II with Victoreen curve (dashed) $1.074\ \lambda^3 - 0.350\ \lambda^4$. b) Normalized EXAFS extracted from (a). c) Magnitude of Fourier transform of $k^3\chi(k)$ with a filtering window (dashed) and d) First shell EXAFS $k^3\chi_1(k)$. Dashed envelope

comparatively sharply peaked for the case II. However the overall trend in both the cases is similar starting with low amplitude and giving a peak around 7 $\overset{\circ}{A}{}^{-1}$. The magnitude of Fourier transform of $k^3 \chi(k)$ (with $E_o = 0$) appears in figure 5.1(c) and 5.2(c). Apart from a sharp main peak corresponding to first coordination shell, a not well resolved small peak at 2.6 $\overset{\circ}{A}$ is observed in case of I. Such type of structure has been previously observed by Sayers et al. (1972) while studying a-GeSe. However this type of structure is absent in II. The position of the main peak in II is at slightly higher distance (~ 0.03 $\overset{\circ}{A}$) than that in I. The other striking feature is the presence of sharp peak at 3.37 $\overset{\circ}{A}$ in I which is not clearly resolved in case of II. The first shell EXAFS and the amplitude function $k^3 \hat{\chi}_1(k)$ are shown in figures 5.1(d) and 5.2(d) for I and II respectively. With the same width (1.25 $\overset{\circ}{A}$) of the filtering window used for filtering out the first shell EXAFS, the amplitude function peaks around 10 $\overset{\circ}{A}{}^{-1}$.

Similar results of EXAFS associated with K X-ray absorption discontinuity of selenium in I and II are shown in figures 5.3 and 5.4 respectively. The absorption spectra shown in part (a) of the figures reveal that the background absorption due to the sample is low in the energy range 12-14 K_{eV}. The inflection points are observed at 12776 eV,

(a)

$\Delta \mu x$

1·70

1·05

0·40

1·20   1·28   1·38

E (eV) $\times 10^4$

(b)

$\chi(k)$

0·04

0·00

-0·02

0·00   8·00   16·00

k (Å^{-1})

(c)

$|F(r)|$

6·00

3·00

0·00

0·00   3·00   6·00

r (Å)

(d)

$k^3 \chi_1(k)$

3·50

0·00

-3·50

0·00   8·00   16·00

k (Å^{-1})
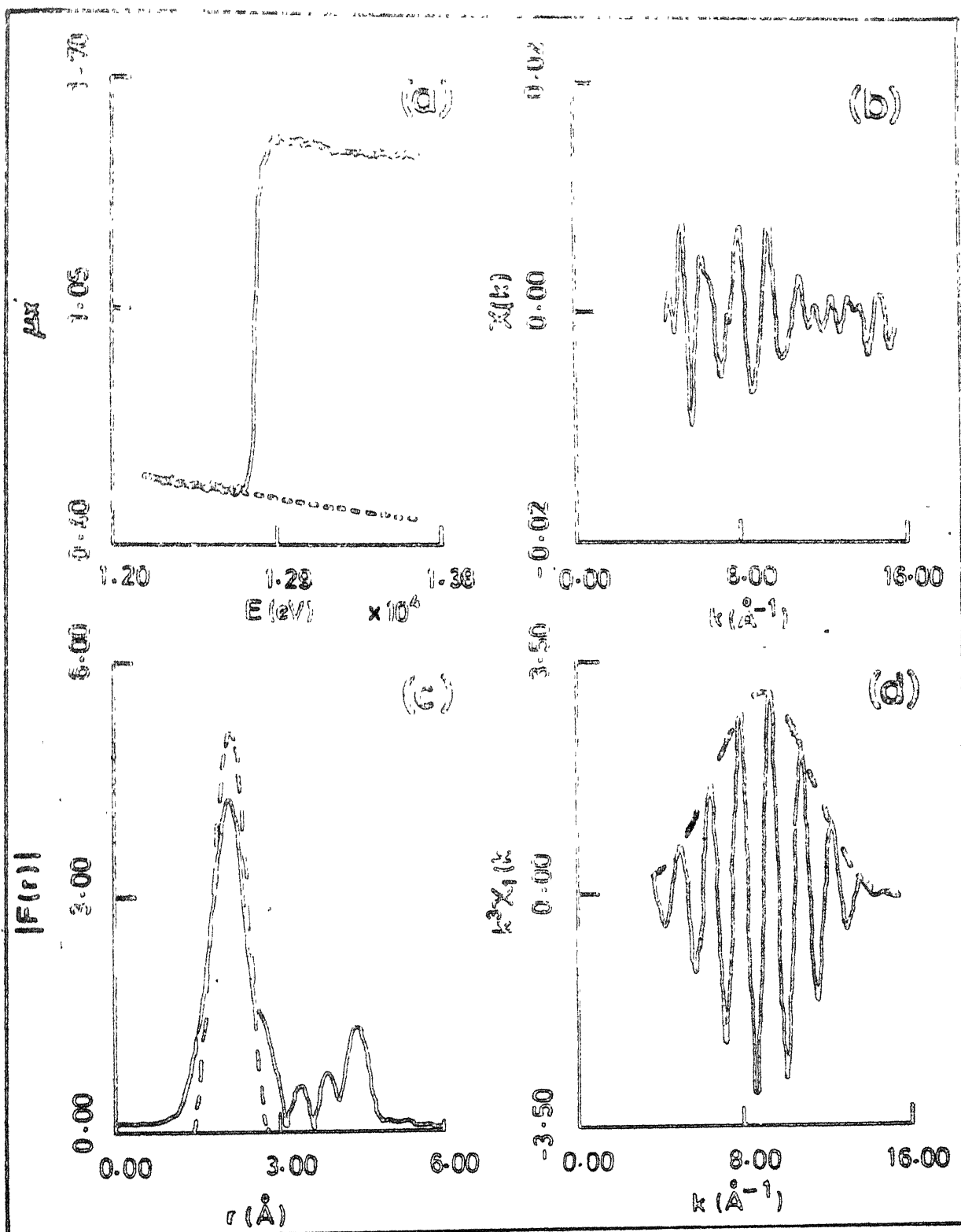
Fig.3.3 a) Absorption spectrum for Se K edge in I. The dashed curve
is the Victoreen curve 1.198 λ^3-0.627 λ^4. b) Normalized EXAFS c) Magni-
tude of Fourier transform of $k^3 \chi(k)$ with filtering window (dashed)
and d) First shell EXAFS $k^3 \chi_1(k)$. Dashed envelope being the amplitude
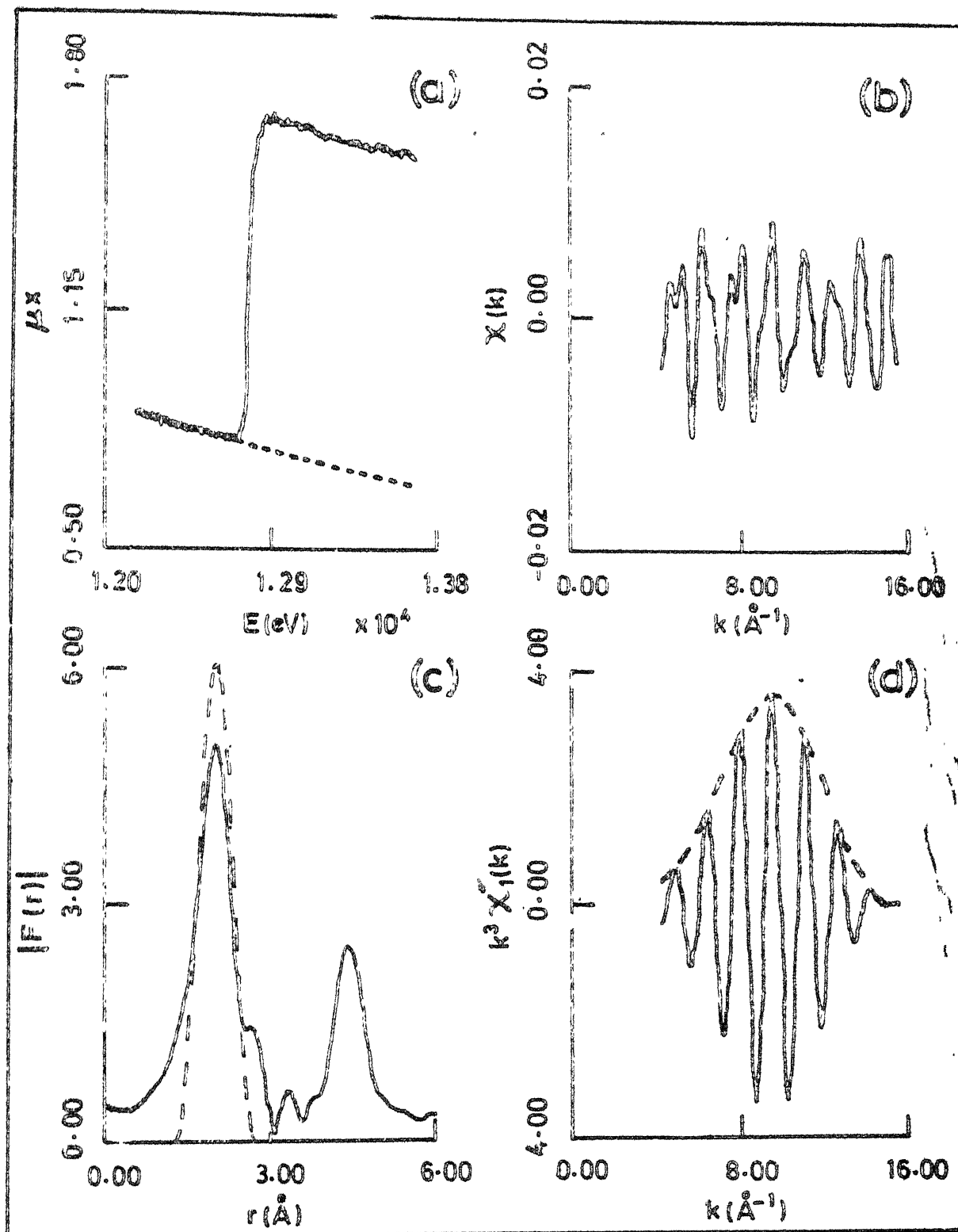
Fig.5.4 a) Absorption spectrum for Se K edge in II with Victoreen fit
1.565 λ^3-0.730 λ^4. b) Normalized EXAFS. c) Magnitude of Fourier
transform of $k^3 \chi(k)$. The dashed curve is the filtering window.
d) First shell EXAFS $k^3 \chi_1(k)$ and amplitude function (dashed) $k^3 A_1(k)$,

12771 eV in I and II respectively. Unlike the case of Ge
K edge, the EXAFS oscillations are not prominent in this
case and also the white line is absent. As is evident
from the figures the patterns of normalised EXAFS oscil-
lations are also very different when compared with the
case of Ge K discontinuity. The first large peak for I
(2.12 $\overset{O}{A}$) is at slightly higher distance compared to the
position of the corresponding peak in II (2.03 $\overset{O}{A}$). As
in case of Ge K edge, the splitting of the first main
peak is observed in this case also both for I and II.
This splitting which is more clearly resolved around Se
atoms may illustrate the tendency of Se atoms to link two
nearby Ge atoms into a chain as the other Ge atom is forced
away.

Although the structure observed beyond first peak
could be of considerable significance, here the analysis
is extended only up to the first coordination shell.

5.3 Determination of Near Neighbour Distances

The determination of near neighbour distance from
experimental phase function by comparing theoretical and
experimental phase shifts requires that the phase function
be extracted using $E_O = E_C$. The critical value E_C for
all the cases (four) was determined by the procedure
described in section 4.5. Table 5.1 summarizes the

Table 5.1

E_C values in I and II for first peak

Compound	Absorbing atom	E_C (eV)	Peak position at E_C (Å)	Peak position at E_O (= 0)(Å)
I	Ge	−50	2.230	2.040
I	Se	5	2.100	2.120
II	Ge	−10	2.050	2.017
II	Se	42	1.820	2.030

results of E_c determination. Moreover the calculation
of theoretical phase shift which is given by

$$\phi(k) = \phi_a + \phi_b - \pi$$

where ϕ_a is central atom phase shift and ϕ_b is the
backscattering atom phase shift, requires that the atom
pair i.e., the central or the absorbing atom and the back-
scattering atom is identified.

Unlike the case of crystalline and amorphous
germanium where the backscattering atoms in the coordina-
tion shell are of same kind, in case of Ge_xSe_{1-x} system
due to the proximity of atomic numbers of Ge and Se, either
Ge or Se can act as the backscattering atom. For example
consider the first shell phase function obtained from EXAFS
associated with Ge K absorption discontinuity in I. The
experimental phase function for the first shell represents
the resultant of phase function of possible bonding of
central Ge atom with another Ge atom and Se atom. However
the two possible bondings may not occur with equal probabi-
lities as the concentrations of Ge and Se are very different.

One can assume that the backscattering atom is a
germanium atom and determine the near neighbour distance
r_1 and change in threshold ΔE_o by fitting the experimental
phase shift with theoretical one. Figure 5.5 shows the
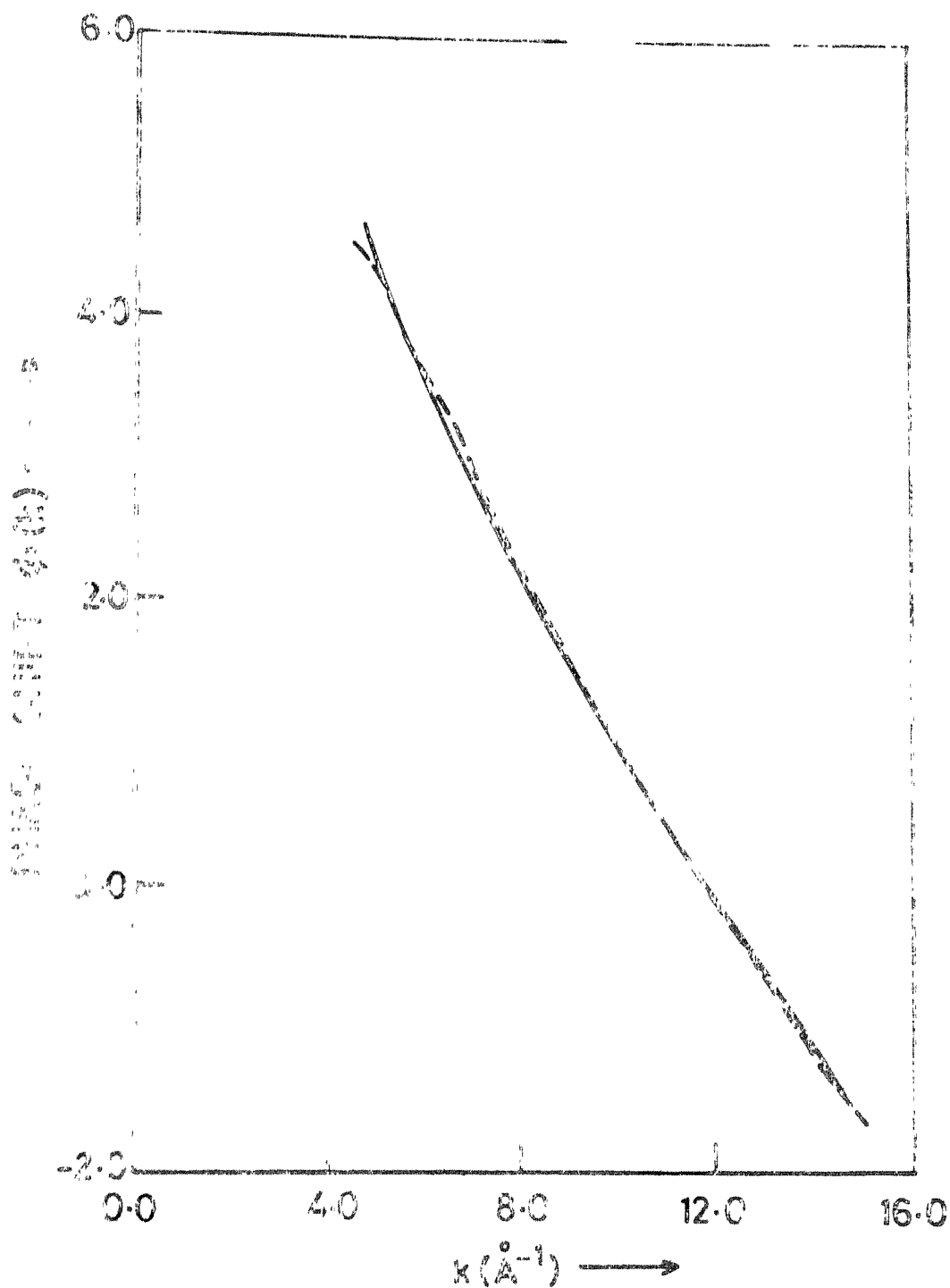
Fig.5.5 Comparison of experimental and theoretical (dashed) phase shifts of Ge K edge in 1. Backscattering atom is Ge.

two phase shifts obtained after the minimization run. The
dashed curve is the theoretical phase shift. The sum of
squares of the deviations obtained after this fitting is
a measure of the quality of fit. On the other hand the
fit would be better if Ge itself (assumed to be backscattering
atom) is the more probable neighbour. Denoting the sum
of squares of deviations by $(F)_x$, where x is the kind of
backscattering atom, the probability P_x of x being the
nearest neighbour is inversely proportional to $(F)_x$. This
probability would also depend on the concentration C_x of
the X-atoms in the compound.

Thus we have

$$P_x \propto \frac{C_x}{(F)_x}$$

$$\text{or} \quad P_x = \frac{K \, C_x}{(F)_x}$$

where K is the constant of proportionality which in general
will depend upon the quality of experimental data itself
but not on the kind of backscattering atom.

For the present case of Ge edge in I

$$P_{Ge} = \frac{K \, C_{Ge}}{(F)_{Ge}} = \frac{0.1 \, K}{(F)_{Ge}} \tag{5.1}$$

Similarly one can assume that the backscattering
atom is Se and obtain

$$P_{Se} = \frac{K \ C_{Se}}{(F)_{Se}} = \frac{0.9 \ K}{(F)_{Se}} \qquad (5.2)$$

Here K remains same as the same experimental phase function is under consideration.

Since the backscattering atom is either Ge or Se, one must have

$$P_{Ge} + P_{Se} = 1.0 \qquad (5.3)$$

Using equations (5.1), (5.2), (5.3) the probabilities P_{Ge} and P_{Se} could be determined. Around Ge and Se in both I and II we have in all eight different cases to be considered. Similar calculations have been carried out for all these cases and results are tabulated in Table 5.2. The probability P_x appear in the last column of the table. The values of ΔE_o obtained are consistent with respective E_c values. The near neighbour distance determined for I corresponds to covalent bond between Ge and Se. However for II the value of r_1 is smaller by ~ 0.04 $\overset{o}{A}$.

From the probabilities for all the cases it follows that Se is the most probable nearest neighbour around Ge as well as Se. Also there is a finite probability of Ge being nearest neighbour of Ge and this casts some doubt on the chain crossing model proposed earlier (Fawcett et al., 1972). In the so called "chain crossing model (CCM)", the

Table 5.2

Probabilities P_{Ge} and P_{Se} obtained
from phase functions

Compound	Central atom	Backscattering atom (x)	$r_1(\overset{o}{A})$	ΔE_o (eV)	$(F)_x$	$P_x(\%)$
I	Ge	Ge	2.378	57.49	0.0121	13.9
	Ge	Se	2.370	61.33	0.0176	86.1
II	Ge	Ge	2.338	7.23	0.0415	27.0
	Ge	Se	2.328	10.88	0.0370	73.0
I	Se	Ge	2.387	12.48	0.0293	8.5
	Se	Se	2.378	16.00	0.0249	91.5
II	Se	Ge	2.341	−44.10	0.0344	28.0
	Se	Se	2.330	−40.60	0.0318	72.0

Se chain structure is maintained but the four fold tetra-
hedrally coordinated Ge atoms act as chain crossing points.
In this model, Ge atoms are not allowed to bond to one
another. The present results, obtained from the experimental
phase functions, do not seem to support fully this particular
model. However it is clear that it is mostly Se which is
found around Ge as well as Se and the probability of Ge
bonding with another Ge is low. In the other model called
the "random covalent model (RCM)" the four fold coordinated
Ge atoms are allowed to bond with other Ge atoms as readily
as the two fold coordinated Se atoms. The markedly differ-
ing probabilities around Ge and Se do not warrant the vali-
dity of RCM too.

5.4 Proposed Model

In determining the bond lengths from experimental
phase functions it was assumed that a particular kind of
atom (either Ge or Se) can act as the backscattering atom.
This means that if Ge is four fold coordinated, either it
is bonded to all the four Ge atoms or to all the four Se
atoms. However the possibility of both kinds of atoms
being present in the first shell can not be excluded. For
example Ge,which is tetrahedrally coordinated to other
four atoms, one can have five different possible configu-
rations. The probabilities P_{Ge} and P_{Se} obtained from phase

shift analysis themselves will determine the probability of individual configuration, i.e. if Ge is surrounded by four Ge atoms, probability of occurrence of this particular configuration would be P_{Ge}^4. Figure 5.6 shows the different configurations for four fold Ge and two fold Se atoms with their respective probabilities.

The probability of ith configuration around the central Ge atom is given by

$$P_i = M_i P_{Ge}^{i-1} P_{Se}^{5-i}$$

where M_i = 1 for i = 1,5

= 4 for i = 2,4

= 6 for i = 3

and

$$\sum_{i=1}^{5} P_i = (P_{Ge} + P_{Se})^4 = 1.0$$

Then the first shell EXAFS $\chi_I(k)$ can be expressed as

$$\chi_I(k) = \sum_{i=1}^{5} P_i \chi_i(k) \tag{5.4}$$

where $\chi_i(k)$ represents the first shell EXAFS of ith configuration.
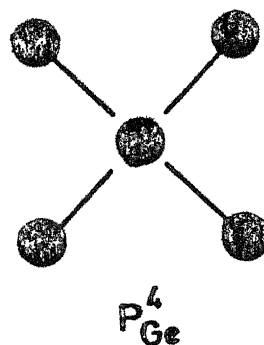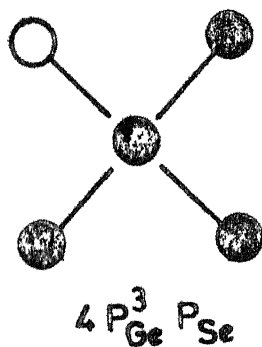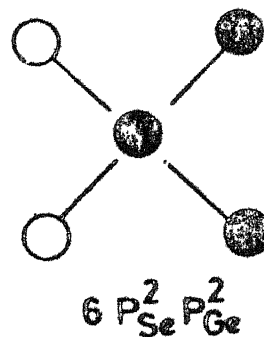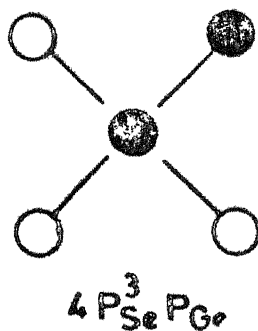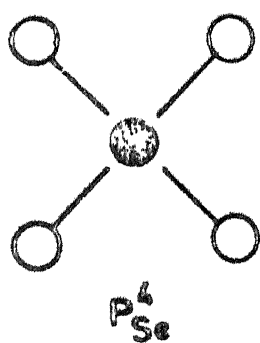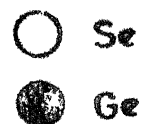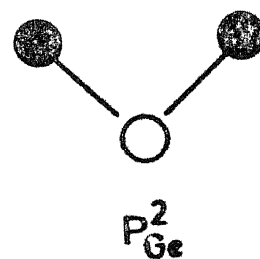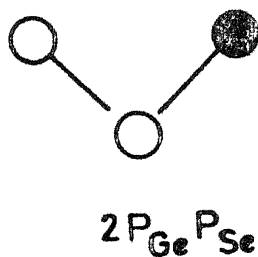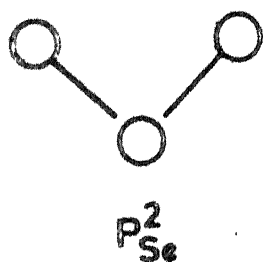
Fig.5.6 Different possible configurations of first shell with (a) Ge as central atom and (b) Se as central atom.

5.4.1 Calculation of $\chi_i(k)$

The expression for the first shell EXAFS is given by

$$\chi_I(k) = \frac{N_1}{kr_1^2} F_1(k) \, e^{-\frac{2r_1}{\lambda}} \, e^{-2\sigma_1^2 k^2} \sin\left[2kr_1 + \phi_1(k)\right]$$

where N_1 is the number of particular kind of atoms surrounding the central atom at an average distance r_1. $\phi(k)$ is the phase shift calculated by taking the backscattering phase shift of that particular kind of atom. The expression can be visualised as sum of N_1 terms, with each term representing contribution from individual bond. Thus the first shell EXAFS for i th configuration can be calculated by taking such a sum. For example if a particular configuration has number of Ge neighbours equal to N_{Ge} and number of Se neighbours equal to N_{Se} such that $N_{Ge} + N_{Se} = N_1$ then

$$\chi_i(k) = \left\{ N_{Ge} \, F_{Ge}(k) \sin\left[2kr_1 + \phi_{Ge}(k)\right] + N_{Se} \, F_{Se}(k) \right.$$
$$\left. \sin\left[2kr_1 + \phi_{Se}(k)\right] \right\} \frac{e^{-\frac{2r_1}{\lambda}} \, e^{-2\sigma_1^2 k^2}}{kr_1^2}$$

where $F_{Ge}(k)$ and $F_{Se}(k)$ are the backscattering amplitudes for Ge and Se respectively, $\phi_{Ge}(k)$ and $\phi_{Se}(k)$ are the total phase shifts calculated using the same central atom phase shift but different backscattering atom phase shifts

corresponding to Ge and Se respectively. Here the Ge-Ge and Ge-Se bondlengths (or Se-Se and Se-Ge) have been assumed to be same and equal to r_1. In evaluating equation 5.4 it was assumed that the temperature dependent Debye-Waller type factor remains same for all the configurations and hence could be pulled out of the summation. The mean free path term could be absorbed in an overall scaling factor.

5.4.2 Determination of structural parameters from the model

The first shell EXAFS was extracted from the experimental data as described in section 5.2 with $E_O = E_C$. The method of determination of structural parameters involves fitting the theoretically evaluated first shell EXAFS (equation 5.4) with the experimental first shell EXAFS with a set of four parameters namely the change in the threshold ΔE_O, the first shell radius r_1, the Debye-Waller type factor σ^2 and an overall scaling factor N. A least squares minimization routine MINFUN (see Appendix I) was used for this purpose. In figures 5.7 and 5.8 are compared the experimental first shell EXAFS (associated with Ge edge and Se edge in II respectively) with the one obtained from the proposed model. The results are summarised in table 5.3. The average first shell radius around Ge as well as Se in both I and II turns out to be 2.39 ± 0.01 Å.
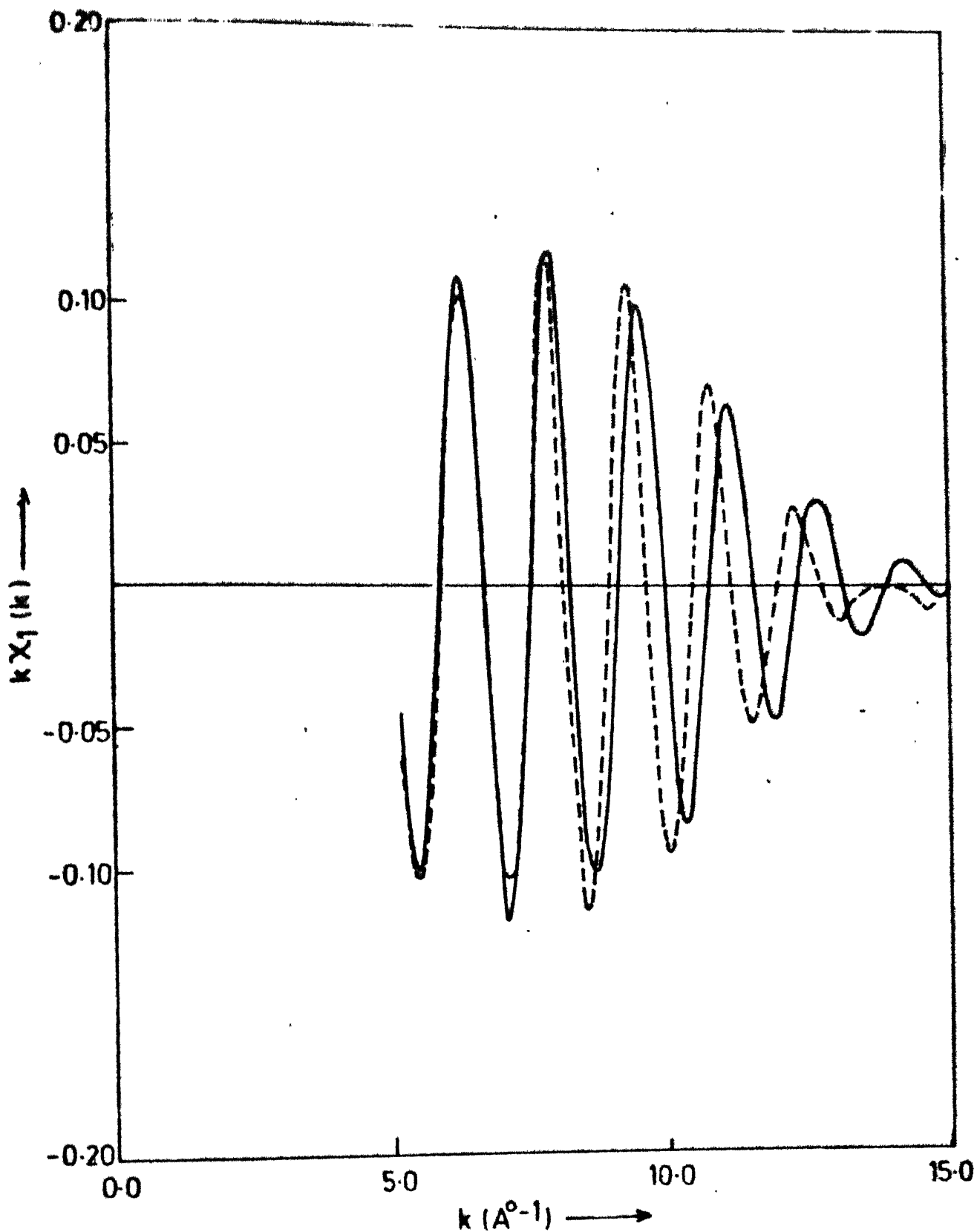
Fig.5.7 Fitting of experimental $k\chi_1(k)$ of Ge K edge in II with the one calculated from the proposed model (dashed curve)
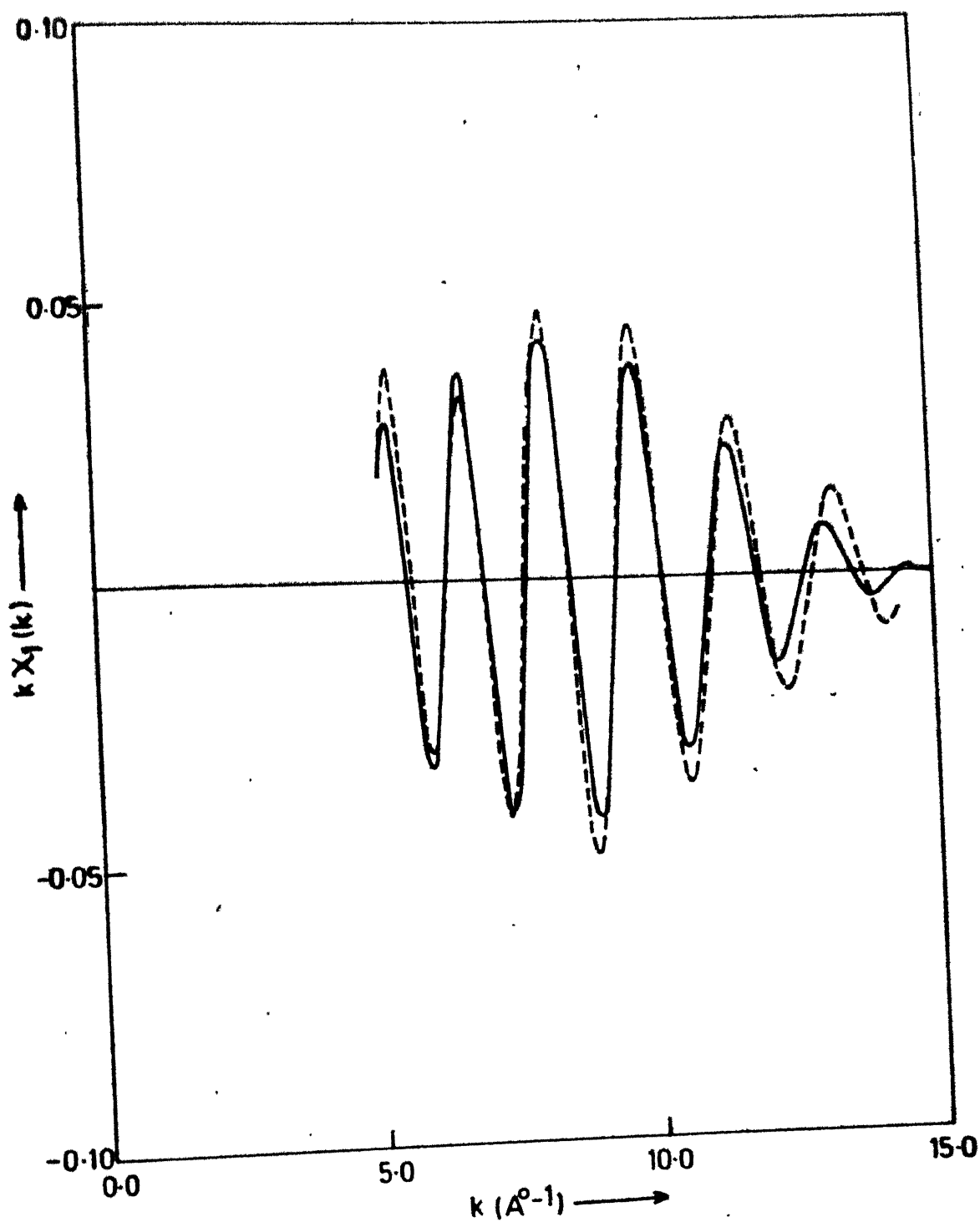
Fig.5.8 Comparison of experimental and theoretical
(equation 5.4) $k\chi_1(k)$ for Se K edge in II.

Table 5.3

Parameters obtained from proposed model

Compound	Central atom	ΔE_o (eV)	r_1 (Å)	σ^2 (Å^2)	N
I	Ge	37.5	2.39	0.0055	−0.120
I	Se	−4.3	2.40	0.0054	−0.0688
II	Ge	15.3	2.39	0.0044	−0.099
II	Se	−52.6	2.39	0.0040	−0.058

The values of ΔE_o are consistent with their respective E_c values. The factor σ^2 remains constant for particular compound irrespective of the kind of central atom. The overall scaling factors obtained for different cases could not be interpreted in simple way due to the various factors which affect the EXAFS amplitudes.

5.5 Results: DRDF

X-ray diffraction patterns for both I and II have been recorded. Broad halos and absence of any sharp diffraction peaks indicated the amorphous state of the samples. Figure 5.9 shows the diffraction pattern for II. The experimental data for DRDF analysis consisted of the diffracted intensity from the sample (with substrate), I, and from the substrate, I_o. The data were corrected for substrate scattering, absorption, polarization, compton scattering and dispersion of form factors. The data was then normalized to electron units by high angle method (Halder et al., 1966). The interference function F(s) is obtained by equation

$$F(s) = s \left\{ I_{coh} - \langle f^2 \rangle \right) \langle f \rangle^2 \right\}$$

where I_{coh} is the first ordered coherently scattered intensity obtained by removing the modified component from the normalised intensity,

$$\langle f \rangle = \sum_i x_i f_i(s) \quad , \quad \langle f^2 \rangle = \sum_i x_i f_i^2(s)$$
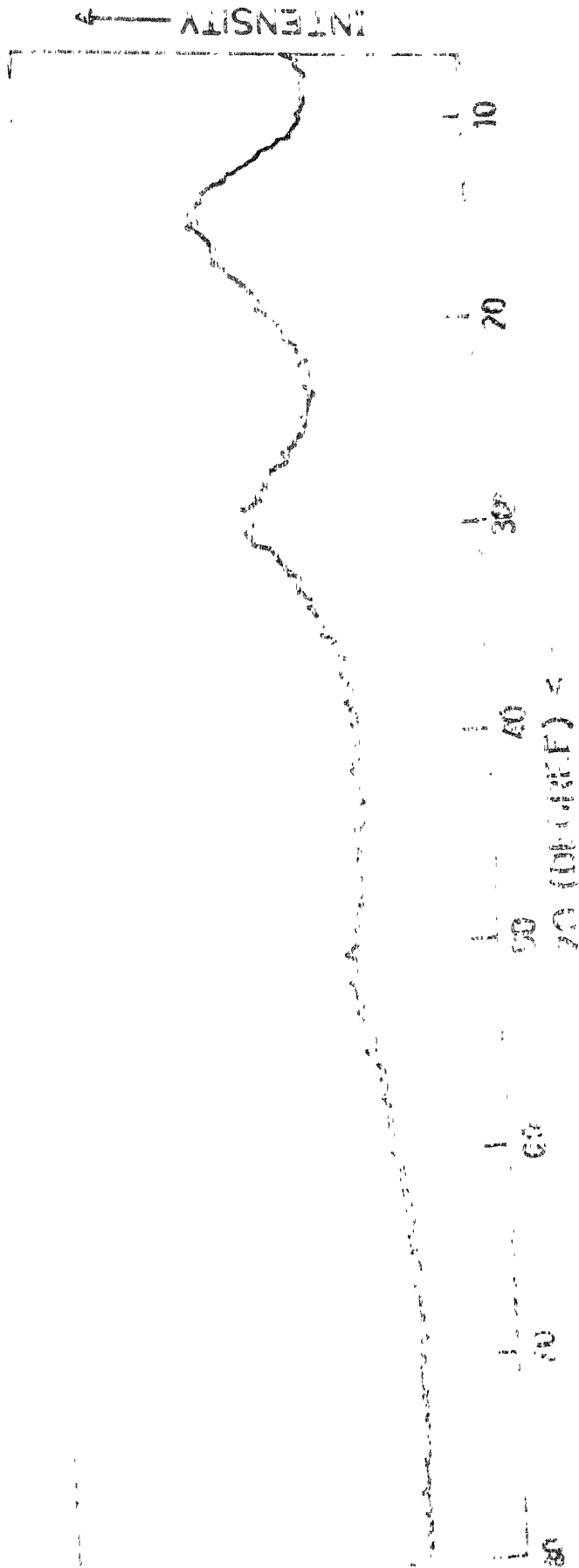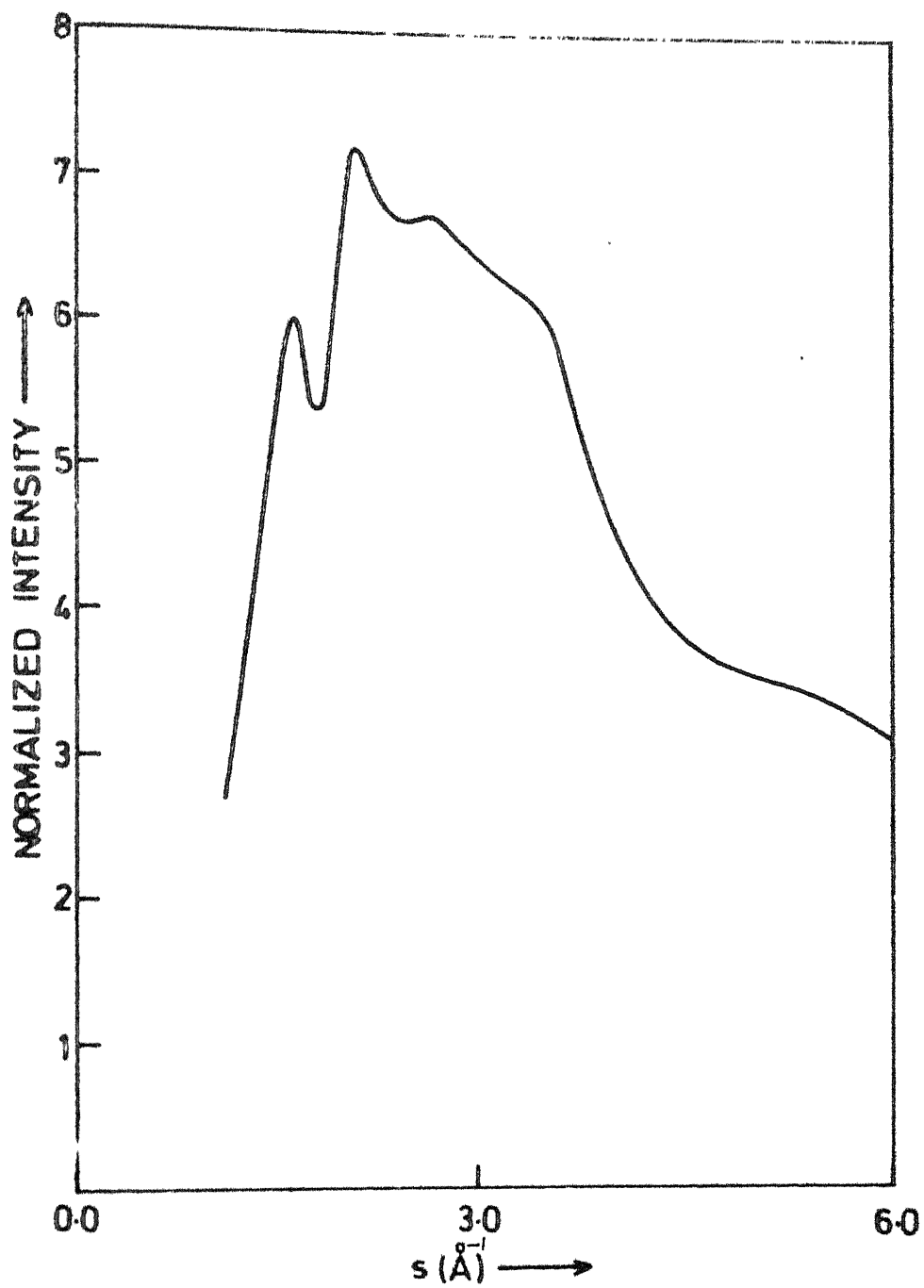
INTENSITY

Fig.5.10   Intensity in electron units for II

Fig. 3.11 G(r) function for Xe.

Axis labels:
r (Å) ⟶

3·5

7·0

0·0

4πr² (ρ − ρ₀)

2·0

1·0

0·5

−0·5

−1·0

−2·0
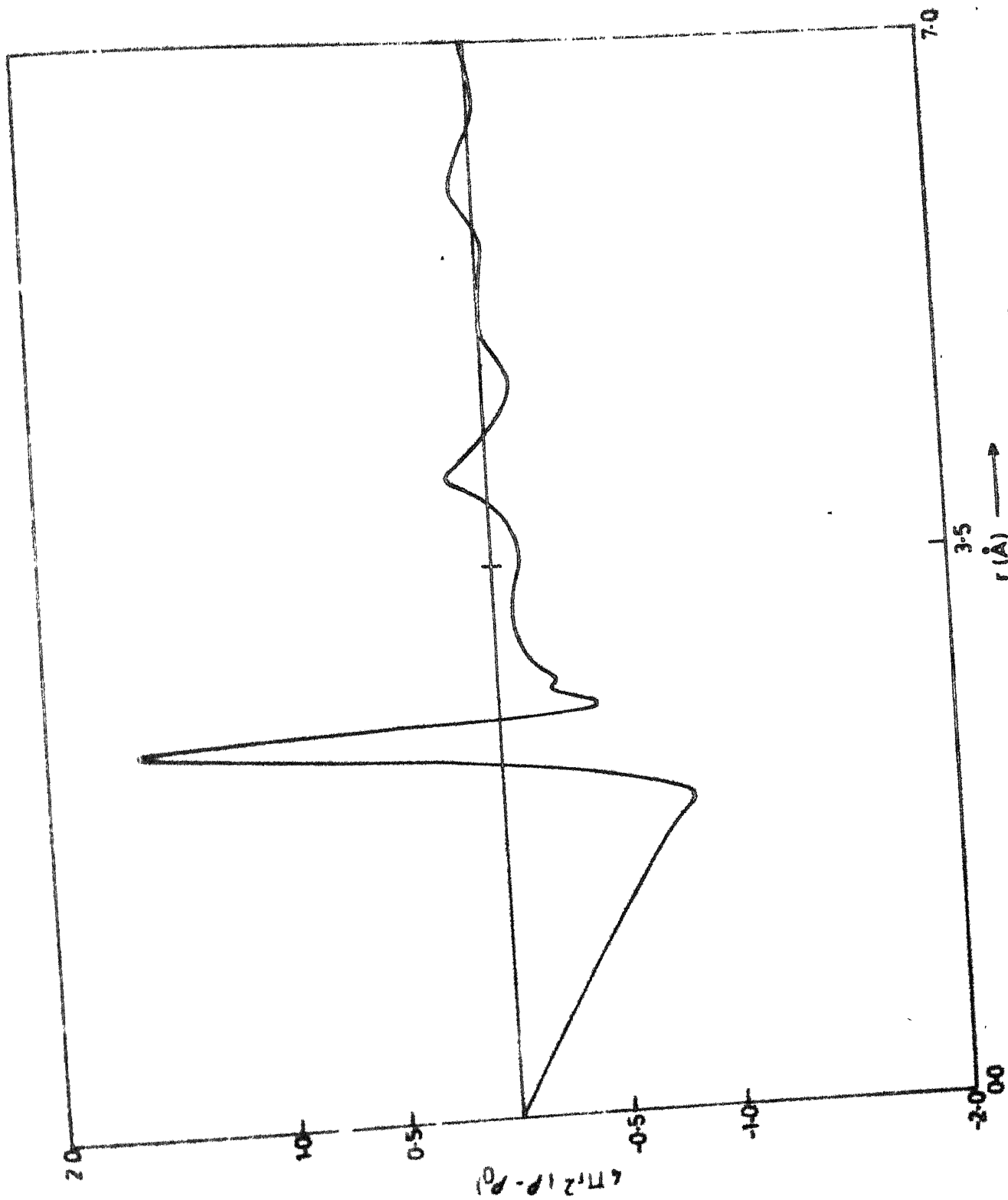
with x_i and $f_i(s)$ representing the atom fraction and scattering factor of element i respectively and

$$s = 4\pi \sin\theta/\lambda .$$

The interference function $F(s)$ is related to the radial distribution function as follows :

$$F(s) = \int_0^\infty G(r) \sin sr \, dr$$

where $G(r)$ equals $4\pi r(\rho - \rho_o)$. ρ_o is the average density and r is the radial distance. Fourier inversion of the above equation yields

$$G(r) = \frac{2}{\pi} \int_0^\infty F(s) \sin rs \, ds$$

The termination of data at $s_{max} < \infty$ introduces spurious details in the resultant $G(r)$. Following the procedure for termination correction (Kaplow et al., 1965), the final $G(r)$ function was determined.

To illustrate, the normalised intensity and the $G(r)$ function for sample II are shown in figures 5.10 and 5.11 respectively. The near neighbour distance from $G(r)$ function indicate a value 2.38 ± 0.03 $\overset{o}{A}$. Similar analysis for sample I also yields the same near neighbour separation.

CHAPTER VI

SUMMARY

The present work includes the structural study of crystalline and amorphous germanium and amorphous Ge_xSe_{1-x} system by X-ray diffraction, X-ray fluorescence and EXAFS techniques. More emphasis is placed on the relatively new technique - EXAFS. Although the revival of interest in EXAFS is due to the improvements in theory and experimentation, in particular the synchroton related developments, we have in our laboratory recorded the EXAFS data with a conventional X-ray source. By operating the tube at higher ratings the requirement of high photon flux was met. However this would introduce systematic errors in the experimental data as the harmonics contribute to the measured intensity. It has been assumed, while analysing the EXAFS data, that this harmonic contribution is relatively small and thus could be neglected. Adequate resolution ($\sim 4eV$) in the vicinity of absorption edge was obtained by using an exit of .05 mm width (which allows minimum increment of 0.01° in 2θ). Because of the slight variation in the intensity of radiation from the source with time, it is expected that the incident and transmitted intensities (I_o , I) be measured simultaneously. However in the present work we have measured the transmitted intensity (in preset count mode, 10^5 counts) at all the experimental points (441 points for Ge edge and 331 points for Se edge) and then repeated the scan without the absorber in the path of the beam. The

variation in the intensity with time was found to lie well within the statistical precision.

The analysis of EXAFS data involved number of steps with extensive use of computer. The programmes needed for the analysis were developed (see Appendix I). The experimental data of crystalline and amorphous germanium served to standardize the analysis procedure. In a bid to determine the near neighbour distance by direct comparison of experimental and theoretical phase shifts it was found that it is possible only when the phase functions are extracted at $E_O = E_C$. When near neighbour distances were determined with values of E_O other than E_C, no physical significance could be attached to the parameter ΔE_O, the change in the threshold. The distances determined also varied by as much as 0.03 A^O. On the other hand analysis with $E_O = E_C$ yields the bond lengths to an accuracy of 0.01 A^O. Also the values of ΔE_O were of the order of E_C with change in sign. This means that the threshold which was shifted by E_C, to obtain linear phase shift, is again shifted towards $E_O = o$ thereby introducing non linearity in the phase shift.

Calculation of theoretical phase shifts require the knowledge of both the central atom phase shift and back-scattering atom phase shift. These have been tabulated by Teo and Lee (1979). The phase shifts calculated by them using the Herman-Skillman wave functions were not used

as variation in the backscattering phase shift with atomic
number posed a problem in interpolation of the tabulated
data. The figure 6.1 shows the backscattering phase shifts
at $k = 3.7795 \, A^{O \, -1}$ calculated using Clementi-Roetti wave
functions and Herman-Skillman wave functions (dashed curve)
as a function of the atomic number. In our analysis we
found the phase shifts calculated using Clementi-Roetti
wave functions suitable.

In the Fourier filtering technique which has been
used to separate out the first coordination shell contri-
bution to EXAFS, normally a 'sufficiently' large window
encompassing the first peak is used. A systematic study
has been carried out to illustrate the effect of the width
of the filtering window on the phase and amplitude func-
tions and subsequently on the local structure parameters
determined using these functions. The near neighbour
distance determined from phase functions for different
widths of the filtering window was found to remain constant
(see Table 4.1). This indicates that the phase part of
first shell EXAFS is hardly affected by the width of the
filtering window. Contrary to this the amplitude function
was found to be very sensitive to the window function.
For 'narrow' window the amplitude function simply dies
away almost exponentially as the photoelectron wave vector
increases. With increasing width of the filtering window
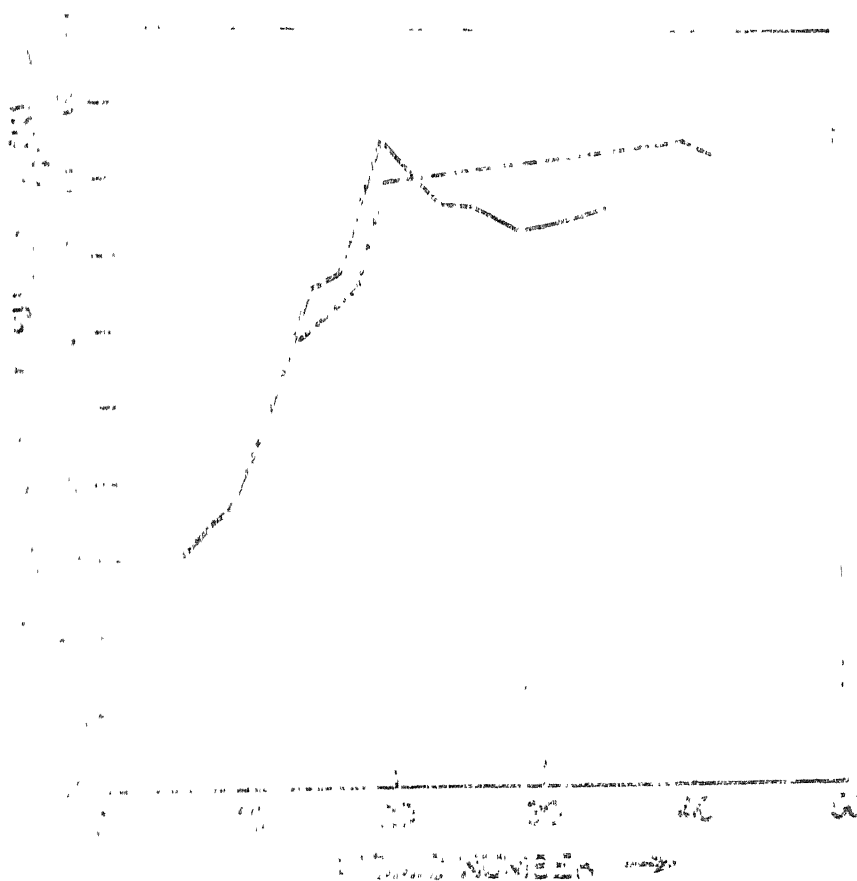
the trend of the amplitude function approaches to that of the backscattering amplitudes tabulated by Teo and Lee (1979). In our analysis we have used an optimum width (1.25 A^o) which retains the details in the amplitude function (see section 4.6).

Concepts of chemical transferability for both the phase and amplitude functions have been used while analysing the crystalline and amorphous germanium data. Transferability of phase functions yielded the near neighbour distance for a-Ge which was in agreement with the one obtained by comparison of theoretical and experimental phase shifts. The DRDF obtained from X-ray diffraction studies (see sec.4.10) also indicate almost the same near neighbour distance. Transferability of amplitude functions was used to determine the coordination number of a-Ge. The logarithmic ratio of the amplitude functions when plotted against k^2 yields a non linear curve (see figure 4.12). The determined value of the coordination number was found to be very sensitive to the range of k-values used for fitting the straight line. Thus the coordination number could be determine only with a limited accuracy (4.49 ± 0.8). The other method which has been used for determining the coordination number of a-Ge involves determination of an overall scaling factor for c-Ge amplitude function and then using the same for a-Ge amplitude. This method also gave a value of

coordination number slightly greater than four with as
much an accuracy as that in case of transferability of
amplitude functions. The results obtained for a-Ge are
in agreement with the earlier RDF and EXAFS studies except
for the coordination number which appears to be greater
than four, a result which is hard to credit. The reason
for obtaining higher value of coordination number also
suggests that the mean free path in case of a-Ge is large
as compared with that in c-Ge. Earlier studies (Temkin
et al., 1973, 1972; Shvchik and Paul, 1972; Richter and
Breitling, 1951) have predicted coordination number of
a-Ge to be less than four. Our results when corrected for
mean free path and the accuracy with which the coordination
number can be calculated with EXAFS is taken into account
would not contradict the earlier results.

In the present work, the study of Ge_xSe_{1-x} system
has been limited to compounds with low concentration of
germanium. The earlier studies with X-ray diffraction
proposed two possible models namely the CCM and RCM. In
recent times many authors have supported the former model
for Ge_xSe_{1-x} system with $x \leqslant 0.33$ (Ball and Chamberlain, 1978;
Hanenstock, 1976). In the present work we have studied
the two composition $x = 0.1$ and $x = 0.3$. X-ray fluorescence
measurements were used to ascertain the compositions of these
compounds. The DRDF obtained from X-ray diffraction studies

of these samples indicate the first neighbour separation

to be equal to 2.38 A^O. This would correspond^{to} all the

three bonds Ge-Ge, Ge-Se and Se-Se.

In order to see whether EXAFS can give some information tion regarding the local structure, the EXAFS associated with both Ge as well as Se absorption discontinuities has been studied. While EXAFS typically measures first shell distances with an accuracy of 0.01 A^O, the resolution of different bond lengths is much poorer of the order of 0.2A^O. With much work and in favourable circumstances the limit can be pushed down to $\leq$ 0.10 A^O (Shulman et al., 1978). For the Ge$_x$Se$_{1-x}$ system thus the distances Ge-Ge and Ge-Se (or Se-Se and Se-Ge around Se) coud not be resolved. Therefore the first shell phase function could be on account of the two possible bondings. Out of the different procedures suggested for determination of first shell radius we choose the method of comparison of theoretical and experimental phase shifts. While comparing the phase shifts again one requires the knowledge of backscattering atom. Depending on the quality of fit obtained with each of the atoms as backscattering atom and their concentration in the compound, we talk in terms of the probability of the particular atom being the nearest neighbour of the central atom. This approach was found to be quite satisfactory but does not support any of the earlier models. Therefore we make use

of these probabilities in the proposed model which describes the first shell EXAFS in terms of all the possible configurations but with different probabilities. The comparison of the experimental first shell EXAFS with the one calculated from the probability model yields the parameters which are quite consistent as discussed in section 5.4.2. Thus it has been possible to determine the distribution of atoms (in terms of probabilities) surrounding the absorbing atom using the EXAFS phase functions.

The method developed in the present work for GeSe system may well be extended to study systems like As_2Se_3 or As_xSe_{1-x} system and the multicomponent systems such as GeSeTe and so on. It is desirable to record the EXAFS data at liquid nitrogen temperature and this could help in the accurate determination of disorder parameter σ^2 (Gregor and Lytle, 1979).

Although the structure in FT beyond the first peak is significant, the present study was limited to only first coordination shell. However with the determined probabilities P_{Ge} and P_{Se} it is possible to simulate a structure which would explain the details in the Fourier transform beyond the first shell.

References

Agrawal B.K. (1979) : "X-Ray Spectroscopy" Springer-Verlag Heidelberg New York

Ashley C.A. and Doniach S. (1975), Phys. Rev. B11, 1279

Azaroff L.V. (1974) : "X-Ray Spectroscopy" Mc-Graw Hill USA

Ball G.J. and Chamberlain J. (1978), J. Non-cryst. Solids 29, 239

Bearden J.A. (1928), Proc. Natl. Acad. Sci. 14, 539

Beni G. and Platzman P.M. (1976), Phys. Rev. B14, 9514

Bergland G.D. (1969), IEEE Spectrum 6(7), 41

Bernal J.D. (1937), Trans. Far. Soc. 33, 27

Bernal J.D. (1959), Proc. Roy. Inst. (GB) 37, 355

Bernal J.D. and Fowler R.H. (1933), J. Chem. Phys. 1, 515

Bienenstock A. (1973a), Proceedings of Fifth International Conference on Amorphous and Liquid Semiconductors ed. Stuke J., p. 49

Bienenstock A. (1973b), J. Non-cryst. Solids 11, 447

Bienenstock A. (1976) : "The Structure of Non-crystalline Materials", Proceedings of the Symposium ed. P.H. Gaskell, p. 5

Bienenstock A., Mortyn F., Narashimhan S. and Rowland S.C. (1976) In "Material Science", edited by L.E. Murr and C. Stein, Marcel Dekker, p. 1

Biscoe J. and Warren B.E. (1938), J. Am. Ceram. Soc. 21, 287

Bletskan D.l. and Gerasimenko V.S. (1978), Ukr. Fiz. Zh. (USSR) 23, 1106

Bragg W.H. and Bragg W.L. (1913), Proc. Roy. Soc. 88a, 428

Brentano J.C. and Landasy I. (1954) Rev. Sci. Inst. 25, 1028

Cargill G.S. (1970), J. Appl. Phys. 41, 12

Cauchois Y. (1948), Les Spectres de Rayons X et la Structure Electronique de la Matiere (Gauthier-Villars, Paris)

Citrin P.H., Eisenberger P. and Kincaid B.M. (1976), Phys. Rev. Lett. 36, 1346

Citrin P.H., Eisenberger P. and Hewitt R.C. (1979), Surf. Sci. 89, 28

Cook Jr. and Sayers D.E. (1981), J. Appl. Phys. 52, 5024

Cramer S.P., Hodgson K.O., Steifel E.I. and Newton W.E. (1978), J.Am. Chem. Soc. 100, 2748

Crozier E.D., Lytle F.W., Sayers D.E. and Stern E.A. (1977), Can. J. Chem. 55, 1968

Crozier E.D. and Seary A.J. (1980), Can. J. Phys. 58, 1388

Crozier E.D. and Seary A.J. (1981), ibid. 59, 876

Dessaner J.H. and Clarks H.E. (1965) : "Xerography and Related Processes" Focal Press, London and New York

Eisenberger P. and Brown G.S. (1979), Solid State Commun. 29, 481

Eisenberger P. and Lengeler B. (1980), Phys. Rev. B22, 3551

Evans D.L. and King S.V. (1966), Nature, 212, 1353

Fawcett R.W., Wagner C.N.J. and Cargill III G.S.(1972), J. Non-cryst. Solids 8-10, 369

Fienleib J., Deneufville J.P., Moss S.C. and Ovshinsky S.R. (1971), Appl. Phys. Lett. 18, 254

Germer L.H. and White A.W. (1941), Phys. Rev. 60, 447

Glaser H. (1951), Phys. Rev. 82, 616

Goldschmidt D., Bernstein T. and Rudman P.S. (1977), Phys. Status Solidi A41, 283

Graczyk J.F. and Choudhari P. (1973), Phys. Status Solidi B58, 163

Greegor R.B. and Lytle F.W. (1979), Am. Phy. Soc. 20, 4902

Grigorvici R. and Manila (1969), J. Non-cryst. Solids $\underline{1}$, 371

Gurman S.J. (1982), J. Mater. Sci. 17(6), 1541

Halder N.C., Metzger R.J. and Wagner C.N.J. (1966), J. Chem. Phys. $\underline{45}$, 1259

Hanawalt J.D. (1931), Z. Physik $\underline{70}$, 293

Hartree D.R., Kronig R. de. and Petersen H. (1934), Physica $\underline{1}$, 895

Hastings J.B., Eisenberger P., Lengeler B. and Perlman M.L. (1979), Phys. Rev. Lett. $\underline{43}$, 1807

Hayasi T. (1949), Sci. Repts. TOHOKU Univ. $\underline{33}$, 123

Hayes T.M., Sen P.N. and Hunter S.H. (1976), J. Phys. $\underline{C9}$, 4357

Hilton A.R., Jones C.E. and Brau M. (1966$\underline{a}$), Infrared Physics $\underline{6}$, 183

Hilton A.R., Jones C.E., Dobrott R.D., Klein H.M., Bryant A.M. and George T.D. (1966$\underline{b}$), Phys. Chem. Glasses $\underline{7}$, 116

Jaklevic J., Kirby T.A., Klein M.P., Robertson A.S., Brown G.S. and Eisenberger P. (1977), Sol. State Commun. $\underline{23}$, 679

Kaplow Roy, Strong S.L. and Averbach B.L. (1965), Phys. Rev. $\underline{138}$, 1336

Kawamura H., Matsumura M. and Ushida S. (1982) 'Spectroscopic Studies of a-GeSe System' in book - Amorphous semiconductor technologies and devices, ed. Y. Hamakawa, North-Holland, 328

Kincaid B.M. and Eisenberger P. (1975), Phys. Rev. Lett. $\underline{34}$, 1361

Klug H.F. and Alexander L.E. (1954) : "X-Ray Diffraction Procedures" (JOHN WILEY & SONS INC.)

Knapp G.S., Chen H. and Kleppert T.E. (1978), Rev. Sci. Inst. $\underline{49}$, 1658

Kossel W. (1920), Z. Phys. $\underline{1}$, 119

Kostarev A.I. (1941), Zhur. eksph. Teoret. Fiz. $\underline{11}$, 66

Kostarev A.I. (1949), ibid. $\underline{19}$, 413

Kostarev A.I. (1951), ibid. 21, 917

Kronig R. de. (1931), Z. Physik 70, 317

Kronig R. de. (1932), ibid. 75, 468

Lagarde P. (1976), Phys. Rev. B13, 741

Lee P.A. and Beni G. (1977), Phys. Rev. B15, 2862

Lee P.A. and Pendry J.B. (1975), ibid. B11, 2795

Lee P.A., Teo B.K. and Simpson A.L. (1977), J.Am. Chem. Soc. 99, 3856

Lindh A. and Nilson A. (1943), arc. mat. astron. Fys. 29A, 17

Lytle F.W. (1963), developments in applied spectroscopy (New York: Plenum), 2, 285

Lytle F.W. (1966), Adv. X-ray ann. (ed. G.R. Mallet, M.J. Fay and W.M. Mullar), 9, 398

Lytle F.W., Sayers D.E. and Stern E.A. (1975), Phys. Rev. B11, 4825

Lytle F.W., Via G.H. and Sinfelt J.H. (1980) : SYNCHROTRON RADIATION RESEARCH Edited by Herman Winick and S. Doniach (Plenum Publication Corporation), p. 401

Mande C. and Nigavekar A.S. (1967), Proc. Ind. Acad. Sci. 65, 376

Martens G., Rabe P., Schwentntner N. and Werner A. (1978), Phys. Rev. B17, 1481

Moss S.C. and Graczyk J.F. (1969), Phys. Rev. Lett. 23, 1167

Mozzi R.L. and Warren B.E. (1969), J. Appl. Cryst. 2, 164

Neale R.G. and Aseltine J. (1973), IEEE Trans. Electron Devices ED-20, 195

Nermanich R.J., Connell G.A.N., Hayes T.M. and Street R.A. (1978), Phys. Rev. B18, 6900

Ordway F. (1964), Science 141, 800

Ovshinsky S.R. (1968), Phys. Rev. Lett. 21, 1450

Ovshinsky S.R. and Fritzsche H. (1973), IEEE Trans. Electron Devices ED-20, 91

Parrat L.G., Hempstead C.F. and Jossem E.L. (1957), Phys. Rev. 105, 1228

Petersen H. (1933), Z. Physik 80, 258

Pettifer R.F. and Mcmillan P.W. (1977), Phil. mag. 35, 871

Piggott M.R. (1966), J. Appl. Phys. 37, 2927

Polk D.E. (1971), J. Non-cryst. Solids 5, 365

Reed J., Eisenberger P., Teo B.K. and Kincaid B.II. (1977), J. Am. Chem. Soc. 99, 5217

Reed J., Eisenberger P., Teo B.K. and Kincaid B.M. (1978), ibid. 100, 2375.

Richter H. (1972), J. Non-cryst. Solids 8-10, 388

Richter H. and Breitling G. (1951), Z. Naturf A6, 721; (1958), ibid. 13, 988

Sandstrom D.R. and Lytle F.W. (1979), Ann. Rev. Phys. Chem. 30, 215

Sayers D.E., Lytle F.W. and Stern E.A. (1970), Adv. X-ray ann. 13, 248

Sayers D.E., Lytle F.W. and Stern E.A. (1972), J. Non-cryst. Solids 8-10, 401

Sayers D.E., Lytle F.W. and Stern E.A. (1974), Vth Int. Conf. on Amorphous Semiconductors ed. J. Stuke, North-Holland, 403

Sayers D.E., Stern E.A. and Herriot J.R. (1976), J. Chem. Phys. 64, 427

Sayers D.E., Stern E.A. and Lytle F.W. (1971), Phys. Rev. Lett. 27, 1204

Schmit V.V. (1961), Bull. Acad. Sci. USSR Ser. Phys. 25, 988; ibid. 27, 392

Shaw C.V. (1946), Phys. Rev. 70, 643

Shevchik N.J. and W. Paul (1972), J. Non-cryst. Solids 8-10, 381

Shulman R.G., Eisenberger P., Blumberg W.E. and Stombaugh N.A. (1975), Proc. Natl. Acad. Sci. (USA) 72, 4003

Shulman R.G., Eisenberger P., Teo B.K., Kincaid B.M. and Brown G.S. (1978), J. mol. Biol. 124, 304

Shiraiwa T., Shimura T.I. and Sawada M. (1958), J. Phys. Soc. Japan, 13, 847

Stearns M.B. (1982), Phys. Rev. B25, 2382

Stephensen S.T. (1947), Phys. Rev. 71, 81

Stern E.A. (1974), Phys. Rev. B10, 3027

Stern E.A., Bunker B.A. and Heald S.N. (1980), Phys. Rev. B21, 5521

Stern E.A. and Kim K. (1981), Phys. Rev. B23, 3781

Stern E.A., Sayers D.E. and Lytle F.W. (1975), Phys. Rev. B11, 4836

Temkin R.J., Connell G.A.N. and Paul (1972), Solid State Commun. 11, 1591

Temkin R.J., Paul W. and Connell G.A.N. (1973), Adv. Phys. 22, 581

Teo B.K., Eisenberger P. and Kincaid B.M. (1978 a), J. Am. Chem. Soc. 100, 1735

Teo B.K., Kijima K. and Ban R. (1978b), ibid. 100, 621

Teo B.K. and Lee P.A. (1979), ibid. 101, 2815

Teo B.K., Lee P.A., Simons A.L., Eisenberger P. and Kincaid B.M. (1977), ibid. 99, 3854

Terao M., Yamamoto H., Asai S. and Maruyana E. (1972), J. Japan. Soc. Appl. Phys. (Suppl.) 41, 68

Tronc P. Bensoussan M., Brenac A. and Sebnne C. (1977), Solid State Commun. (USA), 24, 79

Turnbull D. and Polk D.E. (1972), J. Non-cryst. Solids, 8-10, 19

Wagner C.N.J., Light T.B., Halder M.C. and Lukens W.E. (1968), J. Appl. Phys. 39, 3690

Warren B.E., Krutter H. and Morningstar O. (1936), J. Am. Ceram. Soc. 19, 202

Yoshimura M., Tada M., Hayashi Y., Matsumoto S. and Nimi T. (1978), Jpn. J. Appl. Phys. 17, 1457

Zacharaisen W. (1932), J. Am. Chem. Soc. 54, 3841

Zembutsu S., Toyoshima Y., Igo T. and Nagai H. (1975), Appl. Opt. 14, 3073

APPENDIX I

PROGRAMMING NOTES

1. Elementary Analysis

A fairly simple programme was constructed (PROG-I) which reads the times T, T_o for preset number of counts with absorber in the path of the beam and without the absorber. The subroutine VICTOR gives the Victoreen coefficients A and B. The subroutine INTER has been used to interpolate the data onto a grid of equally spaced k values (Kaplow et al., 1965). The input data is stored in file opened with unit 23. The output is written on X.CDR (unit 25) which gives the contribution to absorption exclusively due to K shell as a function of photoelectron wave vector k. D.CDR file (unit 24) contains the absorption μx as a function of energy at all the experimental points. V.CDR gives the extrapolated curve $A\lambda^3 + B\lambda^4$.

2. Fourier Transform

A single subroutine FOUR (PROG-II) was used to perform the Fourier Transforms and Inverse Fourier Transforms required in the analysis of EXAFS. A NAG LIBRARY program C06FCF gives the Fourier coefficient a_n's and b_n's. Combination of C06FCF and C06GCF (for taking complex conjugate) results in inverse transforming the data. DELR is

the spacing in r at which the coefficients are calculated.
It is given by

$$DELR = \pi / (N*DEL)$$

where DEL is the spacing in k-values at which input data
is tabulated at N points.

3. Minimization : MINFUN

The program was written by W.E. Humphrey at the
Lawrence Radiation Laboratory (W.E. Humphrey, "A general
minimizing routine - MINFUN", Programmer's notes P.6,
9.7.62, UCRL, Berkeley). The program was modified for
some of its input requirements. Purpose of the program
is to minimize a function of several variables. It can
be used for the following two distinct purposes :

(a) Finding the minimum of a function of n parameters as
a mathematical problem.

(b) Finding a fit for a set of experimental data to a
given function by minimizing the sum of chi-squares
or negative logarithm of maximum likehood function.

PROG - I

```
C      ELEMENTARY DATA PROCESSING PROGRAM FOR EXAFS

C      PROGRAM READS N1 AS TOTAL POINTS, N2 NO. POINTS

C      FOR VICTOREEN FIT

C      N3 IS THE POINT CORRESPONDING TO MINIMUM VALUE OF K

C      SWITCH IF POSITIVE, ENERGY, LAMDA AND MUE ARE

C      PRINTED AND PAUSE

C      MM IS NO. OF POINTS LESS 1 REQUIRED FOR FOURIER

C      FILTERING

C      TTHM LAST VALUE OF 2θ

C      DATA IS IN DECREASING ORDER OF    2θ

C      NBAD IS NO. OF BAD DATA POINTS AND NB IS ARRAY CONTAINI

C      CORRESPONDING LOCATIONS.

       DIMENSION ALAMDA(500),E(500),AK(1500),AMUE(1500),AA(144

       ,AA1(300,2),NB(10),T0(500),T(500),TTH(500),AMUE1(500),

       V(500),AMUE2(500),AK1(500)

       OPEN (UNIT=23,DEVICE='DSK',FILE='CGE.CDR')

       OPEN (UNIT=24,DEVICE='DSK',FILE='D.CDR')

       OPEN (UNIT=25,DEVICE='DSK',FILE='X.CDR')

       OPEN (UNIT=26,DEVICE='DSK',FILE='V.CDR')

       DATA IN,IN1,IN2,IN3/23,24,25,26/

       READ(IN,1)AA

1      FORMAT(72A1/36A1/36A1)

       READ(IN,*)N1,N2,N3,SWITCH,TTHM

       MM=1023

       PRINT2,N1,N2,N3,SWITCH,MM,TTHM
```

```
2        FORMAT(10X,3I6,5X,F10.4,5X,I6,5X,F10.4)

         READ(IN,*)(T(I),I=1,N1)

         READ(IN,*)(T0(I),I=1,N1)

         READ(IN,*)E0,NBAD,(NB(I),I=1,NBAD)

         DO 3 I=1,N1

         AMUE1(I)=ALOG(T(I)/T0(I))

         TTH(I)=TTHM-(I-1)*0.01

         ALAMDA(I)(I)=4.0262*SIND(TTH(I)/2.0)

3        E(I)=12398.52/ALAMDA(I)

C        REMOVE BAD DATA POINTS

         IF(NBAD.EQ.0)GOTO4

         DO 5 I=1,NBAD

         NB1=NB(I)

5        AMUE1(NB1)=AMUE1(NB1+1)

4        WRITE(IN,*)N1

         WRITE(IN1,90)(E(I),AMUE1(I),I=1,N1)

90       FORMAT(10F10.3)

         IF(SWITCH)6,7,6

7        PRINT1,AA

         PRINT8,(I,TTH(I),E(I),AMUE1(I),ALAMDA(I),I=1,N1)

8        FORMAT(33X,'S.NO.',8X,'TTH',11X,'E',15X,'MUET'///
       1(30X,I6,4F15.4))

         PAUSE

6        CONTINUE

         READ(IN,*)NE1,NE2
```

```
          SL1=(AMUE1(NE1+1)-AMUE1(NE1))/(E(NE1+1)-E(NE1))

          do 20 I=nE1+1,NE2

          SL2=(AMUE1(I+1)-AMUE1(I))/(E(I+1)-E(I))

          PRINT*,I,E(I),SL1,SL2

          TYPE*,I,E(I),SL1,SL2

          IF (SL2.LT.SL1)GOTO21

   20     SI1=SL2

   21     E01=(E(I-1)+E(I))/2.0

          E0=E01

          DO 9 I=1,N2

          X1=ALAMDA(I)**3

          X2=X1*ALAMDA(I)

          AA1(I,1)=X1

   9      AA1(I,2)=X2

          CALL VICTOR(AA1,AMUE1,N2,2,C,D)

          PRINT*,C,D

   C      EXTRAPOLATION AND SUBTRACTION

          DO 100 I=1,N1

          X1=ALAMDA(I)**3

          X2=X1*ALAMDA(I)

   100    V(I)=C*X1+D*X2

          DO 10 I=N3,N1

          J=I-N3+1

          AMUE2(J)=AMUE1(I)-V(I)

          AK1(J)=SQRT(0.263*(E(I)-E0))
```

```
10      CONTINUE

        N13=N1-N3+1

        DEL=(16.0*3.14159265/857.0)

        N111=(AK1(N13)-AK1(1))/DEL+1

        CALL INTER(AK1,AMUE2,N13,AK,AMUE,N111,DEL,I1)

        PAUSE

        WRITE(IN2,*)N111,DEL,I1,AK(N111)

        WRITE(IN2,11)(AK(I),AMUE(I),I=1,N111)

        WRITE(26,*)N1

        WRITE(26,90)(E(I),V(I),I=1,N1)

11      FORMAT(10F10.7)

        STOP

        END
```

PROG - II

```
SUBROUTINE FOUR(X,Y,N,NL,NH,I1,I2,DELR)
DIMENSION X(8192),Y(8192),WORK(8192),XX(1000),R1(1000),
1WW(1000)
DIMENSION WR(500),WR1(100),WW1(100)
COMMON CONT
OPEN (UNIT=50,DEVICE='DSK',FILE='R.CDR')
OPEN (UNIT=51,DEVICE='DSK',FILE='W.CDR')
C    X IS AN ARRAY CONTAINING REAL PART Y IS THE ARRAY
C    CONTAINING IMPARINARY PART OF THE DATA TO BE ANALYSED
     IFAIL=0;PI=3.14159265
     CALL C06FCF(X,Y,N,WORK,IFAIL)


C    IF I1=NL=0 THE NEGATIVE R-PART IS REMOVED AND I.F.T.
C    COMPLEX FUNCTION IS RETURNED
C    IF I2=2 SMOOTH FILTERING WINDOW IS USED BEFORE I.F.T.
C    REAL FUNCTION IS RETURNED
     IF(I1.EQ.3)GOTO4
     IF(NL.EQ.0)GOTO5
     MMM=8.0/DELR+1
     DO 6 I=1,MMM
     R1(I)=(I-1)*DELR
     XX(I)=SQRT(X(I)**2+Y(I)**2)
6    CONTINUE
     IF(I2.EQ.1)GOTO7
```

```
        WRITE(50,*)MMM
        WRITE(50,8888)(R1(I),XX(I),I=1,MMM)
8888    FORMAT(10F10.4)
7       TYPE 8
8       FORMAT(5X,'TYPE 1 IF NL NH ARE KNOWN ELSE 0')
        ACCEPT*,TR
        IF(TR.EQ.1.0)GOTO9
        CONT1=0.0
        DO 786 I=1,500
        IF(CONT1.NE.0.0) GO TO 888
        IF(XX(I+1).GT.XX(I)) GO TO 786
        TYPE 11,(R1(I),X(I),Y(I),I,XX(I))
        CONT1=1.0
        GO TO 786
888     IF(XX(I+1).LT.XX(I)) GO TO 786
        CONT1=0.0
786     CONTINUE
2222    TYPE 10
10      FORMAT(5X,'GIVE NO OF COEFFICIENTS TO BE TYPED
        1FROM N1 TO N2')
        ACCEPT*,MM1,MM2
        IF(MM2.EQ.1)GOTO10000
        TYPE11,(R1(I),X(I),Y(I),I,XX(I),I=MM1,MM2)
10000   CONTINUE
```

```
11        FORMAT(5X,3F16.7,I6.7)

          TYPE 5555

5555      FORMAT('    TYPE 1 TO CONTINUE, 0 TO GO BACK')

          ACCEPT*,KK

          IF(KK.EQ.0)GO TO 2222

          TYPE 454

454       FORMAT ('    DO YOU WANT TO RETURN : Y/N')

          ACCEPT 1, CONT

1         FORMAT (A4)

          IF (CONT.EQ.'Y') RETURN

9         TYPE 12

12        FORMAT(5X,'GIVE NL NH')

          ACCEPT*,NL,NH

          IF(NL.EQ.0)GOTO13

          IF(NL.EQ.1)GOTO88

          X(1)=0.0;Y(1)=0.0

          DO 14 I=1,NL-1

          X(I+1)=0.0;Y(I+1)=0.0

          X(N-I+1)=0.0;Y(N-I+1)=0.0

14        CONTINUE

          IF(NH.EQ.0)GOTO4

88        DO 16 I=NH-1,N/2-1

          X(I+1)=0.0;Y(I+1)=0

          X(N-I+1)=0.0;Y(N-I+1)=0.0

16        CONTINUE
```

```
        IF(I1.EQ.2)GOTO 22
4       CALL C06GCF(Y,N,IFAIL)
        CALL C06FCE(X,Y,N,WORK,IFAIL)
        CALL C06GCF(Y,N,IFAIL)
        RETURN
13      DO 20 I=1,N/2-1
        Y(N-I+1)=0.0;Y(N-I+1)=0.0
20      CONTINUE
        GOTO4
22      XMAX=SEA(XX,MM,NL,NH)
        DO 21 I=NL-1,NH-1
        I1=I+1
        WI=0.6*(1-COS(2.*PI*(I1-NH)/(NL-NH)))
        WW(I+2-NL)=WI*XMAX
        WR(I+2-NL)=R1(1+I)
        X(I+1)=X(I+1)*WI;X(N-I+1)=X(N-I+1)*WI
        Y(I+1)=Y(I+1)*WI;Y(N-I+1)=Y(N-I+1)*WI
21      CONTINUE
        NLN=NH-NL+1
        NLA=100;D = (WR(NLN)-WR(1))/(NLA-1)
        CALL INTER(WR,WW,NLN,WR1,WW1,NLA,D,I1)

        WRITE(51,*)NLA
        WRITE(51,*) (WR1(I),WW1(I),I=1,NLA)
        GOTO4
        END
```

```
      FUNCTION SEA(A,N,N1,N2)

      DIMENSION A(N)

      XMAX=A(N1)

      DO 10 I=N1+1,N2

      IF(XMAX.GE.A(I) ) GO TO 10

      XMAX=A(I)

10    CONTINUE

      SEA=XMAX

      RETURN

      END
```

APPENDIX II

SEPARATION OF PHASE AND AMPLITUDE FUNCTIONS

The expression for the first shell EXAFS is

$$\chi_1(k) = \frac{N_1}{kr_1^2} e^{-\frac{2r_1}{\lambda}} e^{-2\sigma^2 k^2} \sin\left[2kr_1 + \phi(k)\right]$$

$$= A(k) \sin \psi(k) \tag{i}$$

where $A(k)$ and $\psi(k)$ are the amplitude and phase functions respectively.

The Fourier transform has the ability to decompose a sine wave into a unique amplitude and phase function. We can write (i) in the form

$$\chi_1(k) = \frac{1}{2i} A(k) e^{i\psi(k)} - \frac{1}{2i} e^{-i\psi(k)} \tag{ii}$$

If $\chi_1(k)$ is Fourier transformed to $F(r)$ and $\chi_1(k)$ is sufficiently bandlimited in r (guaranteed by filtering), then the term $e^{i\psi(k)}$ in (ii) corresponds to positive r values and $e^{-i\psi(k)}$ term negative ones. If, before transforming $F(r)$ back to $\chi_1(k)$, the negative r part of $F(r)$ is replaced by zero, then resulting inverse transform produces

$$z(k) = \frac{1}{2i} A(k) e^{i\psi(k)},$$

The phase and amplitude functions are readily obtained as

$$A(k) \quad = \quad 2 \, \bigl| Z(k) \bigr|$$

$$\psi(k) \quad = \quad \arg \bigl[Z(k) \bigr] + \frac{\pi}{2}$$